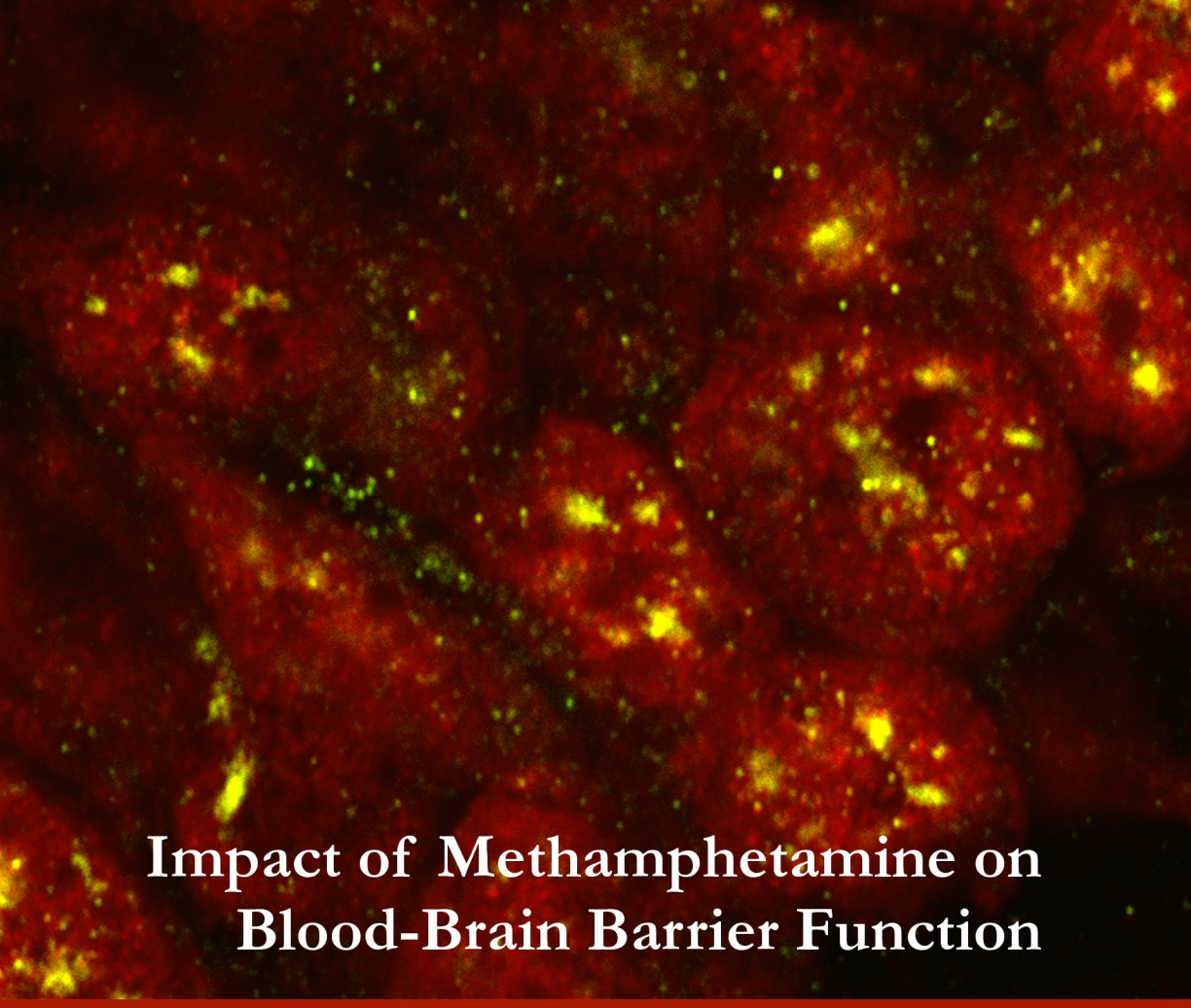

Impact of Methamphetamine on Blood-Brain Barrier Function

Tânia Sofia Cordeiro Martins

Universidade de Coimbra
2012

Cover:
Image of pyramidal neurons expressing matrix metalloproteinase-9 in the mouse hippocampus, obtained by confocal microscopy.

Tânia Sofia Cordeiro Martins

Impacto da metanfetamina na função da barreira hematoencefálica

Impact of methamphetamine on blood-brain barrier function

Universidade de Coimbra

2012

Dissertação apresentada à Faculdade de Medicina da Universidade de Coimbra, para prestação de provas de Doutoramento em Ciências da Saúde, no ramo de Ciências Biomédicas.

Este trabalho foi realizado no Laboratório de Farmacologia e Terapêutica Experimental, no Instituto Biomédico de Investigação em Luz e Imagem (IBILI), da Faculdade de Medicina da Universidade de Coimbra, sob orientação da Doutora Ana Paula Silva e co-orientação do Doutor António Francisco Ambrósio, e no Departamento de Biologia Celular do Instituto de Oftalmologia, *University College of London*, Londres, Reino Unido, sob supervisão do Professor John Greenwood e do Doutor Patric Turowski, ao abrigo de uma bolsa de doutoramento financiada pela Fundação para a Ciência e a Tecnologia (SFRH/BD/41019/2007), co-financiada pelo QREN (Fundo Social Europeu).

Agradecimentos/Acknowledgments

À Doutora Ana Paula Silva pela orientação, discussões e críticas construtivas cruciais à realização deste trabalho. Obrigada pelo voto de confiança e incentivo no início da minha carreira científica que me lançou neste projecto e pelo apoio constante ao longo destes últimos anos.

Ao Doutor António Francisco Ambrósio pela co-orientação, disponibilidade e interesse sempre manifestados na elaboração deste trabalho. Obrigada pelo apoio e pelas críticas e sugestões que contribuíram para o enriquecimento do trabalho realizado.

To Professor John Greenwood and Dr. Patric Turowski for giving me the opportunity to do part of my PhD work in the Institute of Ophthalmology, UCL. Thank you for all the help, trust and support, and for the scientific discussions that greatly improved the quality of this work.

À Professora Doutora Tice dos Reis Macedo, ao Professor Doutor Frederico Teixeira, e ao Professor Doutor Carlos Fontes Ribeiro pelo apoio e oportunidade de desenvolver este trabalho no Laboratório de Farmacologia e Terapêutica Experimental, Faculdade de Medicina da Universidade de Coimbra.

Ao Ermelindo, Joana, Sofia e restantes colegas da Faculdade de Medicina da Universidade de Coimbra, IBILI e Centro de Neurociências de Coimbra por toda a ajuda na realização deste trabalho.

To my colleagues in London, thank you for all your help, support and friendship. A special thanks to Brett, Caroline, Fran, Jenny, Natalie and Xiomang.

À Lena Valente por toda a ajuda e apoio que me deu quando estive em Londres!

A todos os meus amigos que me proporcionaram os melhores anos da minha vida de estudante e cuja amizade se manteve após cada um seguir o seu caminho. Um especial obrigado à Lisa, Joana, Milú e Tiago por estarem presentes nos momentos em que mais precisei e que sempre acreditaram em mim! Obrigada Rita por toda a amizade e ajuda e por teres tornado a minha estadia em Londres mais agradável!

Obrigada Sara por todos os bons momentos que partilhámos, pelas longas conversas e por me ouvires quando eu chegava a casa depois de um dia difícil!

Um especial obrigado também à Catarina, Patrícia e Zé sem os quais não teria sido possível ultrapassar muitos obstáculos e que me ajudaram a manter à tona!

Obrigada Teresa Louro, Teresa Roque e restantes amigos pela vossa amizade e apoio!

Aos meus pais e irmãos pelo amor incondicional, apoio e encorajamento sempre demonstrados, sem o qual não teria sido possível chegar ao final de mais uma etapa da minha vida.

A todos aqueles que de alguma forma contribuíram para a realização deste trabalho.

Agradeço ainda à Fundação para a Ciência e a Tecnologia a bolsa de doutoramento que me atribuiu [(SFRH/BD/41019/2007), co-financiada pelo QREN (Fundo Social Europeu)].

FCT Fundação para a Ciência e a Tecnologia
MINISTÉRIO DA EDUCAÇÃO E CIÊNCIA

The results presented in this dissertation have been published or were submitted for publication in international peer-reviewed journals:

Martins, T., Baptista, S., Gonçalves, J., Leal E., Milhazes, N., Borges, F., Ribeiro, C.F., Quintela, O., Lendoiro, E., Lopez-Rivadulla, M., Ambrosio, A.F., Silva, A.P., 2011. Methamphetamine transiently increases the blood-brain barrier permeability in the hippocampus: Role of tight junction proteins and matrix metalloproteinase-9. Brain Res. 1411, 28-40.

Martins, T., Burgoyne, T., Kenny, B.A., Hudson, N., Futter, C.E., Ambrósio, A.F., Silva, A.P., Greenwood, J., Turowski, P., 2012. Methamphetamine-induced nitric oxide promotes vesicular transport in blood-brain barrier endothelial cells. (Neuropharmacology, in press).

The present dissertation also contributed to the following review:

Silva, A.P., Martins, T., Baptista. S., Gonçalves, J., Agasse, F., Malva, J.O., 2010. Brain injury associated with widely abused amphetamines: neuroinflammation, neurogenesis and blood-brain barrier. Curr Drug Abuse Rev. 3, 239-254.

Note: The results presented in this dissertation, included in Chapter 2 and 3, are formatted according to the style of the journal where the papers were published or submitted for publication, with some modifications.

Table of contents

Abbreviations

AMPH	Amphetamine
BBB	Blood-Brain Barrier
BMVECs	Brain Microvascular Endothelial Cells
BSA	Bovine Serum Albumin
CA1	Cornu Ammonis Field 1
CA3	Cornu Ammonis Field 3
CNS	Central Nervous System
DAB	Diaminobenzide
DG	Dentate Gyrus
EB	Evans Blue
eNOS	Endothelial Nitric Oxide Synthase
FBS	Fetal Bovine Serum
FITC	Fluorescein Isothiocyanate
GFAP	Glial Fibrillary Acidic Protein
HRP	Horseradish Peroxidase
iNOS	Inducible Nitric Oxide Synthase
JAMs	Junctional Adhesion Molecules
LBRC	Lateral Border Recycling Compartment
L-NAME	L-NG-Nitroarginine Methyl Ester
METH	Methamphetamine
MMPs	Matrix Metalloproteinases
MMP-9	Matrix Metalloproteinase-9
MTT	3-(4,5-Dimethylthiazol-2-yl)-2,5-Diphenyltetrazolium Bromide

nNOS	Neuronal Nitric Oxide Synthase
NO	Nitric Oxide
NOS	Nitric Oxide Synthase
PBS	Phosphate-Buffered Saline
PFA	Paraformaldehyde
RITC	Rhodamine B Isothiocyanate
RNS	Reactive Nitrogen Species
ROS	Reactive Oxygen Species
TJs	Tight Junctions
TEM	Transendothelial Migration
VEC	Vascular Endothelial Cadherin
VVOs	Vesiculo-Vacuolar Organelles
ZO-1	Zonula Occludens-1

Resumo

A metanfetamina (MET) é uma droga de abuso psicoestimulante com um elevado poder de viciação. A sua popularidade tem crescido por todo o mundo, essencialmente devido ao facto de aumentar o estado de alerta, a actividade física e diminuir o apetite. Esta droga de abuso é neurotóxica causando danos irreversíveis nas células cerebrais, levando por sua vez a anomalias neurológicas e psiquiátricas. Estudos recentes demonstraram também que a MET é capaz de causar disfunção da barreira hematoencefálica (BHE). Devido ao papel crucial que a BHE desempenha em manter a homeostase cerebral e proteger o cérebro de substâncias tóxicas e organismos patogénicos, a sua disfunção pode ter consequências graves. Assim, a ruptura da BHE induzida pela MET tem emergido como um outro mecanismo através do qual a MET exerce os seus efeitos neurotóxicos. Para tentar compreender melhor os mecanismos através dos quais a MET induz disfunção da BHE, administrou-se uma dose aguda elevada de MET (30 mg/kg) a murganhos jovens adultos, o que constitui um modelo de intoxicação aguda, e os efeitos na permeabilidade da BHE foram analisados após 1 h, 24 h ou 72 h da injecção de MET em diferentes regiões cerebrais. Observou-se que a MET aumenta a permeabilidade da BHE, mas este efeito foi apenas detectado 24 h após a administração e apenas no hipocampo, mostrando que este foi um efeito transitório e que o hipocampo foi a região cerebral mais susceptível, comparando com o córtex frontal e o estriado. Com o objectivo de identificar os mediadores celulares envolvidos na disfunção da BHE induzida pela MET, investigaram-se possíveis alterações nas proteínas das junções oclusivas e na metaloproteinase-9 da matriz (MMP-9). A MET diminuiu os níveis de

proteína de *zonula occludens* (ZO)-1, claudina-5 e ocludina no hipocampo 24 h após a administração, e aumentou a actividade e a imunoreactividade da MMP-9. O pré-tratamento com BB-94 (30 mg/kg), um inibidor das MMPs, preveniu o aumento da imunoreactividade da MMP-9 e o extravasamento do azul de Evans no hipocampo induzidos pela MET. Em conjunto, estes resultados demonstram que a MET aumenta de forma transitória a permeabilidade da BHE no hipocampo, o que parece ser causado por alterações nas proteínas das junções oclusivas e na MMP-9.

Para investigar os efeitos directos da MET ao nível da BHE, culturas primárias de células endoteliais microvasculares cerebrais (CEMVC) de rato foram expostas a MET (1 μM), uma concentração fisiologicamente relevante, semelhante à encontrada no plasma sanguíneo de consumidores de MET. A permeabilidade a dextranos de massa molecular de 4, 70 e 250 kDa duplicou em resposta à MET, de forma independente ao seu peso molecular. Este aumento na permeabilidade ocorreu sem alterações tanto na resistência eléctrica transendotelial como na distribuição das proteínas das junções aderentes e oclusivas, nomeadamente da caderina vascular endotelial, ocludina, claudina-5 e ZO-1. Além disso, a exposição a MET aumentou o transporte vesicular de peroxidase de rábano, mostrando que a MET promove o transporte vesicular e não o paracelular em culturas de CEMVC de rato. Para além do efeito da MET na permeabilidade endotelial a moléculas, a MET também causou um aumento da migração de linfócitos-T através de monocamadas de células endoteliais após 30 min e 2 h. Mais ainda, verificámos que a MET aumentou significativamente a activação da sintetase do óxido nítrico endotelial (eNOS) após 30 min. Concluímos também que o pré-tratamento das CEMVC com um inibidor da NOS, L-NG-Nitroarginina metil ester (L-NAME), preveniu o aumento

de permeabilidade e migração de linfócitos induzido pela MET. Em conjunto, estes resultados mostram que a MET compromete tanto a permeabilidade das células endoteliais a moléculas através da promoção da transcitose, como a função de imunidade através do aumento da migração de linfócitos. Para além disso, o óxido nítrico derivado da activação da eNOS parece ser um mediador chave na resposta da BHE à MET.

Abstract

Methamphetamine (METH) is a psychostimulant drug of abuse highly addictive. METH is widely abused for its ability to increase wakefulness and physical activity and decrease appetite. This drug of abuse is neurotoxic and causes irreversible damage of brain cells leading to neurological and psychiatric abnormalities. Recent studies demonstrated that METH has the ability to induce blood-brain barrier (BBB) dysfunction. Due to the crucial role of BBB in maintaining brain homeostasis and protecting the brain from toxic substances and pathogenic organisms, its dysfunction can have severe consequences. Thus, METH-induced BBB disruption has emerged as another mechanism by which METH induces its neurotoxic effects. To better understand the cellular mechanisms underlying METH-induced BBB dysfunction, young adult mice were administered with an acute high dose of METH (30 mg/kg), representing an acute intoxication model, and the effects on BBB permeability were assessed after 1 h, 24 h or 72 h post-METH injection in different brain regions. We observed that METH increased BBB permeability, but this effect was detected only at 24 h after administration and only in the hippocampus, showing that this was a transitory effect and that the hippocampus was the most susceptible brain region to METH, comparing to frontal cortex and striatum. In order to identify the key players in METH-induced BBB dysfunction, potential alterations in tight junction (TJ) proteins and matrix metalloproteinase-9 (MMP-9) were analysed. We observed that METH decreased the protein levels of zonula occludens (ZO)-1, claudin-5 and occludin in the hippocampus at 24 h post-injection, and increased the activity and immunoreactivity of MMP-9.

The pre-treatment with BB-94 (30 mg/kg), a MMP inhibitor, prevented METH-induced increase in MMP-9 immunoreactivity and Evans blue leakage in the hippocampus. Overall, these results demonstrate that METH transiently increases the BBB permeability in the hippocampus, which seems to be caused by alterations on TJ proteins and MMP-9.

To investigate the direct effects of METH in the BBB, primary rat brain microvascular endothelial cells (BMVECs) were exposed to 1 μM METH, a concentration physiologically relevant, i.e. found in the plasma of METH abusers. The macromolecular flux of 4, 70 and 250 kDa dextrans across the EC monolayers doubled in response to METH, irrespective of the tracer size. Interestingly, the increase in the permeability occurred without changes in the transendothelial electrical resistance and in the junctional distribution of the adherens or tight junction proteins, namely vascular endothelial-cadherin, occludin, claudin-5 and ZO-1. In addition, METH exposure increased the vesicular uptake of horseradish peroxidase, showing that METH promoted vesicular but not junctional transport in primary rat BMVECs. Besides the effect of METH on endothelial permeability to molecules, METH also enhanced the migration of T-lymphocytes across EC monolayers after 30 min or 2 h. We also found that METH significantly increased the activation of endothelial nitric oxide synthase (eNOS) within 30 min in BMVECs. In addition, the pre-treatment of BMVECs with the NOS inhibitor L-NG-Nitroarginine methyl ester (L-NAME) prevented METH-induced permeability and lymphocyte migration. Taken together, these results indicate that METH compromises not only the permeability function of endothelial cells to molecules by promoting transcytosis, but also the immune function by increasing

lymphocyte migration. Moreover, eNOS-derived nitric oxide seems to be a key mediator of BBB in response to METH.

Chapter 1

General Introduction

1.1. Methamphetamine (METH)

Methamphetamine (METH) is a member of the Amphetamine (AMPH) family, a group of synthetic psychomotor stimulants. The AMPH-type substances (ATS) comprise the AMPH-group (AMPH, METH and non-specified AMPH) and the ecstasy-group substances [3,4-methylenedioxymethamphetamine (MDMA) and its analogues]. METH is the most widely manufactured ATS worldwide. The United Nations Office on Drugs and Crime estimates that, in 2009, between 13.7 and 56.4 million people used AMPH-group substances at least once in the preceding year, with a corresponding annual prevalence range of 0.3% to 1.3% of the population aged 15 to 64 (UNODC, 2011). METH consumption is particularly common in East/South-East Asia, Oceania, North America and Central Europe (namely, Czech Republic and Slovakia). METH is available in diverse forms and varies in purity, so it can be found in powder, tablet, paste or crystalline form. Typical street names for METH are "crystal", "meth", "speed", "crank", and "ice", among others. The drug can be taken orally, snorted, injected intravenously or smoked. At relatively low doses, the acute effects of METH include feelings of euphoria, well-being, alertness, positive mood, behavioural disinhibition, short-term improvement in cognitive domains, increased libido and reduced appetite. Higher doses of METH may induce acute effects such as anxiety, paranoia, hallucinations, aggression, insomnia, tachycardia, hypertension and hyperthermia (Cruickshank and Dyer, 2009; Hart et al., 2001; Nordahl et al., 2003). The long-term use of METH may lead to non-ischemic cardiomyopathy, congestive heart failure, pulmonary hypertension, cognitive impairment, and lasting psychosis (Schep et al., 2010).

Although METH can be abused, its oral forms are also used for therapeutic purposes. Oral METH (Desoxyn, OVATION Pharmaceuticals) is approved in the United States of America for the treatment of attention-deficit hyperactivity disorder in children and for the short-term treatment of obesity (Kish, 2008).

1.1.1. Physico-chemical properties

METH is part of a class of sympathomimetic drugs denominated phenylethylamines, which consist of an aromatic ring with a two-carbon side chain leading to a terminal amine group (phenylethylamine structure), with attached groups to the amine, the carbons or on the aromatic ring. METH possesses a methyl derivative on the alpha carbon of the ethylamine side chain and also an additional methyl derivative on the amine (Fig. 1.1) (Schep et al., 2010). METH is a small molecule (molecular weight of 149.24), and has a relatively high lipophilicity (Schep et al., 2010). There are two isomeric forms of METH: (+)-methamphetamine and (–)-methamphetamine (Fig. 1.1) and their pharmacological profiles are distinct. The former enantiomer is the dominant stimulant of central nervous system (CNS) and is five times more biologically active than the (–) enantiomer (Cho, 1990), which has greater peripheral sympathomimetic activity.

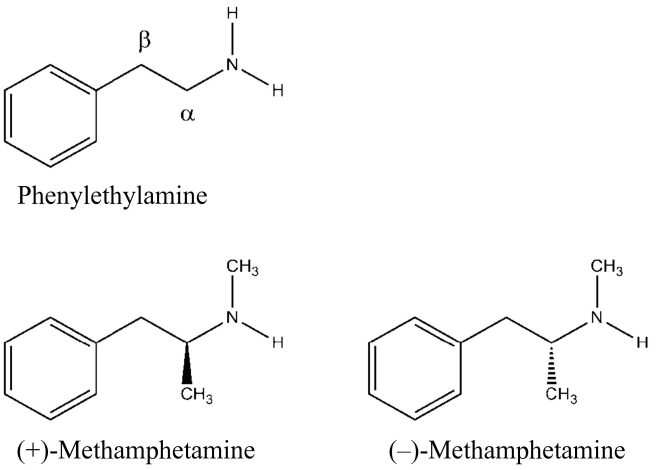

Fig. 1.1. Chemical structure of phenylethylamine and the stereoisomers of methamphetamine (adapted from Schep et al., 2010).

1.1.2. Pharmacokinetics

METH metabolism occurs predominantly in the liver, mainly involving the cytochrome isoenzyme, CYP2D6. In humans, the major metabolic pathways are: (i) aromatic hydroxylation, producing 4-hydroxymethamphetamine, and (ii) N-demethylation to produce AMPH; other minor metabolic pathways include (iii) β-hydroxylation to produce norephedrine; (iv) oxidative deamination, producing benzyl methyl ketoxime; and (v) side chain oxidation to produce benzoic acid (Fig. 1.2) (Caldwell et al., 1972; Cruickshank and Dyer, 2009; Lin et al., 1997; Schep et al., 2010). Thus, in humans, the major metabolites produced are 4-hydroxymethamphetamine and AMPH. The metabolites of METH are unlikely to contribute significantly to clinical effects. In fact, the plasma levels of AMPH arising from the metabolism of 30 mg METH is

substantially lower than that of the ingested drug, with peak occurring after 12 hours, at which time acute effects are minimal (Cook et al., 1993).

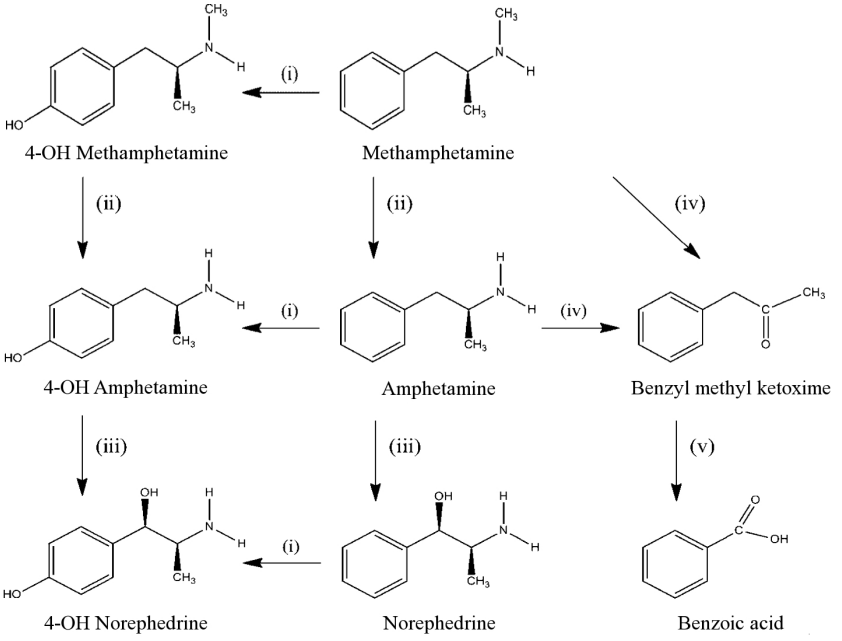

Fig. 1.2. Metabolic pathways of methamphetamine. (i) Aromatic hydroxylation, (ii) N-demethylation, (iii) β-hydroxylation, (iv) oxidative deamination, and (v) side chain oxidation (adapted from Schep et al., 2010).

1.1.3. Molecular pharmacology

The small molecular size and the lipophilic property of METH enable a rapid and extensive transport across the blood-brain barrier (BBB) by passive diffusion. Due to chemical structure similarity, METH is an indirect agonist at dopamine (DA), noradrenaline (NE) and serotonin (5-HT) receptors, causing the release of these monoamine neurotransmitters

(Fig. 1.3). Thus, METH substitutes for monoamines at membrane-bound transporters, namely the DA transporter (DAT), NE transporter (NET), serotonin transporter (SERT) and vesicular monoamine transporter-2 (VMAT-2) (Cruickshank and Dyer, 2009).

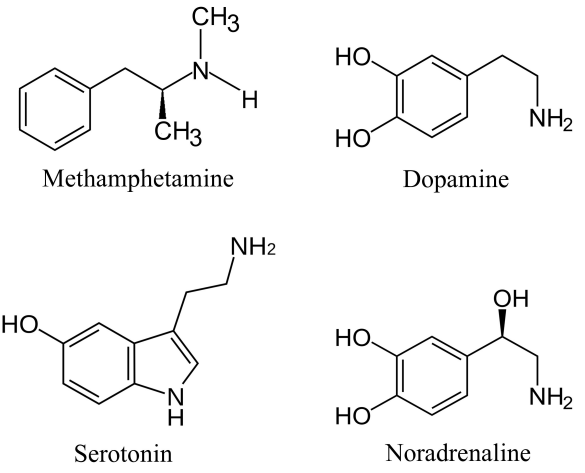

Fig. 1.3. Chemical structures of methamphetamine and the neurotransmitters dopamine, serotonin and noradrenaline.

METH exerts multiple pharmacological effects *via* different molecular processes (Fig. 1.4). METH enters the presynaptic terminals by passive diffusion across the lipid membrane and through the DAT, NET and SERT (Schep et al., 2010; Sulzer et al., 2005). Within the cytosol, METH enters the presynaptic vesicle through VMAT-2, leading to the redistribution of the monoamines into the cytosol by reversing the function of VMAT-2 and disrupting the pH gradient, which is essential for the accumulation of the monoamines into the vesicles (Cruickshank and

Dyer, 2009; Sulzer et al., 2005). The increase in the levels of DA, NE and 5-HT in the cytosol leads in turn to the reverse function of DAT, NET and SERT, resulting in the release of monoamines from the cytosol into synapses (Fischer and Cho, 1979). The elevated concentrations of monoamines within the synapse compete with, and are partially blocked, by METH for reuptake through the transporters, thus promoting prolonged neuronal activity (Schmitz et al., 2001). In addition, METH also decreases the expression of catecholamine transporters at the cell surface, increases the activity and expression of the DA-synthesizing enzyme, tyrosine hydroxylase, and inhibits the activity of monoamine oxidase, attenuating monoamine metabolism (Barr et al., 2006; Cruickshank and Dyer, 2009; Schep et al., 2010; Sulzer et al., 2005). With these combined mechanisms, METH acts as a highly potent releaser of monoamines, mainly DA, from the sympathetic nerve terminals. Major CNS dopaminergic (DAergic) circuits include the mesolimbic, mesocortical, and nigrostriatal pathways, which are responsible for the emotional motivation responses, reward systems, and motor control (Wise, 2004). Noradrenergic (NEergic) regions of particular interest include the hippocampus, involved in memory consolidation, the prefrontal cortex, which processes cognitive functions, and the medial basal forebrain, which mediates arousal (Berridge and Waterhouse, 2003). The serotonergic (5-HTergic) neurons are involved in the regulation of several functions, like reward, impulsiveness, sexual behaviour, higher cognitive functions, anxiety, pain perception, hyperthermia and respiration (Hornung, 2003).

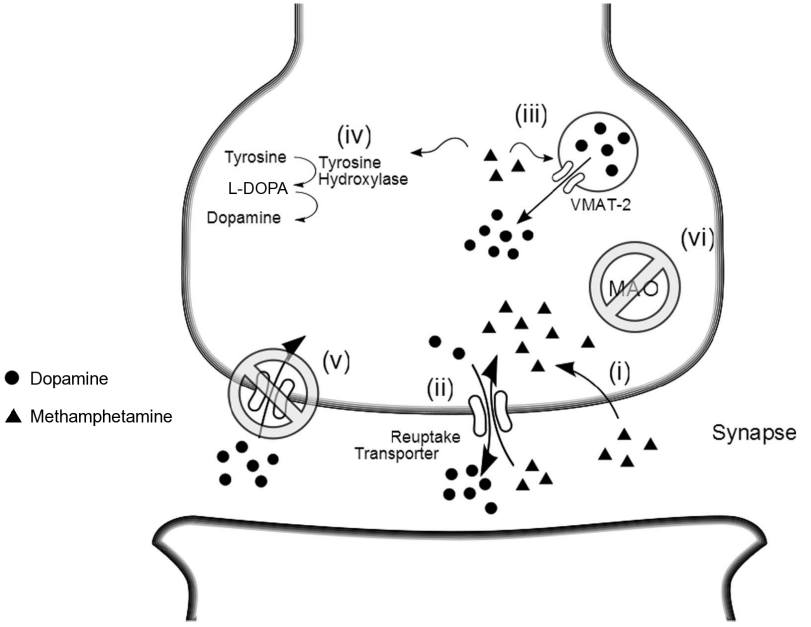

Fig. 1.4. Mechanisms through which methamphetamine (METH) increases dopamine (DA) and other catecholamines release from neuronal terminals into the synapse. (i) METH enters the cell by passive diffusion or (ii) *via* membrane-bound DA reuptake transporters. (iii) METH causes the redistribution of DA from presynaptic vesicles into the neuronal cytosol and (iv) promotes the activity and expression of tyrosine hydroxylase, thereby contributing to elevated DA concentrations within the cytosol, (ii) leading to increased movement into the synapse *via* the DA transporter. METH also prolongs monoamine neuronal activities by (v) blocking their presynaptic reuptake, decreasing the expression of transporters at the cell surface and (vi) inhibiting monoamine oxidase activity. Abbreviations: L-DOPA, L-3,4-dihydroxyphenylalanine; MAO, monoamine oxidase; VMAT-2, vesicular monoamine transporter-2 (adapted from Schep et al., 2010).

1.1.4. Neurotoxicity of METH

It is well documented that METH produces long-term damage to DAergic and 5-HTergic nerve terminals, such as impairment in the enzyme activity, monoamine content, and monoamine transporters (Hotchkiss et al., 1979; Wagner et al., 1980). METH produces long-term decreases in the activity of tyrosine and tryptophan hydroxylases (DA and 5-HT-synthesising enzymes, respectively) (Hotchkiss and Gibb, 1980). Moreover, studies have shown that METH induces long-lasting depletions in DA and its metabolites, and DA reuptake sites in the striatum, but not in other DA rich areas such as the nucleus accumbens and the prefrontal cortex (Eisch and Marshall, 1998; Finnegan et al., 1982; Quinton and Yamamoto, 2006; Seiden et al., 1976; Wagner et al., 1980). In contrast, METH neurotoxicity to 5-HTergic terminals occurred in several brain areas, including prefrontal cortex, striatum and hippocampus (Green et al., 1992; Ricaurte et al., 1980). Several evidences suggest that METH-induced neurotoxicity involves the production of reactive oxygen species (ROS) and reactive nitrogen species (RNS), leading to oxidative stress (Quinton and Yamamoto, 2006). METH also induces brain hyperthermia, which contributes for the toxicity to the DAergic and 5-HTergic terminals (Kiyatkin, 2005). In addition, there are also pieces of evidence showing axonal degeneration after METH administration (Eisch et al., 1998; O'Dell and Marshall, 2005; Ricaurte et al., 1982), as well as an increase in the reactivity of astrocytes (Miller and O'Callaghan, 1994; Pu et al., 1994; Simões et al., 2007), and microglial activation (Sekine et al., 2008; Thomas et al., 2004). The excitotoxicity resultant from the increase in the extracellular levels of glutamate (Glu) induced by METH has also been

implicated in the neurotoxicity of this drug of abuse (Stephans and Yamamoto, 1994). Moreover, alterations in energy metabolism *via* mitochondrial function impairment have been suggested to mediate METH-induced neurotoxicity (Brown et al., 2005).

1.1.4.1. Oxidative stress

The production of free radicals and the consequent oxidative stress has been pointed as one of the most important causes of METH-induced toxicity. This is based on the facts that METH administration leads to the production of ROS, RNS and lipid peroxidation products; besides, the administration of antioxidants and free radical scavengers attenuates the neurotoxic effects induced by METH (Fukami et al., 2004; Quinton and Yamamoto, 2006; Wagner et al., 1986; Yamamoto et al., 2010). Furthermore, METH decreases the levels of endogenous antioxidants in DAergic and 5-THergic terminals (Jayanthi et al., 1998), and oxidative stress has also been reported in METH users (Fitzmaurice et al., 2006; Mirecki et al., 2004). The excessive intracellular DA concentrations, resulting from METH-mediated disruption of vesicular proton gradient and vesicular monoamine transport function (Fleckenstein et al., 2007), can be oxidized enzymatically and nonenzymatically, leading to the formation of reactive dopamine quinones and ROS, thus increasing the oxidative stress (Fig. 1.5) (Hanson et al., 2004; Michel and Hefti, 1990; Wrona et al., 1997). Also, the generation of the highly reactive hydroxyl radicals has been reported in rats (Fleckenstein et al., 1997; Giovanni et al., 1995) and mice (Imam et al., 2001) administered with METH, demonstrating that METH can increase the formation of free radicals in the brain. This drug

of abuse also increases the formation of lipid peroxidation products and protein oxidation in the striatum of rats (Acikgoz et al., 1998; Gluck et al., 2001; Yamamoto and Zhu, 1998) and in the striatum and hippocampus of mice (Gluck et al., 2001). The neurotoxicity induced by METH can also be caused by the production of RNS. In fact, METH increases the levels of striatal nitrotyrosine in rodents, an indirect index of nitric oxide (NO) synthesis (Quinton and Yamamoto, 2006; Zhu et al., 2009). NO can react with superoxide resulting in the formation of the oxidant peroxynitrite (Pacher et al., 2007; Radi et al., 1991), which in turn induces the nitration of tyrosine residues on various proteins. Moreover, the inhibition of nitric oxide synthase (NOS) by 7-nitroindazole and the peroxynitrite decomposition catalyst FeTPPS attenuates METH-induced toxicity in the mouse striatum (Imam et al., 2000; Itzhak and Ali, 1996). The increase in NO and peroxynitrite induced by METH can potentiate the nitration of tyrosine residues on various proteins, such as tyrosine or tryptophan hydroxylase or monoamine transporters, which are crucial to the correct function of DAergic or 5-HTergic terminals (Eyerman and Yamamoto, 2007; Kuhn et al., 1999; Kuhn and Arthur, 1997; Kuhn and Geddes, 1999; Kuhn et al., 2002). In fact, it was shown that METH administration induces a rapid nitrosylation of VMAT-2 and a decrease in striatal VMAT-2 protein levels, and these effects are blocked or attenuated, respectively, by the pre-treatment with S-methyl-L-thiocitrulline, a neuronal NOS inhibitor (Eyerman and Yamamoto, 2007). So, it is well established that protein oxidation and nitration, as well as lipid peroxidation play an important role in the toxicity of METH to DAergic or 5-HTergic terminals.

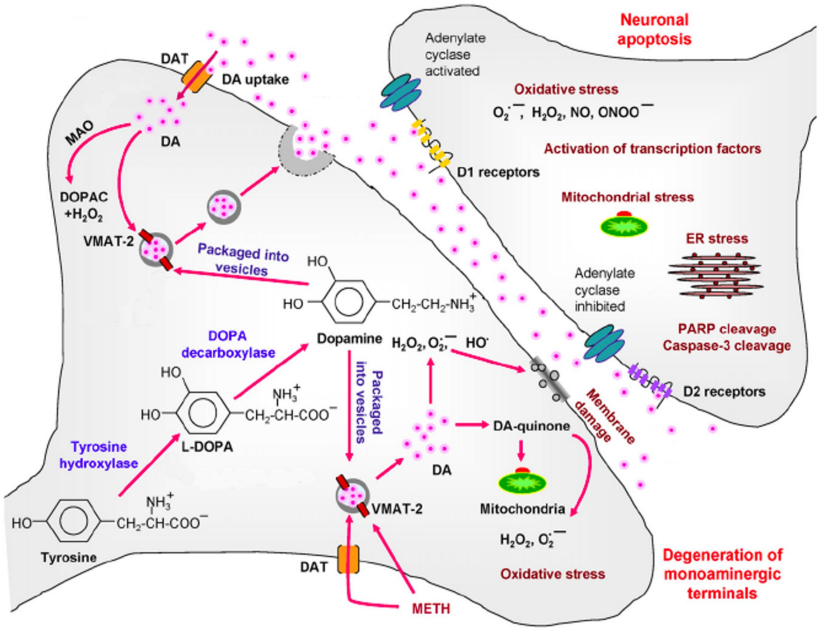

Fig. 1.5. Mechanisms involved in methamphetamine (METH)-induced dopaminergic terminal degeneration and neuronal apoptosis within the striatum. After dopamine (DA) release into the cytoplasm by METH, DA rapidly auto-oxidizes to form potentially toxic substances, such as DA quinones, superoxide radicals, hydroxyl radicals and hydrogen peroxide. The increased production of reactive oxygen species can damage lipids, proteins, mitochondrial and nuclear DNA, causing the dysfunction of cellular organelles, which can lead to terminal degeneration and neuronal apoptosis. Abbreviations: DAT, dopamine transporter; DOPAC, 3,4-dihydroxyphenylacetic acid; L-DOPA, L-3,4-dihydroxyphenylalanine; ER, endoplasmic reticulum; MAO, monoamine oxidase; PARP, Poly (ADP-ribose) polymerase; VMAT-2, vesicular monoamine transporter-2 (adapted from Krasnova and Cadet, 2009).

1.1.4.2. Excitotoxicity

The excitotoxicity resultant from the increase in the extracellular levels of Glu has also been implicated in METH-induced neurotoxicity. The excessive extracellular Glu can lead to the overactivation of ionotropic Glu receptors [N-methyl-D-aspartate (NMDA), α-amino-3-hydroxy-5-methyl-4-isoxazolepropionic acid receptor (AMPA) and kainate receptors (KA)], and group I metabotropic Glu receptors (mGluR1 and mGluR5), resulting in the increase of neuronal cytosolic calcium ion (Ca^{2+}). The increased Ca^{2+} levels can lead to the activation of several kinases, proteases, and lipases, resulting in the breakdown of cytoskeletal proteins, generation of free radicals, and DNA damage, that ultimately can culminate in neuronal death (Arundine and Tymianski, 2003; Sattler and Tymianski, 2000). In fact, METH administration leads to the increase in the extracellular levels of Glu in the striatum and hippocampus (Mark et al., 2004; Rocher and Gardier, 2001; Stephans and Yamamoto, 1994). Besides, it was shown that the blockade of NMDA Glu receptor attenuated the toxicity to DAergic terminals induced by METH (Sonsalla et al., 1989), and the blockade of mGluR5 attenuated the DA depletions induced by METH, effect that was proven to be independent of the hyperthermic effects of the drug (Battaglia et al., 2002). Moreover, METH increases calpain-mediated spectrin proteolysis, a cytoskeletal protein, and this effect is blocked by an antagonist of AMPA receptors (Staszewski and Yamamoto, 2006).

The increase of intracellular Ca^{2+} levels resulting from the excessive extracellular Glu, can lead to the formation of ROS and to the increase of NO levels *via* NOS activation, resulting in RNS formation (Kahlert et al.,

2005; Schmidt et al., 1996). This increase in ROS and RNS can in turn aggravate the neurotoxic effects of METH.

1.1.4.3. Hyperthermia

Brain hyperthermia can occur at normal environment temperatures during metabolic neural activation, which is triggered by environmental stimuli, and maintained within physiological limits by a compensatory increase in heat dissipation to the external environment. However, sometimes it may rise to pathological levels (Kiyatkin, 2005). It has been extensively described that METH induces hyperthermia, and metabolic neural activation seems to be the primary factor for the intra-brain heat production (Brown et al., 2003). Prevention of hyperthermia blocked the long-term toxicity of METH and prevented ROS formation (Bowyer et al., 1994; Bowyer et al., 1992; Fleckenstein et al., 1997; LaVoie and Hastings, 1999; Miller and O'Callaghan, 1994). The increase of brain temperature triggered by METH seems to be also correlated with BBB disruption, intra-brain water accumulation and shifts in brain ionic homeostasis (Kiyatkin et al., 2007; Sharma and Kiyatkin, 2009). Nevertheless, other studies demonstrated that some effects of METH are dissociated from hyperthermia. For instance, prevention of hyperthermia did not reverse METH-induced mitochondrial inhibition (Brown et al., 2005). Moreover, inhibition of neuronal NOS protected against METH-induced neurotoxicity without affecting the hyperthermic response subsequent to METH (Itzhak et al., 2000; Sanchez et al., 2003). Also, potentiation of the toxic effect of METH on DA neurons and protective effects of DA uptake inhibition were independent of increased temperature (Callahan et al.,

2001). METH induces DA and tyrosine hydroxylase depletions in hypothermic mice, and the blocking of METH neurotoxicity by phenobarbital and diazepam occurred without altering the hypothermic profile (Bowyer et al., 2001). Additionally, METH-induced damage to DA and 5-TH terminals, apoptotic cell death, and reactive gliosis are attenuated in interleukin-6 (IL-6) knockout (KO) mice, but animals still develop hyperthermia in response to METH (Ladenheim et al., 2000). Similarly, KO mice partially deficient of c-Jun are protected against METH-induced neuronal apoptosis, which was not dependent on thermoregulation (Deng et al., 2002b). These studies demonstrate that brain hyperthermia *per se* is not the only cause of METH-induced toxicity. Although high temperature has deleterious effects on neural, glial and endothelial cells, it is also an integral physiological index of METH-induced metabolic activation (Kiyatkin, 2005), which manifests by an enhancement in oxidative stress (Seiden and Sabol, 1996), as well as an increase in arterial blood pressure and heart rate (Arora et al., 2001; Yoshida et al., 1993).

1.1.4.4. Mitochondrial dysfunction

Functional mitochondria are responsible for the maintenance of normal cell bioenergetics. Besides the generation of cellular adenosine triphosphate (ATP), these organelles also perform critical functions like hosting essential biosynthetic pathways, Ca^{2+} buffering and apoptotic signalling (Tata and Yamamoto, 2007). Mitochondrial dysfunction has also been pointed as another mechanism by which METH induces its neurotoxic effects. METH is a cationic lipophilic molecule, and so it can diffuse into and be retained by mitochondria, which can lead eventually to the dissipation of

the electrochemical gradient and to the inhibition of ATP synthesis, causing energy deficiency and subsequent mitochondrial dysfunction (Davidson et al., 2001; Krasnova and Cadet, 2009). Neurotoxic doses of METH cause striatal ATP loss that precedes the long-term DA depletions in tissue (Chan et al., 1994). Also, METH was shown to decrease the activity of complex I (Thrash et al., 2010), complex II (Brown et al., 2005) and complex IV of the mitochondrial electron transport chain, which is associated with a reduction on ATP stores in the brain (Burrows et al., 2000). In neuroblastoma cells, METH exposure induces a decrease in mitochondrial membrane potential, an increase of ROS production, and disturbances in mitochondrial biogenesis (Wu et al., 2007). In addition to the involvement of mitochondrial dysfunction in METH-induced terminal degeneration, drug-related neuronal apoptosis also involves mitochondria-dependent death pathways (Deng et al., 2002a; Jayanthi et al., 2001; Jayanthi et al., 2004). The release of an essential cofactor of the complex IV, the cytochrome c, from dysfunctional mitochondria acts as a pro-apoptotic factor. In fact, METH-induced cell death involves a cascade, which is initiated by the cytochrome c release from mitochondria followed by activation of caspases-3 and -9 (Deng et al., 2002a). METH also causes an increase in pro-apoptotic proteins, Bax, Bad and Bid, and a decrease in anti-apoptotic proteins, namely Bcl-2 and Bcl-XL (Deng et al., 2002a; Jayanthi et al., 2001). Such alterations can lead to the formation of channels, resulting in mitochondrial membrane potential loss and releasing of mitochondrial proteins such as cytochrome c and apoptosis-inducing factor (AIF) into the cytosol (Breckenridge and Xue, 2004).

1.1.4.5. Neuroinflammation

Microglia are the resident antigen presenting cells in the CNS, and under conditions of insult or disease become activated and migrate to the sites of injury (Streit, 2002). When activated, these immune-like cells secrete a variety of reactant species, including proinflammatory cytokines, prostaglandins, superoxide, and NO, which can cause injury to the neuronal tissue (Hanisch, 2002; Kreutzberg, 1996). Microglial activation has been detected in the brain of human METH abusers (Sekine et al., 2008). Also, in rodents, METH administration stimulates microglia activation in the striatum (LaVoie et al., 2004; Thomas et al., 2004), cortex and hippocampus (Escubedo et al., 1998; Gonçalves et al., 2010; Kuczenski et al., 2007). The activation of microglia was shown to precede the robust expression of DAergic axonal pathology in the rat striatum after METH administration (LaVoie et al., 2004), and a single high dose of METH induced microglial activation in the mice hippocampus, also accompanied by neuronal dysfunction (Gonçalves et al., 2010). These cells might be involved in METH-induced neurotoxicity *via* increase in the release of cytokines such as IL-1β, IL-6, and tumour necrosis factor-α (TNF-α), which in turn initiate and promote neuroinflammation (Stoll and Jander, 1999; Streit et al., 1999). In fact, mice administered with a single dose of METH showed an increase in mRNA levels of IL-1α, IL-6 and TNF-α in the brain (Gonçalves et al., 2008; Sriram et al., 2006). Additionally, KO mice for IL-6 showed protection against METH-induced toxicity to DAergic and 5-HTergic neurons (Ladenheim et al., 2000), demonstrating the importance of cytokines in mediating METH toxicity. Despite the correlation between microglial response and METH-induced

neurotoxicity, studies using anti-inflammatory drugs to block METH toxicity are controversial. Although the nonsteroidal anti-inflammatory drug ketoprofen was shown to attenuate METH-induced decreases in striatal DAT and microglial activation (Asanuma et al., 2003), other study showed that this drug had no effect in blocking METH-induced decreases in striatal DA content (Thomas and Kuhn, 2005b). Similarly, minocycline was able to attenuate METH-induced microglial activation but failed to block METH-induced increases in TNF-α or striatal DA toxicity (Sriram et al., 2006). Also, the pretreatment with indomethacin prevented METH-induced glia activation, as well as the increase in both TNF-α and TNF receptor 1 protein levels, and the decrease in neuronal-specific class III beta-tubulin protein levels in the hippocampus (Gonçalves et al., 2010).

Astrocytes, the major glial components of the CNS, play an important role in rescuing neurons in the injury area and in clearing up excessive Glu at the synaptic level. However, they can also play a role in the pathogenesis of several CNS diseases (De Keyser et al., 2008), as well as in METH-induced neurotoxicity. Reactive astrocytosis was observed in the striatum, cortex and hippocampus of rats administered with METH (Pubill et al., 2003). Rodents administered with a single high dose of METH also showed an increase in astrocyte reactivity in the hippocampus (Gonçalves et al., 2010; Simões et al., 2007). Overall, astrocytes can mediate METH-induced neurotoxicity through modulation of Glu-mediated excitotoxicity and inflammation. In fact, these cells regulate extracellular concentrations of Glu mainly by uptake of the neurotransmitter, but, upon activation, the intracellular Ca^{2+} levels increase, leading to the release of Glu by astrocytes (Parpura and Haydon, 2000). Under physiological conditions, astrocytes may suppress microglial activation by releasing anti-inflammatory cytokines

(Aloisi, 2001; Vincent et al., 1997). Nevertheless, astrocytes can mediate an increase in inflammation trough the release of chemokines when stimulated by IL-1β and TNF-α (Oh et al., 1999). It is, indeed, the crosstalk between the different brain cells, including glial cells and neurons, that usually determines the death or survival of neurons after an insult.

METH consumption can cause neurotoxicity through the mechanisms mentioned above. Although each of these mechanisms has a clear role in the toxic effects of METH, each process does not occur in isolation. In fact, the neurotoxicity induced by this drug is likely to be mediated by the convergence of oxidative stress, excitotoxicity, hyperthermia, metabolic compromise, and inflammation, among others, which interact with each other leading to brain toxicity.

1.2. Blood-brain barrier (BBB)

The homeostasis of the neural microenvironment is regulated and maintained by barrier layers localised at three main interfaces between blood and neural tissue or its fluid spaces (Fig. 1.6). In the CNS of mamals, the microvascular endothelial cells form the blood-brain barrier (BBB), which constitutes the primary interface for the exchanges between the blood and the brain (Abbott, 2005). The blood-cerebrospinal fluid barrier (BCSFB) is created by the epithelial cells of the choroid plexus facing the cerebrospinal fluid (CSF), providing a second interface (Abbott et al., 2006). Although the choroid plexus epithelium contributes to the regulation of brain homeostasis, the endothelium plays a major role in this process due to its large surface area (between 12 and 18 m^2 in human

adult) and short difusion distance between neurons and capillaries (Abbott et al., 2010). The arachnoid epithelium, underlying the dura, forms the third interface, which constitutes an effective seal between the CNS extracellular fluids and that of the rest of the body (Abbott et al., 2010). Due to the avascular nature of the arachnoid epithelium and its relatively small surface area, the arachnoid barrier does not constitute a significant interface for blood-brain exchange (Abbott et al., 2010).

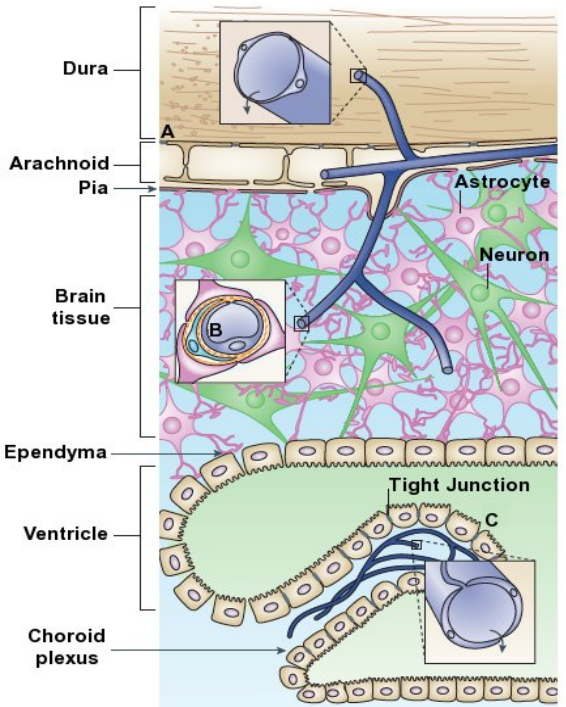

Fig. 1.6. Location of barrier sites in the brain. The barriers in the brain localise at three main sites: (A) the arachnoid epithelium, that forms the middle layer of the meninges, (B) the brain endothelium forming the blood-brain barrier, and (C) the choroid plexus epithelium, which secretes cerebrospinal fluid (CSF) and forms the blood-CSF barrier. At each interface, the tight junctions between cells provide a physical barrier, reducing flux *via* the paracellular pathway (adapted from Abbott et al., 2006).

1.2.1. Functions of the BBB

The barrier function results from the combination of: (1) physical barrier, due to complex tight junctions (TJs) between adjacent endothelial cells (ECs) that limit the paracellular flux; (2) transport barrier, due to the existence of specific transport systems that regulate the transcellular traffic of solutes; and (3) metabolic barrier, given by the presence of extracellular and intracellular enzymes responsible for metabolizing molecules in transit (Abbott et al., 2010; Abbott et al., 2006).

The BBB plays several important roles. It supplies the brain with essential nutrients, mediates the efflux of several waste products, and protects the brain from neurotoxins circulating in the blood (Abbott et al., 2010; Abbott et al., 2006). The BBB also provides a combination of specific ion channels and transporters that keeps the ionic composition of the interstitial fluid optimal for neuronal function, protecting, thus, the brain from fluctuations in ionic composition that can occur following exercise or a meal, or resulting from several pathological conditions, which would disturb the synaptic signalling function (Abbott, 2005). The BBB also helps separating the CNS and peripheral nervous system transmitter pools, minimising potential "crosstalk" between neurotransmitters used centrally and peripherally (Abbott, 2005; Abbott et al., 2010; Bernacki et al., 2008). So, the proper function of the BBB is crucial for the optimal neuronal function.

1.2.2. Neurovascular unit

The endothelium represents the effective physical, biochemical, and metabolic barrier between the blood and the brain. However, its specialized phenotype is dependent on interactions between the ECs of the microvessels with astrocytes, pericytes, neurons, microglia, and the extracellular matrix of the basal lamina (Cardoso et al., 2010; Hawkins and Davis, 2005; Hawkins and Egleton, 2008). Altogether these form the neurovascular unit (Fig. 1.7). The complex interactions within this unit induce, maintain, and regulate the specialized functions of the endothelium.

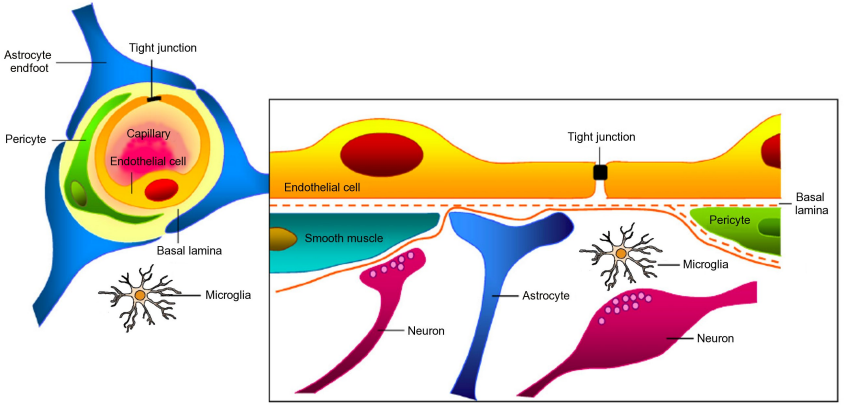

Fig. 1.7. Schematic representation of the neurovascular unit composed of endothelial cells, basement membrane, astrocytes, pericytes, neurons and microglia (adapted from Abbott et al., 2010).

Endothelial cells (ECs)

The ECs that form the BBB differ from ECs in the rest of the body by (i) the absence of fenestrations that is correlated with more extensive TJs, (ii)

reduced pinocytic vesicular transport and paracellular diffusion of hydrophilic compounds, (iii) a high number of mitochondria, associated with a high metabolic activity, and (iv) the polarized expression of membrane receptors and transporters which are responsible for the active transport of blood-borne nutrients into the brain or the efflux of potentially toxic compounds from brain to blood (Petty and Lo, 2002; Weiss et al., 2009). The hallmark of BBB endothelium is its highly restricted and regulated permeability to plasmatic compounds and ions, characterized by a very high transendothelial electrical resistance (TEER) (Butt et al., 1990; Petty and Lo, 2002; Weiss et al., 2009).

Pericytes

Pericytes embrace the abluminal endothelial surface of almost all arterioles, venules and capillaries, and their association with blood vessels has been suggested to regulate endothelial cell proliferation, survival, migration, differentiation, and vascular branching (Lai and Kuo, 2005; Persidsky et al., 2006). The location of pericytes and the degree of coverage to the vascular endothelium differs between microvessel types, and are correlated with the degree of tightness of the interendothelial junctions (Cardoso et al., 2010). Pericytes have a close physical association with the ECs and communicate with each other through gap junctions, TJs, adhesion plaques and soluble factors (Cardoso et al., 2010). In addition, the rich expression of a contractile protein α-smooth muscle actin in pericytes suggests that they may regulate the blood flow (Lai and Kuo, 2005). Pericytes were shown to induce up-regulation of the BBB function by significantly reducing the paracellular permeability to small molecules in cell monolayers (Dohgu et

al., 2005). In addition, pericytes-derived angiopoetin can induce endothelial expression of occludin, a component of BBB TJs (Hori et al., 2004). Pericytes migrate away from brain microvessels under conditions associated with increased BBB permeability such as hypoxia or brain trauma (Dore-Duffy et al., 2000; Gonul et al., 2002). Also, the lack of pericytes results in endothelial hyperplasia and abnormal vascular morphogenesis (Persidsky et al., 2006). These observations suggest that pericytes have an important role in the induction and maintenance of structural integrity of the BBB.

Astrocytes

Astrocytes communicate with the other neurovascular cells *via* their numerous "foot processes" (Zlokovic, 2008). *In vitro* studies have demonstrated that astrocytes can upregulate many BBB features, leading to tighter TJ (physical barrier), the expression and polarized localization of transporters (transport barrier), and specialized enzyme systems (metabolic barrier) (Abbott et al., 2006). Astrocytes promote the synthesis of proteoglycan, which results in an increase in the charge selectivity of brain microvascular ECs, playing thus an important role in the induction of the BBB functions (Cardoso et al., 2010). In addition, an *in vivo* study showed that the temporary loss of astrocytes in the inferior colliculus resulted in the loss, followed by restoration, of barrier integrity (Willis et al., 2004). Studies demonstrated that the secretion of factors by astrocytes contributes to the barrier properties of brain microvascular ECs by upregulating TJ proteins and decreasing the transendothelial permeability across ECs, thus

showing that astrocytes may modulate the BBB phenotype without being directly involved in the physical BBB properties (Cardoso et al., 2010).

Neurons

The high neural activity and the metabolic needs of nervous tissue require a tight regulation of the microcirculation of the brain. The microvascular endothelium and associated astrocyte endfeet are directly innervated by NEergic, 5-HTergic, cholinergic, and GABAergic neurons, among others (Hawkins and Davis, 2005). Also, chemical lesion of the locus coeruleus, which sends the NEergic projections to the microvasculature, increases the vulnerability of the BBB to acute hypertension (Ben-Menachem et al., 1982). In addition, in Alzheimer's disease, the significant loss of cholinergic innervation of cortical microvessels is associated with impaired cerebrovascular function (Tong and Hamel, 1999). Thus, there is multiple evidence showing that neurons regulate critical aspects of BBB function.

Microglia

Microglia plays critical roles in innate and adaptive immune responses of the CNS. These cells are found in the perivascular space, suggesting that interactions between microglia and ECs can contribute to the BBB properties (Choi and Kim, 2008). On the other hand, microglia are a source of cytotoxic mediators that can induce disruption of TJs (Poritz et al., 2004). Yet, the exact mechanisms how microglia influence the BBB integrity remain unknown.

Extracellular matrix

The extracellular matrix of the basement membrane interacts with the cerebral microvascular endothelium. Brain ECs, astrocytes and pericytes all contribute to the generation and maintenance of the basement membrane that is constituted by three apposed laminas (Cardoso et al., 2010), which are composed of various types of collagen, glycoproteins and proteoglycans (Weiss et al., 2009). The basement membrane not only anchors the ECs in place, but also regulates their functions through signalling molecules on the abluminal surface of the cells (Carvey et al., 2009). In fact, multiple basal lamina proteins, such as matrix metalloproteinases (MMPs) and tissue inhibitor of metalloproteinases (TIMPs), are involved in the dynamic regulation of the BBB in both physiological and inflammatory conditions (Weiss et al., 2009). Besides, the disruption of the extracellular matrix is strongly associated with increased BBB permeability in pathological conditions (Persidsky et al., 2006).

1.2.3. Endothelial cell-cell junctions

Junctional proteins control paracellular permeability, restrain cell migration, inhibit proliferation, and contribute to the maintenance of apical-basal polarity. In the endothelium, junctional complexes comprise tight junctions (TJs) and adherens junctions (AJs), that are linked to intracellular cytoskeletal and signalling partners (Fig. 1.8) (Aghajanian et al., 2008; Dejana et al., 2009; Gonzalez-Mariscal et al., 2008). At the BBB, the disruption of AJs can lead to an increase in the permeability (Abbruscato and Davis, 1999), however, it is primarily the TJs that confer the low

paracellular permeability and high electrical resistance (Romero et al., 2003). The junctions are generally formed by both transmembrane and cytoplasmic components. Transmembrane proteins mediate cell-cell adhesion, while cytoplasmic proteins function as a bridge between the transmembrane proteins and the actin cytoskeleton.

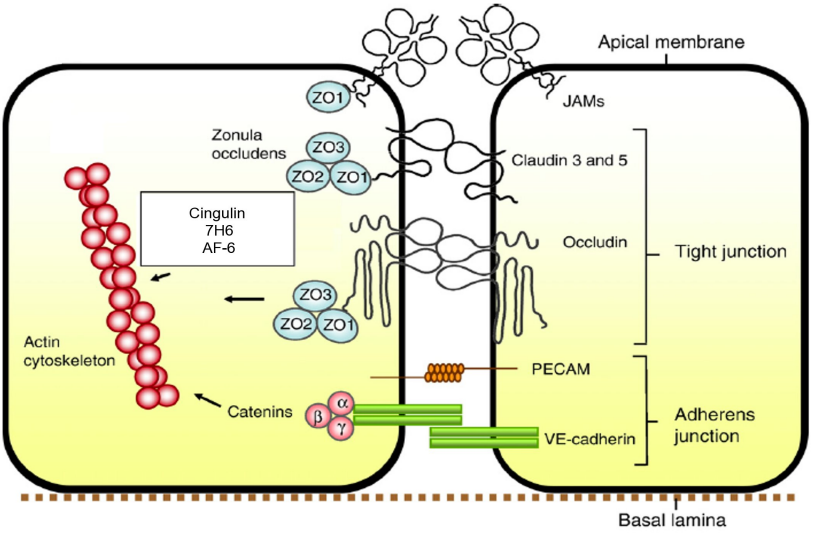

Fig. 1.8. Schematic representation of the junctional complex between adjacent endothelial cells. Abbreviations: JAMs, junctional adhesion molecules; PECAM, platelet/endothelial cell adhesion molecule; VE-cadherin, vascular endothelial cadherin; ZO1, -2, -3, zonula occludens-1, -2, -3 (adapted from Abbott et al., 2010).

1.2.3.1. Tight junctions (TJs)

TJs are well developed in brain vessels, where they play a major role in the function of the physical barrier of BBB, and less organized in other organs, which are characterized by high rate trafficking (Dejana et al., 2009;

Simionescu et al., 1975). TJs are composed by three major transmembrane proteins, namely, occludin, claudins and junction adhesion molecules (JAMs), and by several cytoplasmic accessory proteins including zonula occludens (ZO)-1, ZO-2, ZO-3, and cingulin, among others. Cytoplasmic proteins link the transmembrane proteins to actin, the primary cytoskeleton protein, for the maintenance of structural and functional integrity of the endothelium (Ballabh et al., 2004).

Occludin

Occludin is the first transmembrane protein of TJs that had been identified, and is expressed in both endothelial and epithelial cells (Furuse et al., 1993). Occludin is a 60-65 kDa integral membrane protein with four transmembrane domains, amino- and carboxy-termini in the cytosol and two extracellular loops (Fig. 1.9) (Aijaz et al., 2006; Furuse et al., 1993). The cytoplasmic domain of occludin is directly associated with ZO proteins (Ballabh et al., 2004). Occludin expression is much higher in brain ECs, showing a continuous distribution, when compared to nonneural tissues that display a discontinuous pattern, and seems to contribute to intercellular adhesion and to be involved in the regulation of paracellular permeability (Ballabh et al., 2004; Hirase et al., 1997). Although occludin is a component of the TJs, several studies demonstrated that increased or reduced expression of occludin or expression of occludin mutants do not affect TJ morphology, suggesting that it is not a critical structural component of the TJs (Balda et al., 1996; McCarthy et al., 1996; Saitou et al., 2000; Yu et al., 2005). Accordingly, Saitou and colaborators (2000) showed that occludin deficient mice are viable, and form TJs with no

alterations in the barrier function in intestinal epithelium. However, these mice display several abnormalities, including brain calcification, defects in epithelial differentiation in several tissues, growth retardation, and are unable to reproduce (Saitou et al., 2000).

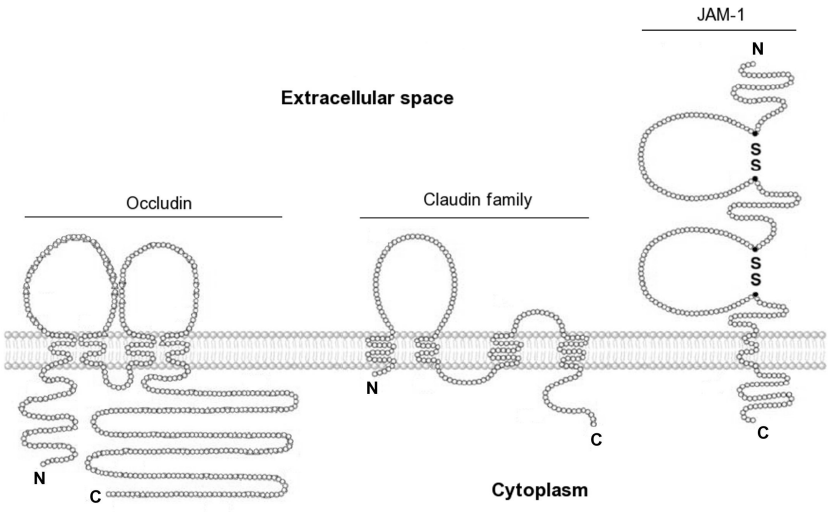

Fig. 1.9. Structure of the transmembrane proteins of the tight junctions. Occludin and claudins have four transmembrane domains, two extracellular loops and a N- and C-terminal cytoplasmic domain. Junctional adhesion molecule 1 (JAM-1) has a single transmembrane domain, and its extracellular portion contains two domains with intrachain disulfide bonds typical of immunoglobulin-like loops of the V-type (adapted from Forster, 2008).

Claudins

Claudins are small transmembrane proteins with a molecular mass around 20-27 kDa, and 24 members of this family have been identified so far (Cardoso et al., 2010). Similar to occludin, claudins possess four transmembrane domains, two extracellular loops, and two cytoplasmic

termini, however, claudins do not show any sequence similarity to occludin (Fig. 1.9) (Furuse et al., 1998a). The homophilic interactions between the extracellular loops of claudins of adjacent ECs form the primary seal of the TJs (Petty and Lo, 2002). The carboxy terminal of claudins binds to cytoplasmic proteins including ZO-1, -2 and -3 (Furuse et al., 1999). Overexpression of claudins in fibroblasts induce cell aggregation and formation of TJ-like strands, and recruit occludin to the strands (Furuse et al., 1998b). In contrast, occludin expression does not result in TJ formation, thus showing that claudins constitute the backbone of TJ strands, while occludin acts as an additional support structure, playing a role in the regulation of permeability by incorporating into the claudin-based strands (Forster, 2008). Claudins are not only important for barrier formation but are also responsible for the selective permeability of the paracellular pathway, showing once again that they are important structural components of the TJs (Furuse et al., 1998b; Tsukita et al., 2001; Van Itallie and Anderson, 2004). The distribution of some claudins is limited, and appears to follow a tissue-specific pattern. Furthermore, the claudin repertoire that is expressed in the cells confers the different size and charge selectivity properties, and the combination of claudin isoforms results in cell- or tissue-type specific barrier function (Forster, 2008). At the BBB, the endothelial cells express claudin-1, -3, -5 and -12 (Hawkins and Davis, 2005; Krause et al., 2008; Lippoldt et al., 2000; Nitta et al., 2003; Persidsky et al., 2006). Claudin-1 and -5 are associated with the maintenance of normal BBB function (Liebner et al., 2000). Also, claudin-5 KO mice exhibited a size-selective loosening of the BBB to molecules smaller than 800 Da (Nitta et al., 2003), showing the importance of claudin-5 in the

regulation of paracellular pathway of BBB. Such mutant mice developed normally but died within 10 h after birth.

Junctional adhesion molecules (JAMs)

JAMs are 40 kDa proteins that belong to the immunoglobulin superfamily, and bind directly to ZO-1 (Ebnet et al., 2000). JAMs have a single transmembrane domain and its extracellular portion has two immunoglobulin-like loops (Fig. 1.9) (Petty and Lo, 2002). Three members of this family have been identified, JAM-1, -2 and -3. JAM-1 and -3 are expressed in the brain blood vessels but not JAM-2 (Aurrand-Lions et al., 2001). JAMs are also expressed in circulating monocytes, neutrophils, lymphocytes subsets, and platelets (Ueno, 2007). This third type of transmembrane TJ proteins is involved in cell-cell adhesion and contributes to the control of permeability and monocyte migration through the BBB (Palmeri et al., 2000; Vorbrodt and Dobrogowska, 2003).

Cytoplasmic accessory proteins

Cytoplasmic proteins involved in TJ formation include ZO-1, -2, -3, cingulin, 7H6, and AF-6, among others. ZO proteins belong to the family of membrane-associated guanylate kinase (MAGUK) proteins, and have sequence similarity with each other (Ballabh et al., 2004). MAGUKs contain three postsynaptic density-95 protein/Drosophila disc large tumor suppressor DlgA/zonula occludens-1 (PSD-95/DlgA/ZO-1; PDZ) domains (PDZ1, PDZ2, and PDZ3), one Src homology 3 (SH3) domain, and one guanylyl kinase-like (GUK) domain (Fig. 1.10), that function as

protein binding domains, playing a role in organizing proteins at the plasma membrane (Funke et al., 2005).

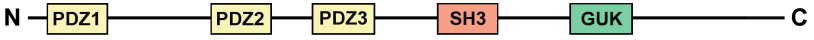

Fig. 1.10. Schematic representation of the molecular structure of zonula occludens proteins. Abbreviations: GUK, guanylyl kinase-like; PDZ, postsynaptic density-95 protein/Drosophila disc large tumor suppressor DlgA/zonula occludens-1; SH3, src homology 3.

ZO-1, a 220 kDa phosphoprotein, was the first component of TJs to be identified (Stevenson et al., 1986). This protein is expressed in endothelial and epithelial cells, as well as in many cell types that do not form TJ, such as astrocytes, cardiac muscle cells, and fibroblasts (Howarth et al., 1992; Itoh et al., 1999b). ZO-1 plays a critical role in the stability and function of the TJs by linking the transmembrane proteins of the TJs to the actin cytoskeleton (Fanning et al., 1998), and the dissociation of ZO-1 from the junctional complex is associated with increased permeability (Abbruscato et al., 2002). In addition, ZO-1 may also act as a signalling molecule by communicating the state of the TJ to the interior of the cell, or vice-versa (Hawkins and Egleton, 2008). Under conditions of proliferation and injury, ZO-1 localizes to the nucleus (Gottardi et al., 1996) where it will interfere with transcription factors (Balda and Matter, 2000). ZO-2 (160 kDa) like ZO-1 binds to transcription factors (Betanzos et al., 2004), localizes to the nucleus during stress and proliferation (Islas et al., 2002; Traweger et al., 2003), and has also been found in non-TJ-containing tissues (Itoh et al., 1999b). ZO-3 (130 kDa) has been found in some TJ-containing tissues

(Inoko et al., 2003), however, while KO mice for ZO-1 and ZO-2 exhibited embryonic lethality, KO mice for ZO-3 were viable, suggesting that ZO-3 is not essential *in vivo* (Katsuno et al., 2008; Xu et al., 2008). ZO proteins bind each other, and specifically, ZO-1 binds ZO-2 or ZO-3, but ZO-2 does not bind ZO-3 (Wittchen et al., 1999). Consequently, the ZO proteins do not form a ZO-1/ZO-2/ZO-3 trimer, but rather independent ZO-1/ZO-2 and ZO-1/ZO-3 dimers (Bazzoni and Dejana, 2004). PDZ1 domain of ZO proteins binds directly to the carboxyl terminal of claudins (Itoh et al., 1999a), while the carboxyl terminal of occludin interacts with the GUK domain in ZO proteins (Furuse et al., 1994; Haskins et al., 1998; Itoh et al., 1999b; Petty and Lo, 2002). JAM also binds directly to ZO-1 and other PDZ-containing proteins (Ebnet et al., 2000). The primary cytoskeletal protein actin binds to the carboxyl terminal of ZO-1 and ZO-2, and this complex cross-links transmembrane elements, thus providing structural support to the ECs (Fanning et al., 1998; Itoh et al., 1999b).

Cingulin is a 140 – 160 kDa phosphoprotein localized at the endothelial and epithelial cytoplasmic surface of TJs that associates with ZO proteins, myosin and AF-6 (Petty and Lo, 2002). Cingulin may function as a scaffold at the TJ cytoplasmic face by linking the submembrane plaque domain of TJs to the cytoskeleton (Cordenonsi et al., 1999). The phosphoprotein 7H6 antigen (155 kDa) is found at both epithelial and endothelial cell TJs and it likely plays a role in the maintenance of paracellular barrier function (Satoh et al., 1996). In response to cellular ATP depletion, 7H6 reversibly dissociates from the TJ complex (Mitic and Anderson, 1998). AF-6, a 180 kDa protein, contains two Ras-associating domains, a PDZ domain, and a myosin V-like domain, and has been reported either at the TJ or at the AJ (Bazzoni and Dejana, 2004; Hawkins and Davis, 2005). Ras activation

inhibits the interaction between AF-6 and ZO-1, indicating that the disruption of the ZO-1/AF-6 complex may be critical in the modulation of TJs *via* pathways that involve Ras (Yamamoto et al., 1997).

1.2.3.2. Adherens junctions (AJs)

AJs are ubiquitously distributed along the vasculature and mediate the adhesion of ECs to each other, the contact inhibition during vascular growth as well as remodelling, initiation of cell polarity, and the regulation, in part, of paracellular permeability (Hawkins and Davis, 2005). AJs are composed of cadherins associated with catenin proteins, forming a complex that mediates cell-cell adhesion through actin filaments linking.

Cadherins

Cadherins are Ca^{2+}-regulated membrane glycoproteins and are the major transmembrane components of AJs. Cadherins contain a plasma membrane-spanning domain and a cytoplasmic domain associated with other molecular components of the junctional complex, such as catenins (Vorbrodt and Dobrogowska, 2003). ECs express a cell-type-specific cadherin, called vascular endothelial cadherin (VE-cadherin), which mediates cell-cell adhesion *via* homophilic interactions between the extracellular domains of proteins expressed in adjacent cells (Vincent et al., 2004). ECs also express neuronal cadherin (N-cadherin), which is present in other cell types such as neural cells and smooth muscle cells (Bazzoni and Dejana, 2004). Other non-cell-type-specific cadherins, such as placental (P)-cadherin and truncated (T)-cadherin, are variably expressed in different types of ECs (Ivanov et al., 2001; Liaw et al., 1990).

Catenins

The cadherin complex is anchored to the actin cytoskeleton by catenins. VE-cadherin is linked through its cytoplasmic tail to the cytoplasmic anchor proteins β-catenin and γ-catenin (plakoglobin). β- and γ-catenin bind in turn to α-catenin, which couples the cadherin-catenin complex to the actin cytoskeleton (Vincent et al., 2004). In addition to the binding to actin filaments, α-catenin also interacts with several actin-binding proteins, including ZO-1 (Weis and Nelson, 2006). The expression of α-catenin was shown to be required for the cell adhesion activity of cadherins (Nagafuchi et al., 1994; Watabe et al., 1994). β-catenin localizes at the cell junctions and in the cell nuclei, which parallels its role in cell-to-cell adhesion, in signal transduction, and in gene expression associated with morphogenetic and histogenetic functions. γ-catenin is closely related to β-catenin and can substitute for it in the cadherin-catenin complex (Vorbrodt and Dobrogowska, 2003). VE-cadherin and the cadherin binding proteins β- and γ-catenin regulate endothelial monolayer permeability and endothelial growth rates (Venkiteswaran et al., 2002). An additional VE-cadherin partner is p120 catenin, which was originally identified as a Src substrate. Unlike β- and γ-catenin, p120 does not appear to link cadherins to the cytoskeleton but, rather, appears to regulate cadherin clustering and the local organization of actin during the assembly of cadherin-based adhesive contacts (Vincent et al., 2004).

1.2.4. Transport across the BBB

The transfer of solutes between the blood and the brain tissue occurs through a limited number of mechanisms at the level of ECs of the BBB (Fig. 1.11), but the materials transferred include substances as small as electrolytes to as large as immune cells.

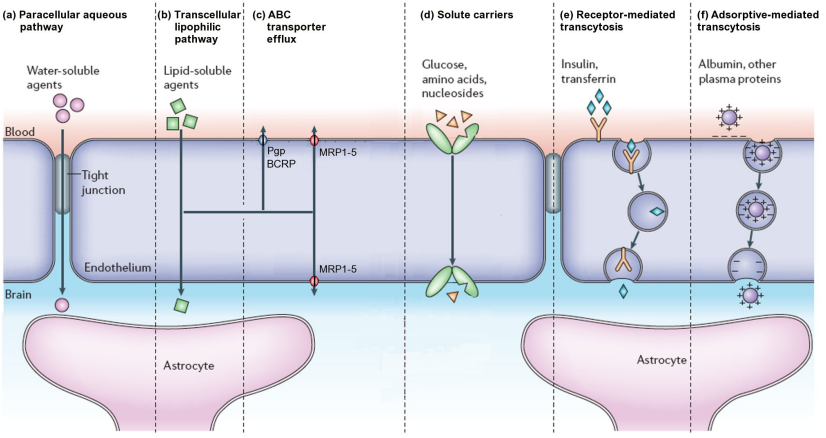

Fig. 1.11. Schematic representation of the transport pathways across the blood-brain barrier. (a) The tight junctions restrict the passage of water-soluble compounds, including polar drugs. (b) Lipid-soluble molecules can diffuse through the lipid membranes of the endothelium. (c) Active efflux carriers (ABC transporters) may intercept some of these lipophilic solutes and pump them out of the endothelial cells. Pgp and BCRP are strategically placed in the luminal membrane of the endothelium, while MRPs 1-5 are inserted into either luminal or abluminal membranes. (d) Carrier-mediated influx *via* solute carriers can transport many essential polar molecules such as glucose, amino acids and nucleosides. (e) Receptor-mediated transcytosis requires receptor binding of ligand and transport a variety of macromolecules such as peptides and proteins across the BBB endothelium, while (f) adsorptive-mediated transcytosis is induced in a non-specific manner by positively charged molecules. Abbreviations: BCRP, Breast Cancer Resistance Protein; MRP 1-5, Multidrug Resistance-associated Proteins 1-5; Pgp, P-glycoprotein (adapted from Abbott et al., 2006).

Passive diffusion

The diffusion of compounds across the BBB is largely determined by the physico-chemical properties of the compounds (e.g., molecular weight, hydrophilicity, lipophilicity, electrical charge, hydrogen bonding potential). The passive transport comprises hydrophilic paracellular and lipophilic transcellular transport (de Boer et al., 2003). Passive hydrophilic transport is dependent on the size and charge of the molecules, and the possibility to form hydrogen bonds, and at the BBB this transport is mainly restricted by the narrow TJs between ECs (de Boer et al., 2003). Passive transcellular transport of a substance across the BBB depends mostly on its lipid solubility. However, other factors that restrict the entry of compounds into the brain by passive transcellular diffusion include a high polar surface area, and a tendency to form more than 6 hydrogen bonds, a factor which greatly increases the free energy requirement of moving from an aqueous phase into the lipid of the cell membrane. The presence of rotatable bonds in the molecule and a molecular mass above 450 Da also appear to restrict the diffusion of the compounds (Abbott et al., 2010; de Boer et al., 2003).

ATP-binding cassette transporters (ABC transporters)

There is a general correlation between the rate at which a compound crosses the BBB and its lipid solubility. However, a large number of solutes and drugs have a much lower CNS entry rate than might be expected considering their lipophilicity. These substances, and many of their metabolites, are actively effluxed from the brain at the BBB endothelium by members of the ATP-binding cassette transporter (ABC transporter) family (Abbott et al., 2010; Begley, 2004). In humans, the ABC superfamily

comprises 48 members, which are grouped into seven major sub-families (from A to G; Begley, 2004).

In the BBB, ABC transporters function as active efflux pumps consuming ATP and transport a diverse range of lipid-soluble compounds out of the brain capillary endothelium and CNS. So, they play a role in removing potentially neurotoxic endogenous or xenobiotic molecules from the brain, having therefore a vital neuroprotective and detoxifying function (Dallas et al., 2006). The multidrug resistance (MDR) transporter P-glycoprotein (P-gp) mediates rapid removal of ingested toxic lipophilic metabolites, and is the best-known MDR protein (Zlokovic, 2008). In addition to P-gp, several multidrug resistance-associated proteins (MRPs) are expressed in brain microvessels, such as the breast cancer resistance protein (BCRP), and both the members of the organic anion transporting polypeptide (OATP) family and the organic anion transporter (OAT) family that mediate mainly the efflux of anionic compounds (Zlokovic, 2008). P-gp and BCRP are expressed in the luminal membrane of the ECs and their function is to transport compounds from endothelium to blood, while other MRP isoforms are expressed in either the luminal or the abluminal membrane, or sometimes both (Roberts et al., 2008). Although the ABC transporters play a crucial role in protecting the brain from neurotoxic compounds, these transporters are also responsible for the limited entry of potential therapeutic drugs to treat CNS diseases.

Carrier mediated transport

Hydrophilic and polar nutrients, such as glucose and amino acids, cannot diffuse through cell membranes, and thus they are actively transported

through the ECs by a variety of membrane transporters, notably the large family of Solute Carriers (SLCs) (Abbott et al., 2010). Some of these SLC proteins are polarised in their expression and are inserted into either the luminal or abluminal membrane, whereas others are inserted into both membranes of the ECs (Abbott et al., 2010). Carrier-mediated transport systems are specific and facilitate the transport of nutrients as follows: hexoses (glucose, galactose); neutral, basic, and acidic amino acids and monocarboxylic acids (lactate, pyruvate, ketone bodies); nucleosides (adenosine, guanosine, uridine); purines (adenine, guanine); amines (choline); and vitamins (Hawkins et al., 2006; Simpson et al., 2007; Zlokovic, 2008). Most of these systems are energized directly by the hydrolysis of ATP or indirectly by coupling to the cotransport of a counterion down its electrochemical gradient (e.g., Na^+, H^+, Cl^-) (Zhang et al., 2002).

Transcytosis

Despite the low levels of pinocytic vesicles present in brain ECs, a range of endocytotic processes do occur at the BBB, and transcytosis across this barrier is the main route by which macromolecules such as proteins and peptides can enter the brain. A variety of large molecules and complexes can thus cross the BBB by specific and non-specific transcytotic mechanisms (Abbott et al., 2010). Transcytosis describes the vectorial movement of molecules within endocytic vesicles across the brain ECs, from the luminal cell side to the abluminal side where exocytosis occurs. BBB ECs contain two kinds of vesicles that are open to the luminal blood capillary space: the caveolae and the clathrin-coated pits/vesicles (Herve et

al., 2008). Fluid-phase transcytosis is a constitutive and non-specific process in which solutes together with extracellular fluid are caught in the lumen of the vesicle that forms at the surface and then enters the cell (Hawkins and Egleton, 2008). This transport process is independent of any interaction between the transported molecules and the vesicle membrane. Solutes that undergo fluid-phase endocytosis at the BBB include horseradish peroxidase (Defazio et al., 1997) and Lucifer yellow (Guillot et al., 1990). While this transcytotic process is the main route for the transendothelial delivery of proteins from blood to underlying tissues in the periphery, in a healthy BBB fluid-phase transcytosis occurs to a very limited degree, due to the low levels of vesicles in brain ECs (Herve et al., 2008).

Adsorptive-mediated transcytosis is a non-specific process that involves molecules such as lectins that bind to carbohydrate moieties on the cell surface, and positively charged (cationized) molecules that bind to negatively charged cell surface components (Ueno, 2007). Solutes that undergo this form of transcytosis include wheat germ agglutinin, basic and cationized peptides, glycoproteins and glycopeptides, and viruses (Hawkins and Egleton, 2008).

Receptor-mediated transcytosis (RMT) is a specific process that implies the binding of a ligand to a cell surface receptor specific for that ligand; the binding then triggers the internalization of the receptor-ligand complex (Ueno, 2007). The receptor-ligand complex cluster together, and a caveolus is formed which pinches off into a vesicle, and then the complex is internalised and exocytosed at the opposite side of the cell. The dissociation of the ligand and receptor probably occurs during cellular transit or during the exocytotic event (Abbott et al., 2010). At the BBB

there are several receptors that can carry ligands into and across the ECs *via* RMT, such as the insulin receptor, the low-density lipoprotein receptor, and the transferrin receptor, the latest being the best characterized receptor system at the BBB (Hawkins and Egleton, 2008).

To achieve transcytosis of an intact protein or peptide, the primary sorting endossomal compartment and its contents need to route away from the lysossomal compartment. Routing away from this degradative compartment appears not to occur in many peripheral endothelia, and may be a specialised feature of the BBB where the intact transcytosis of a significant number of macromolecules becomes a necessity for the correct brain function (Abbott et al., 2010).

1.2.5. Leukocyte migration across the BBB

Leukocyte transendothelial migration (TEM), or diapedesis, occurs during normal physiologic processes such as immune surveillance, antigen recognition, and acute inflammatory responses. The brain acts as an immune privileged organ, and so leukocyte TEM into the brain is low compared to other tissues (Greenwood et al., 2011; Hickey, 1999). This limited diapedesis is mainly regulated by the restricted expression of endothelial cell adhesion molecules (CAMs), which are required for leukocyte capture from the blood. When TEM is excessive or inappropriately localized, it can initiate many pathological processes. For instance, leukocyte TEM is involved in the development of atherosclerotic plaques and in the pathogenesis of multiple sclerosis (Aghajanian et al., 2008). Leukocyte TEM can occur by paracellular diapedesis through the junctions between adjacent ECs, and by transcellular diapedesis through

the body of the EC *via* pore formation (Greenwood et al., 2011; Muller, 2011).

Paracellular TEM

Paracellular TEM involves an elaborate series of rolling, adhesion, and locomotion events to bring the leukocyte close to the endothelial border (Muller, 2003). Clustering of intercellular cell adhesion molecule 1 (ICAM-1) and vascular CAM-1 (VCAM-1) on the EC surface occurs as the leukocyte approaches the EC border (Barreiro et al., 2002; Carman and Springer, 2004). The binding of leukocyte integrin to EC CAMs stimulates signalling in the ECs that further support adhesion and the subsequent process of TEM (Greenwood et al., 2011). Clustering of ICAM-1 stimulates phosphorylation of cortactin, enhancing further actin-induced clustering of ICAM-1. This process leads to the enrichment of ICAM-1 around tightly adherent leukocytes, and ICAM-1 multimerization leads to increases in cytosolic free Ca^{2+} and RhoA activation (Muller, 2011). Clustering of VCAM-1 also stimulates an increase in cytosolic free Ca^{2+}, activation of Rac-1, and production of ROS in ECs (Muller, 2011). The result of these events is the loosening of junctional structures. Signalling of ICAM-1 and VCAM-1 leads to the phosphorylation of VE-cadherin, which dissociates VE-cadherin from its links to the actin cytoskeleton, causing weakness of the endothelial junctions. Also, the increase in cytosolic free Ca^{2+} activates myosin light chain kinase (MLCK), which leads to actin-myosin fiber contraction that is believed to help endothelial cells to contract against weakened junctions, that in turn will promote the paracellular TEM (Hixenbaugh et al., 1997).

The lateral border recycling compartment (LBRC) is an interconnected reticulum of 50-nm vesicle-like structures that resides just beneath the plasma membrane of the EC borders (Mamdouh et al., 2008). In resting ECs, membrane traffics constitutively between the lateral cell border and this compartment, recycling uniformly along the lateral border with a life time of roughly 10 min. However, when a leukocyte transmigrates, membrane from the LBRC is targeted rapidly and extensively to the site of diapedesis to surround the leukocyte (Mamdouh et al., 2003). LBRC contains platelet/endothelial CAM (PECAM), CD99 and JAM-1 proteins (Mamdouh et al., 2003; Mamdouh et al., 2009). These junctional molecules concentrate at EC borders and are required for TEM (Muller, 2011). In addition to the loosening of the junctional structures, the targeted recycling of the LBRC is necessary for efficient paracellular transmigration. During paracellular TEM, the membrane from the interconnected vesicles of the LBRC moves to surround the leukocyte, and the recruitment of the LBRC continues as the leukocyte crosses the EC border (Fig. 1.12) (Muller, 2011).

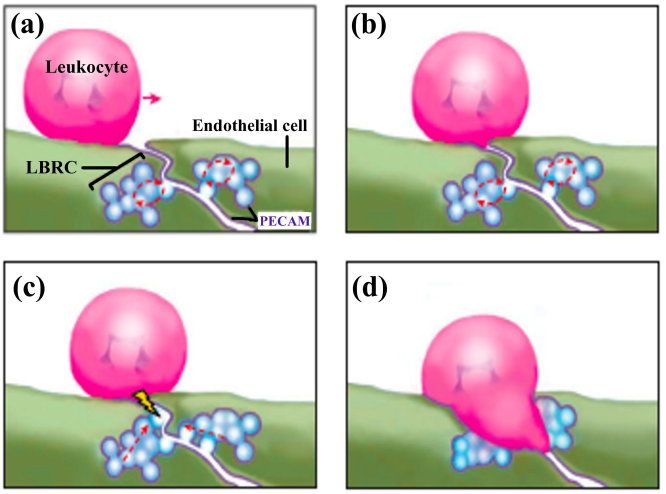

Fig. 1.12. Schematic representation of the movement of the lateral border recycling compartment (LBRC) during paracellular transmigration. (a) Constitutive recycling of the LBRC is ongoing as the leukocyte moves toward the intercellular border. (b) After reaching the luminal side of the endothelial border, leukocyte platelet/endothelial cell adhesion molecule (PECAM) engages endothelial cell PECAM, (c) and this interaction triggers a signal (lightning bolt) that redirects recycling of the LBRC to the site of leukocyte engagement. In cases of PECAM-independent transmigration, some other interaction triggers this signal. (d) Membrane from the interconnected vesicles of the LBRC moves to surround the leukocyte, and the recruitment of the LBRC continues as the leukocyte crosses the endothelial cell border (adapted from Muller, 2011).

Transcellular TEM

Transcellular migration appears to use the same initial steps as paracellular migration, although, for some reason, the leukocytes migrate through the cell body rather than the border. During transcellular TEM, ICAM-1 concentrates at the site of diapedesis and is enriched in the membrane channel that surrounds the crossing leukocyte as it goes through the EC body (Carman et al., 2007; Carman and Springer, 2004; Mamdouh et al.,

2009; Millan et al., 2006; Yang et al., 2005). Other molecules normally considered restricted to the cell borders, such as PECAM, CD99, and JAM-1, are also observed around leukocytes migrating transcellularly (Carman et al., 2007; Mamdouh et al., 2009). These molecules appear to be functional. In fact, by blocking PECAM and CD99 it is possible to prevent transcellular migration, showing that this pathway is dependent on PECAM and CD99 (Mamdouh et al., 2009). Moreover, endothelial vesicles and vesiculo-vacuolar organelles (VVOs) were observed immediately adjacent to the region of transcellular migration (Carman et al., 2007). Caveolin-1 was shown to accumulate in the site of transcellular diapedesis, suggesting that caveolae might be involved in transcellular migration (Millan et al., 2006). However, other studies did not observe any enrichment in caveolin-1 at the site of diapedesis (Carman et al., 2007; Carman and Springer, 2004; Mamdouh et al., 2009). A recent study showed that LBRC is also critical for transcellular migration of leukocytes (Mamdouh et al., 2009). During transcellular TEM, as the leukocyte passes through the EC, LBRC membrane is recruited to surround the leukocyte, forming a transmigration pore lined by molecules that leukocytes need to interact with (PECAM, CD99, and JAM-1) (Fig. 1.13) (Muller, 2011). Although overexpression of ICAM-1 promotes transcellular migration (Yang et al., 2005) and may be a necessary prerequisite, it is not sufficient to promote transmigration in the absence of a functional LBRC (Mamdouh et al., 2009).

The factors that determine the preferred route for TEM are not well understood. However, if the endothelial cell junctions are particularly tight (as in the BBB), or when leukocytes are strongly activated or have difficulty

reaching the cell junctions, transcellular migration tends to occur (Muller, 2011). In inflammatory pathological conditions that can lead to the opening of the TJs, leukocytes may enter by both paracellular and transcellular routes (Abbott et al., 2010).

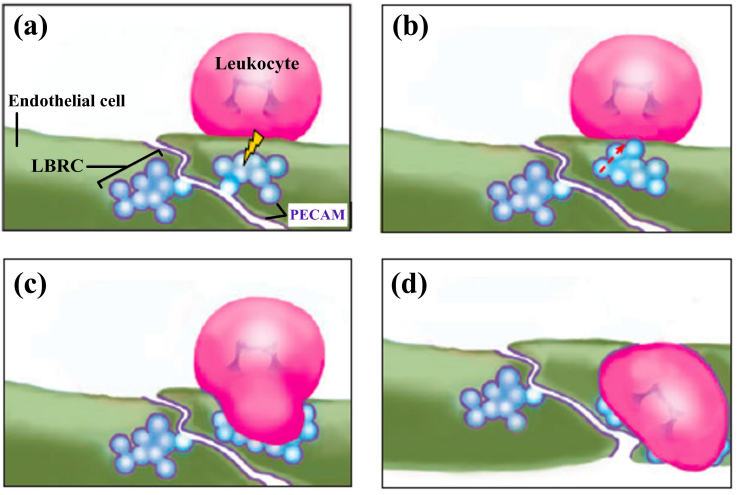

Fig. 1.13. Schematic representation of the movement of the lateral border recycling compartment (LBRC) during transcellular transmigration. (a) During transcellular migration, the signal (lightning bolt) that recruits targeted recycling to the vicinity of the leukocyte is transmitted while the leukocyte is on the luminal surface of the endothelial cell. (b) This process causes targeting of the LBRC membrane along cortical microtubules toward the leukocyte. A single fusion event may be sufficient to allow the entire interconnected LBRC to come in contact with the leukocyte. (c) As the leukocyte passes through the endothelial cell, additional LBRC membrane is recruited to surround the leukocyte, forming thus a transmigration pore lined by molecules that leukocytes need to interact whith [e.g., platelet/endothelial cell adhesion molecule (PECAM), CD99, and junctional adhesion molecule (JAM)-1]. (d) At the basal surface, a second fusion event may be necessary to allow the leukocyte to complete its migration across the endothelial cell (adapted from Muller, 2011).

1.2.6. BBB in pathology

Under physiological conditions, the BBB is relatively impermeable, however, in pathologic conditions, a number of chemical mediators are released, which increase BBB permeability, compromising the barrier function (Ballabh et al., 2004). BBB dysfunction has been claimed to be involved in several CNS pathologies, including hypoxia and ischemia (Kaur and Ling, 2008), infectious or inflammatory processes (Gaillard et al., 2003), multiple sclerosis (Correale and Villa, 2007), Alzheimer's disease and Parkinson's disease (Zlokovic, 2008), epilepsy (Remy and Beck, 2006), brain tumours (Papadopoulos et al., 2004), pain (Huber et al., 2001), and lysosomal storage diseases (Begley et al., 2008). The dysfunction of BBB can range from mild and transient TJ opening to chronic barrier breakdown (Forster, 2008). In addition to TJ disruption, changes in the transport systems and enzymes in BBB ECs can also occur (Abbott et al., 2010). Although BBB disruption is implicated in CNS diseases, in most cases is difficult to determine whether barrier impairment is responsible for the disease onset. Nevertheless, the disruption of BBB has been shown to contribute to and exacerbate developing pathology (Persidsky et al., 2006). A better understanding of the mechanisms underlying BBB dysfunction is important for targeting the brain endothelium to aid recovery from injury and to help in the formulation of therapeutic strategies to prevent or/and treat many CNS diseases.

1.3. Nitric oxide synthase (NOS) and nitric oxide (NO)

Nitric oxide (NO) is a signalling molecule that regulates several physiological processes, such as vascular functions (angiogenesis, blood flow, vascular permeability, leukocyte-endothelial interaction, platelet aggregation and microlymphatic flow) and neurological functions (neurotransmission and development of the nervous system). On the other hand, NO can also be involved in cytotoxic functions (cytostasis and cytolisis) (Fukumura et al., 2006). NO and its metabolites, such as peroxynitrite, nitrate, nitrite, nitrosamines and S-nitrosothiols, mediate many of the cytotoxicity associated with NO, like the inhibition of mitochondrial respiration, protein and DNA damage, loss of protein function, necrosis and apoptosis (Fukumura et al., 2006). NO is synthesized from L-arginine, NADPH and oxygen by nitric oxide synthase (NOS) (Fig. 1.14). NOS is classified into three major isoforms: neuronal NOS (nNOS), endothelial NOS (eNOS), and inducible NOS (iNOS). nNOS and eNOS are constitutively expressed (predominantly in neuronal cells and vascular ECs, respectively) to produce NO mainly for signalling functions, and their activity is dependent on the levels of intracellular Ca^{2+} (Fischmann et al., 1999). However, gene expression of both nNOS and eNOS may also be induced under particular physiological conditions such as hemodynamic shear stress or nerve injury (Michel and Feron, 1997). nNOS-derived NO plays a critical role in the regulation of neurogenesis and hippocampal long-term potentiation and memory. However, when in excessive amounts it changes from a physiological neuromodulator to a neurotoxic factor, playing a role in the pathogenesis of Parkinson's and Alzheimer's diseases, ischemia, excitotoxicity, and depression (Zhou and

Zhu, 2009). Regarding iNOS, this isoform can be expressed in a wide range of cells and tissues beeing its expression triggered by inflammatory mediators. In addition, iNOS produces higher NO levels than the other isoforms, and its activity is independent of Ca^{2+} concentrations (Fukumura et al., 2006). iNOS-derived NO can have beneficial microbicidal, antiviral, antiparasital, and antitumoral effects (Bogdan et al., 2000). However, abnormal iNOS induction appears to be involved in the pathophysiology of human diseases such as asthma, arthritis, neurodegenerative diseases, tumour development, transplant rejection or septic shock (Kleinert et al., 2004).

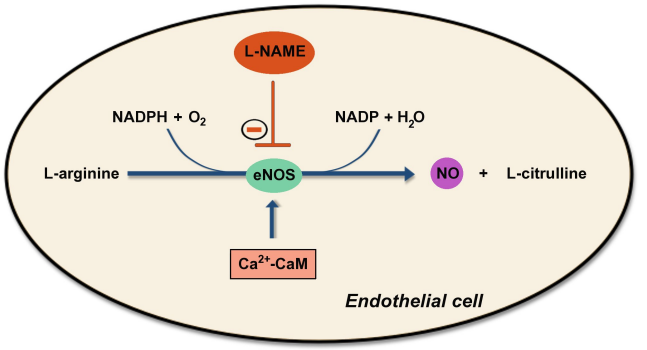

Fig. 1.14. Schematic illustration of the biosynthesis of nitric oxide (NO) in endothelial cells. NO is synthesised from L-arginine by endothelial nitric oxide synthase (eNOS), which is activated by the calcium-calmodulin complex (Ca^{2+}-CaM). NO synthesis can be inhibited by the action of the L-NG-Nitroarginine methyl ester (L-NAME), a NOS inhibitor.

1.3.1. Endothelial NOS (eNOS)

eNOS is expressed not only in ECs, but also in cardiac myocytes, blood platelets, erythrocytes, mast cells, leukocytes, and renal epithelium

(Dudzinski and Michel, 2007). In physiologic conditions eNOS-derived NO regulates vascular permeability, leukocyte-endothelial interaction, neurotransmission, and maintains an anti-proliferative and anti-apoptotic environment in the vessel wall. However, in pathologic conditions, the excessive amounts of NO produced become neurotoxic. In eNOS-deficient mice, the occurrence of vascular leakage during acute inflammation is abolished, suggesting that eNOS-derived NO plays a major role in the increase of vascular permeability (Bucci et al., 2005). Others also showed that NO causes hyperpermeability in response to pro-inflammatory agents such as platelet-activating factor (PAF) and vascular endothelial growth factor (VEGF) (Fukumura et al., 2001; Hatakeyama et al., 2006).

The functional eNOS, like the other isoforms, is a dimmer comprised of two identical subunits, both of which are myristoylated and palmitoylated (Fleming and Busse, 1999) and thus can associate with intracellular membranes. Functional eNOS is present in at least three membrane compartments, the plasma membrane (Hecker et al., 1994), plasmalemmal caveolae (Feron et al., 1996), and the Golgi complex (Sessa et al., 1995), but is also present in the cytosol. Cell membrane-bound and Golgi-bound eNOS have the ability to release more basal NO than cytosolic eNOS. However, the location of the enzyme when it releases NO may be more important than the amount of NO released for development of an extracellular significant function (Duran et al., 2010). NO production must be cautiously controlled, and so the eNOS activity is highly regulated by post-translational modifications and protein-protein interactions (Dudzinski and Michel, 2007).

Intracellular Ca^{2+}: calmodulin binding

The increase in cytoplasmic Ca^{2+} levels activates calmodulin (CaM), which binds to the CaM-binding domain in the eNOS to promote the alignment of the oxigenase and reductase domains of eNOS, leading to efficient NO synthesis (Sessa, 2004). In addition, binding of CaM simultaneously disrupts the inhibitory caveolin-eNOS interaction. The intracellular Ca^{2+} level is a critical determinant of eNOS activation *via* calmodulin, and many pathways converge on the release of Ca^{2+} from intracellular stores to activate eNOS, such as the G protein-dependent signalling pathway (Loscalzo and Welch, 1995). In this pathway, phospholipase C (PLC) cleaves the membrane component phosphatidylinositol 4,5-triphosphate into diacylglycerol and inositol 1,4,5-triphosphate (IP3), which binds to IP3 receptors that are enriched in caveolae and regulate intracellular Ca^{2+} through pleiotropic effects on ion channels (Fujimoto et al., 1992).

eNOS phosphorylation

eNOS can be phosphorylated on serine (S), tyrosine (Y), and threonine (T) residues. Phosphorylation at S1177, S635, S617 or Y83 stimulates eNOS activity, whereas phosphorylation at S116, Y657 or T495 is inhibitory. S1177 phosphorylation activates eNOS by inhibition of CaM dissociation from eNOS and enhancement of the flux of electrons through the reductase domain of eNOS (McCabe et al., 2000). S1177 is phosphorylated by several kinases, such as kinase Akt (protein kinase B), cyclic AMP-dependent protein kinase A (PKA), AMP-activated protein kinase (AMPK), PKG, and Ca^{2+}/CaM-dependent protein kinase II (CaM Kinase II) (Dudzinski and Michel, 2007). The kinase pathways that lead to eNOS

phosphorylation depends on the stimuli applied. S635 is phosphorylated by PKA and increases eNOS activity in response to PKA-dependent agonists, as well as shear stress (Boo et al., 2002; Michell et al., 2002). Phosphorylation at S617 occurs downstream of either PKA or Akt, and seems to sensitize eNOS to CaM binding (Michell et al., 2002) and possibly to modulate phosphorylation at other eNOS sites (Bauer et al., 2003). eNOS can be phosphorylated at S116 by MAPK Erk1/2, which leads to a decrease in eNOS activity (Li et al., 2007; Ruan et al., 2011). Src kinase phosphorylates Y83 and activates eNOS (Fulton et al., 2005; Fulton et al., 2008), whereas Y657 is phosphorylated by proline-rich tyrosine kinase 2 and seems to inhibit eNOS activity (Fisslthaler et al., 2008). Moreover, eNOS can be phosphorylated at T495 by PKC and AMPK, which attenuates the binding of CaM by eNOS (Chen et al., 1999; Michell et al., 2001), decreasing the enzyme activity.

eNOS-associated proteins

Caveolin is the major coat protein of caveolae (Williams and Lisanti, 2004). eNOS contains a consensus caveolin binding motif, and is negatively regulated by the interaction with caveolin-1 (Fulton et al., 2001). Caveolin-1 interacts independently with both oxygenase and reductase domains of eNOS (Ghosh et al., 1998). However, the binding of caveolin-1 with the reductase domain is essential to inhibit eNOS activity, since the binding to this domain compromises eNOS ability to bind CaM and to donate electrons to the eNOS heme subunit, thereby impairing NO synthesis (Ghosh et al., 1998). The reductase interaction is independent of a caveolin-1 binding motif. Despite the inhibitory interaction with caveolin,

the localisation of eNOS in plasmalemmal caveolae seems to be important for eNOS activation by clustering receptors and effector proteins downstream of numerous eNOS agonists (Dudzinski and Michel, 2007).

eNOS interacting protein (NOSIP) binds to the carboxyl-terminal region of the eNOS oxygenase domain. NOSIP decreases eNOS activity possibly by uncoupling it from plasma membrane caveolae and by promoting the translocation of eNOS from caveolae to intracellular compartments (Dedio et al., 2001).

Heat shock protein 90 (Hsp90) is a molecular chaperone responsible for the proper folding of proteins such as steroid receptors and cell cycle-dependent kinases (Pratt, 1997). Hsp90 associates with eNOS, and this association seems to be determined by the reversible tyrosine phosphorylation of Hsp90 in response to diverse eNOS agonists (Garcia-Cardena et al., 1998; Harris et al., 2000). Hsp90 binding stimulates eNOS activity by enhancing the affinity of eNOS for CaM and balancing the output of NO (Pritchard et al., 2001). Hsp90 also stimulates eNOS activity by increasing the rate of Akt-dependent phosphorylation, and may also function as a scaffold for eNOS and Akt (Fontana et al., 2002; Sato et al., 2000; Takahashi and Mendelsohn, 2003).

Dynamin-2 is a large GTPase that is involved in vesicle formation, receptor-mediated endocytosis, caveolae internalization, and vesicle trafficking in and out of the Golgi (Doherty and McMahon, 2009). Dynamin-2 is found in the Golgi and plasma membranes of ECs. Dynamin-2 binds directly to eNOS and colocalizes with this enzyme in the Golgi membranes (Cao et al., 2001). The association between eNOS and dynamin-2 is increased by Ca^{2+} ionophores, and an increase in dynamin levels results in enhanced eNOS catalysis (Cao et al., 2001).

1.3.2. eNOS-derived NO and the BBB

ECs express both iNOS and eNOS, and produce NO in small amounts that will control the local blood flow. In addition, constitutive eNOS-derived NO plays a crucial role as a determinant factor of basal vascular permeability by regulating capillary and venular endothelial junctional integrity and by controlling the dimensions of interendothelial junctions (Predescu et al., 2005). This clearly shows that a restrictive endothelial barrier requires a physiological concentration of NO. Nevertheless, in pathologic conditions, excessive production of NO and the consequent NO redox species increase the BBB permeability (Boje and Lakhman, 2000; Mayhan, 2000; Parathath et al., 2006). eNOS expression was shown to be increased in a rat model of focal cerebral ischemia, which was associated with BBB disruption (Kim and Jung, 2011). In addition, microsphere embolism-induced BBB disruption in the rat brain was attenuated by the inhibition of eNOS activity (Han et al., 2006).

Caveolae are involved in receptor-mediated endocytosis and transcytosis through the BBB, and hydrolysis of guanosine triphosphate (GTP) is involved in the fission of the caveolae structures away from the plasma membrane (Schnitzer et al., 1996). Futhermore, NO increases endocytosis by S-nitrosylation of dynamin, promoting its oligomerization and GTPase activity (Wang et al., 2006). Thus, it seems that NO is important in the regulation of transendothelial permeability.

1.4. Matrix metalloproteinases (MMPs)

1.4.1. MMP family and functions

MMPs are a family, with more than 20 members, of zinc-dependent endopeptidases that catalyse the proteolysis of a number of extracellular matrix and basement membrane proteins, including collagens, laminin, glycoproteins and proteoglycans (Milward et al., 2007). MMPs also cleave a range of other molecules including growth factors, cytokines and chemokines. While some MMPs are secreted into the extracellular space, others are expressed on the cell surface, the membrane-type MMPs (Milward et al., 2007). The activity of MMPs is regulated by their natural inhibitors TIMPs. The MMP/TIMP system is thus involved in the modulation of functional and structural remodelling of the cellular architecture in the context of pathophysiology. MMPs play an important role in developing and normal adult CNS, and during repair of injuries that are inflicted upon adult CNS (Fig. 1.15) (Agrawal et al., 2008).

In the nervous system, the profiles of constitutive and inducible MMP expression differ between regions, cell types and species. Some MMPs and TIMPs are expressed by all the main CNS cell types including neurons, astrocytes, microglia, oligodendrocytes, Schwann cells, vascular ECs, choroid plexus epithelial cells and progenitor cells (Milward et al., 2007). MMP-2 and MMP-9 (also called gelatinases A and B, respectively) are capable of cleaving collagen IV and V, laminin, and chondroitin sulfate proteoglycan, which are associated with cell adhesion. MMP-9 is probably the best characterised MMP expressed in the CNS. MMP-9 expression has been detected in both limbic and non-limbic structures in adult rat brain, with preferential expression within the hippocampus (Szklarczyk et al.,

2002). In contrast, MMP-2 has been found to be uniformly distributed, especially within the brain gray matter, and generally expressed at a lower level than MMP-9 (Szklarczyk et al., 2002). In the hippocampus, MMP-9 is primarily but not exclusively expressed by neurons, while MMP-2 originates primarily from glial cells (Szklarczyk et al., 2002). Importantly, MMP-9 is required for hippocampal long-term potentiation and memory (Nagy et al., 2006). MMPs are often secreted in inactive forms, and so protein levels do not always correlate with activity. Also, the regulation of MMPs activity following secretion allows an additional post-translational level of control to these enzymes (Milward et al., 2007).

Besides the beneficial roles of MMPs in the developing and adult CNS, the MMPs can also play a detrimental role by promoting several diseases such as multiple sclerosis, spinal cord injury, and infection with human immunodeficiency virus (HIV) (Agrawal et al., 2008).

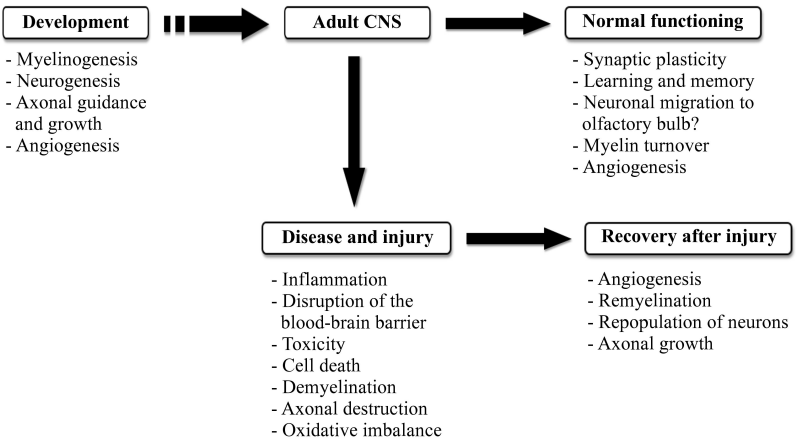

Fig. 1.15. Multiple roles of matrix metalloproteinases (MMPs) in the central nervous system (CNS). MMPs play a crucial role in developing and adult CNS, as well as in recovery after injury. In CNS injury, infection and inflammation, MMPs may lead to degeneration of neurons, axons and myelin, resulting in various disease conditions (adapted from Agrawal et al., 2008).

1.4.2. MMPs and the BBB

One mechanism by which MMPs may promote some of the CNS diseases is their ability to disrupt the BBB. MMP-9 induction by lipopolysaccharide (LPS) increases BBB permeability in rat brain, which is attenuated by treatment with the MMP inhibitor, BB-1101 (Mun-Bryce and Rosenberg, 1998). In addition, both inhibition of MMP-9 and the deletion of MMP-9 gene attenuate the BBB disruption (Rosenberg et al., 1998; Svedin et al., 2007). These effects can be explained by the fact that MMPs are able to degrade the BBB extracellular matrix of the basal membrane as well as TJ proteins. In fact, occludin contains a putative extracellular MMP cleavage site (Bojarski et al., 2004). It was previously shown that claudin-5 and occludin are proteolytically degraded by MMP-2 and MMP-9 in a rat model of focal ischemia (Yang et al., 2007). MMP-3 is also involved in the cleavage of claudin-5 and occludin in LPS-induced inflammation model (Gurney et al., 2006). In human brain microvascular ECs, activation of MMP-1, -2, and -9 by ROS parallels degradation of extracellular matrix proteins and the enhancement of TJ protein phosphorylation, namely occludin, claudin-5 and ZO-1 (Haorah et al., 2007). These effects are prevented by the pre-treatment with an inhibitor of MMPs or an antioxidant (Haorah et al., 2007).

1.4.3. MMPs and METH

METH can activate MMP-2 and MMP-9. Specifically, Mizoguchi et al. (2007b) reported that rats treated repeatedly with METH showed an increase in the protein levels and activity of MMP-2 and MMP-9 in the

nucleus accumbens and frontal cortex. METH also increases MMP-9 gene expression in the whole mice brain (Liu et al., 2008). However, MMP-9 KO mice still exhibited neurotoxicity to METH (Liu et al., 2008). Despite the limited studies addressing the role of MMPs in mediating METH-induced toxicity, a few studies demonstrated that MMPs are involved in the rewarding effects of this drug, namely METH-induced behaviour sensitization and conditioned place preference (CPP). Mizoguchi and colleagues (2007b) reported that MMP-2 and MMP-9 KO mice showed a decrease in METH-induced behavioural sensitization and CPP compared to wild-type mice. METH-increased DA release in the nucleus accumbens was also attenuated in these KO mice (Mizoguchi et al., 2007b). In addition, the inhibition of MMP-2 and MMP-9 attenuates the rewarding effects of chronic low-dose METH (Mizoguchi et al., 2007a). Since learning and memory (MMPs are important mediators of these processes), as well as DAergic transmission in the nucleus accumbens are important in mediating the rewarding effects of drugs of abuse, these evidences show that MMPs may play a crucial role in the reward effects of METH. Several mechanisms that mediate the activation of MMP-2 and MMP-9, including oxidative stress, metabolic compromise, and inflammation, occur after the administration of AMPH-related drugs of abuse (Yamamoto and Raudensky, 2008), suggesting that MMP activation after METH administration might play a role in METH-induced toxicity. In fact, since METH can lead to an increase in the expression and activity of MMPs, and MMPs disrupt the BBB, one possible mechanism by which METH could induce neurotoxicity is *via* BBB dysfunction due to TJ proteins cleavage mediated by MMPs.

1.5. METH and the BBB

Recently, the disruption of the BBB has emerging as another mechanism involved in the toxic effects caused by METH. Several studies showed that METH administration increases the permeability of the BBB in rodents (Bowyer and Ali, 2006; Kiyatkin et al., 2007; Sharma and Ali, 2006). Mice administered with a single high dose of METH showed BBB disruption to large molecules in the cerebral cortex (Sharma and Ali, 2006), hippocampus and amygdala (Bowyer and Ali, 2006), and in the caudate-putamen (Bowyer et al., 2008), which was correlated with severe hyperthermia and status epilepticus. METH administration to rats also increases BBB permeability in the cortex, hippocampus, thalamus and hypothalamus, which was enhanced with the occurrence of brain hyperthermia (Kiyatkin et al., 2007; Sharma and Kiyatkin, 2009). Recent *in vitro* studies demonstrated that METH is capable of altering the BBB properties through direct effects on ECs (Park et al., 2012; Ramirez et al., 2009). Human primary brain microvascular ECs exposed to METH showed a disorganisation and decrease in the protein levels of occludin, claudin-5 and ZO-1, as well as the consequent decrease in the TEER (Ramirez et al., 2009). These changes were also accompanied by an increase in the formation of ROS, activation of MLCK, and an enhancement in monocyte migration across METH-treated endothelial monolayers. Interestingly, antioxidant treatment attenuated or blocked the effects of METH on brain ECs (Ramirez et al., 2009). Park and co-workers (2012) also demonstrated that METH exposure can activate a NADPH oxidase (NOX) complex, followed by the subsequent activation of ERK1/2 signalling and phosphorylation of caveolin-1 at Tyr14 in a human

brain microvascular EC line. The events resultant from METH exposure leads in turn to the generation of ROS, to a decrease in occludin protein levels and immunoreactivity, and to increased monocyte migration across EC monolayers (Park et al., 2012). These evidences show that METH can compromise the BBB function just through direct effects on brain ECs.

1.6. Objectives

The neurotoxicity caused by METH consumption is mediated primarily by excitotoxicity, mitochondrial dysfunction, oxidative stress, and neuroinflammation. METH can also impair the BBB function, and the dysfunction of this barrier is known to contribute to and exacerbate many CNS diseases. Thus, BBB disruption has recently emerged as an important mechanism by which METH could exerts its neurotoxic effects. However, the molecular and cellular mechanisms underlying METH-induced BBB dysfunction are not well understood.

Therefore, we first aimed to clarify the time-course effects of METH on BBB permeability and the susceptibility of different brain regions to this drug in mice administered with a single high dose of METH, corresponding to an acute intoxication model. Furthermore, in an attempt to understand how METH could induce BBB breakdown in this model, we also evaluated changes in TJ proteins and MMP-9 expression and activity.

In order to unravel the mechanisms by which METH affects the BBB, using an *in vitro* BBB model we investigated the direct effects of METH on brain microvascular ECs. METH effects were assessed at concentrations physiologically significant, i.e. at levels found in the blood plasma of drug

abusers. Given that NO production may play a role in METH-induced neurotoxicity, we studied the role of eNOS in the METH-induced EC response. Moreover, since BBB dysfunction often results in increased leukocyte infiltration, we also addressed the alterations to lymphocyte migration in response to METH.

Chapter 2

Methamphetamine transiently increases the blood-brain barrier permeability in the hippocampus: Role of tight junction proteins and matrix metalloproteinase-9

2.1. Abstract

Methamphetamine (METH) is a powerful stimulant drug of abuse that has steadily gained popularity worldwide. It is known that METH is highly neurotoxic and causes irreversible damage of brain cells leading to neurological and psychiatric abnormalities. Recent studies suggested that METH-induced neurotoxicity may also result from its ability to compromise blood-brain barrier (BBB) function. Due to the crucial role of BBB in the maintenance of brain homeostasis and protection against toxic molecules and pathogenic organisms, its dysfunction could have severe consequences. Thus, in this study, we investigated the effect of an acute high dose of METH (30 mg/kg) on BBB permeability after different time points and in different brain regions. For that, young adult mice were sacrificed 1 h, 24 h or 72 h post-METH administration. We concluded that METH increased BBB permeability, but this effect was detected only at 24 h after administration, being therefore a transitory effect. Interestingly, we also found that the hippocampus was the most susceptible brain region to METH, comparing to frontal cortex and striatum. Moreover, in an attempt to identify the key players in METH-induced BBB dysfunction, we further investigated potential alterations in tight junction (TJ) proteins and matrix metalloproteinase-9 (MMP-9). METH was able to decrease the protein levels of zonula occludens (ZO)-1, claudin-5 and occludin in the hippocampus 24 h post-injection, and increased the activity and immunoreactivity of MMP-9. The pre-treatment with BB-94 (30 mg/kg), a matrix metalloproteinase inhibitor, prevented the METH-induced increase in MMP-9 immunoreactivity and METH-induced Evans blue dye leakage in the hippocampus. Overall, the present data demonstrate that METH

transiently increases the BBB permeability in the hippocampus, which can be explained by alterations on TJ proteins and MMP-9.

2.2. Introduction

Methamphetamine (METH) is a psychomotor drug highly addictive and toxic to the brain. Studies with human subjects have shown that METH chronic users demonstrate structural abnormalities in the brain, namely lost of grey-matter, white matter hypertrophy and altered glucose metabolism in specific regions like hippocampus, prefrontal cortex, cingulate gyrus and amygdala (Thompson et al., 2004). These findings could explain some of the problems identified in METH users, such as behavioural problems, recall capacity, and memory and performance deficits observed in verbal memory tests and executive functions (Thompson et al., 2004). In an attempt to better clarify the molecular and cellular mechanisms responsible for these effects, most of the studies have focused on free radical production and oxidative stress, excitotoxicity, inflammation and mitochondrial dysfunction (Quinton and Yamamoto, 2006; Yamamoto and Raudensky, 2008). More recently, a new concept of METH-induced brain dysfunction has been raised based on its ability to disrupt the blood-brain barrier (BBB) (Bowyer and Ali, 2006; Sharma and Ali, 2006; Silva et al., 2010). However, the molecular and cellular mechanisms underlying BBB breakdown due to METH consumption remains to be fully dissected. *In vivo* studies demonstrate that mice administered with an acute high dose of METH show an increase in BBB permeability in the medial and ventral amygdala, hippocampus (Bowyer and Ali, 2006) and caudate-putamen

(Bowyer et al., 2008), which was correlated with severe hyperthermia and extensive seizure activity. Moreover, *in vitro* studies have suggested that METH alters the BBB function through direct effects on endothelial cells by modulating the tight junction (TJ) proteins (Mahajan et al., 2008). Similarly, Ramirez and collaborators (2009) demonstrated that METH decreases the tightness of the BBB not only by decreasing the TJ protein levels but also by enhancing the production of reactive oxygen species resulting in the activation of myosin light chain kinase (MLCK), which in turn can lead to an increase in monocyte migration.

The matrix metalloproteinases (MMPs) are proteolytic enzymes that can be activated by several mechanisms, including oxidative stress (Jian Liu and Rosenberg, 2005) and inflammation (Rosenberg, 2002). Multiple evidence have suggested the involvement of MMPs in some CNS diseases such as multiple sclerosis, spinal cord injury and human immunodeficiency virus encephalitis (Agrawal et al, 2008). A plausible mechanism by which these enzymes can promote brain dysfunction is their ability to disrupt the BBB (Fujimura et al., 1999; Keogh et al., 2003; Yang et al., 2007). In fact, MMPs are involved in the degradation of claudin-5 and occludin in a rat model of focal ischemia (Yang et al., 2007) and in a mouse model of neuroinflammation (Gurney et al., 2006). Moreover, Mizoguchi and collaborators (2007a) showed that METH increases the expression of MMP-2 and MMP-9 in neurons and glial cells in the rat frontal cortex and nucleus accumbens. Another study demonstrated that METH induces the release of MMP-1 in mixed human neuron/astrocyte cultures (Conant et al., 2004).

According to very recent findings, it is clear that METH affects negatively the BBB function, but many questions remain unanswered. Thus, with the

present study we aimed to clarify the time-course effect of METH on BBB permeability and the susceptibility of different brain regions to this drug. Furthermore, in an attempt to better understand how METH can affect BBB, we looked for alterations in TJ proteins and MMP-9 expression and activity.

2.3. Material and methods

2.3.1. Animals

Male C57BL/6J wild-type mice (20 – 30 g), aged three months (Charles River Laboratories, Inc, Barcelona, Spain) were housed under standard 12-h light/dark cycle with *ad libitum* access to food and water. In this study we used an acute intoxication model, and for that mice were administered intraperitoneally (i.p.) with a single dose of METH (30 mg/kg body weight; synthesised at Chemistry Department, Faculty of Sciences, University of Porto, Portugal) dissolved in a maximum volume of 100 µl of sterile 0.9% NaCl, and were then sacrificed 1 h, 4 h, 8 h, 24 h, 48 h or 72 h post-administration. The control animals were administered with 100 µl of sterile 0.9% NaCl (i.p.) and were sacrificed at the same time-points abovementioned. Other group of animals was pre-treated with BB-94 (Batimastat; 30 mg/kg, i.p.; Tocris Bioscience, Bristol, UK), a broad spectrum MMP inhibitor, 10 min prior METH administration with a maximum volume of 200 µl dissolved in 0.01 M phosphate buffer saline (PBS; pH 7.2) with 0.01% Tween-20, being the animals sacrificed 24 h after METH injection. A minimum of three animals per experiment was used, as specified in the figure legends. All procedures involving

experimental animals were performed in accordance with European Community guidelines for the use of animals in laboratory (Directive 2010/63/EU) and the Portuguese law for the care and use of experimental animals (DL nº. 129/92). All efforts were made to minimise animal suffering and to reduce the number of animals used.

2.3.2. Sample preparation for METH and AMPH quantification

Mice were anaesthetised with 100 µl of sodium pentobarbital (25 mg/ml, i.p.; Sigma, St Louis, MO, USA). Blood was collected from mice jugular vein and immediately placed onto sterile K_3EDTA tubes (7.5% K_3EDTA, 3 ml; BD Vacutainer™, Plymouth, UK) in order to avoid blood clotting. Afterwards, 300 µl of blood sample was centrifuged at 14,100×*g* for 10 min and 200 µl of plasma was added to 2 ml borate buffer, pH 9. Regarding brain samples, the mice brains were quickly removed and homogenised at 4ºC in 4 ml borate buffer, pH 9, in a Precellys® 24 tissue homogeniser. Then, brain homogenates were centrifuged at 3,600×*g* for 10 min at 4ºC. Before METH and amphetamine (AMPH) extraction, 100 µl of the internal standard consisting of 100 ng/ml AMPH-d_5 and METH-d_5 (Cerilliant, Round Rock, TX, USA) was added to the plasma and brain samples.

2.3.3. METH and AMPH extraction

For the detection of METH and AMPH, plasma and brain samples were submitted to a solid phase extraction in an Oasis HLB 3cc 60 mg column (Waters, Milford, Massachusetts, USA). First, the column cartridges were

conditioned with 2 ml methanol and 2 ml water, and samples were directly applied into the column. Then, columns were cleaned with 2 ml water with 5% methanol followed by 2 ml of the solution consisting of 60% water, 39.5% methanol and 0.5% NH_4OH. Cartridges were dried for 10 min and then an elution was performed with 2 ml of a solution composed by 75% dichloromethane and 25% isopropanol. Afterwards, eluates were evaporated to dryness with nitrogen and then reconstituted in 100 µl of the following solution: 95% mobile phase (2 mM ammonium formate and 0.1% formic acid) plus 5% methanol.

2.3.4. Liquid chromatography-tandem mass spectrometry

Samples containing METH and AMPH (30 µl) were injected into the HPLC system (Waters Alliance 2795 Separation Module, Milford, Massachusetts, USA) with a Waters Alliance series column heater/cooler (Waters) and separated in an Atlantis T3 column (100 × 2.1 mm, 3 µm; Waters) using the mobile phase at a flow rate of 0.2 ml/min, in gradient mode. Samples were detected on a tandem mass spectrometer Quattro MicroTM API ESCI (Waters) with a triple quadrupole, being the electrospray operated in the positive ionisation mode (ESI+). Moreover, nitrogen was heated at 300ºC and used as nebulisation gas and desolvation gas at a flow rate of 600 (l/h), and as a cone gas at a flow of 60 (l/h). Capillary voltage was set to 3 kV and source block temperature was set to 130ºC. Data was acquired by using MassLynx 4.1 software and processed with QuantLynx 4.0 software (Waters).

2.3.5. Evans blue quantification in the brain

Evans blue (EB; Sigma) dye was used to detect BBB disruption. EB binds to serum albumin (MW of the complex = 65 kDa) and only crosses the BBB if there is an increase in BBB permeability. Animals were anaesthetised with 100 µl of sodium pentobarbital (25 mg/ml, i.p.; Sigma) and injected in the tail vein with 100 µl of 4% EB 30 min before transcardial perfusion with 5 ml of 0.05 M sodium citrate with 1% paraformaldehyde (PFA) (pH 4.2, 37ºC), followed by 10 ml of 4% PFA in 0.01 M PBS, pH 7.4. Brains were removed and for some experiments the cerebellum and hemispheres were separated, whereas in other studies the bilateral hippocampi, frontal cortex and striata were dissected. Each hemisphere and the cerebellum were immersed in formamide (6 µl/mg wet tissue; Sigma-Aldrich), while the hippocampi and striata were immersed in 300 µl and the frontal cortex in 1 ml of formamide. The samples were left for 24 h at 51ºC. Formamide was then centrifuged at 420,000×*g* for 20 min at 4ºC. The absorbance of each sample was measured at 620 nm and 740 nm in a Synergy™ HT Multi-Mode Microplate Reader (BioTek, Winooski, Vermont, USA). The concentration of the dye in the supernatant was calculated by interpolation in a standard curve of EB in formamide (0 – 4 µg/ml).

2.3.6. Detection of Evans blue extravasation in different brain regions

Mice were manipulated as abovementioned for EB quantification and after transcardial perfusion, brains were removed, post-fixed in 4% PFA

solution for 24 h at 4ºC, and transferred to 20% sucrose in 0.01 M PBS, pH 7.4, for at least 24 h at 4ºC. Then, brains were sectioned from the striatum to the hippocampus in coronal slices (14 μm), on a cryostat (Leica CM3050S, Nussloch, Germany) and the slices were mounted directly onto gelatine-coated glass slides. Slices were rinsed in PBS and then stained with 10 μg/ml Hoechst 33342 [in PBS containing 0.25% bovine serum albumin (BSA)] for 10 min at room temperature (RT). After washing once again, slices were coverslipped with Dako fluorescence medium (Dako North America, Carpinteria, USA). Images were recorded using an Axiovert 200 M fluorescence microscope (Carl Zeiss, Oberkochem, Germany).

2.3.7. Western blot analysis

After the treatments, the animals were sacrificed by cervical dislocation, the brain was immediately removed from the skull, placed on an ice-cold dissection disc and the bilateral hippocampi, frontal cortex and striata were dissected. The isolated tissues were homogenised in RIPA buffer (150 mM NaCl, 5 mM EGTA, 50 mM Tris, 1% (v/v) Triton, 0.1% SDS and 0.5% sodium deoxycholate), supplemented with protease inhibitor cocktail tablets (Roche Applied Sciences, Germany) in the ratio of 1 tablet/10 ml RIPA buffer. The homogenates were centrifuged at 14,000×*g* for 10 min, the supernatants were collected and protein concentration was determined by the Pierce BCA Protein Assay Kit (Thermo Fisher Scientific, Northumberland, UK). Protein samples (25 μg, 100 μg or 200 μg for occludin, ZO-1 and claudin-5, respectively) were separated by electrophoresis on 6 – 12% SDS-PAGE, and then transferred electrophoretically onto a PVDF membrane (Millipore, Madrid, Spain).

Membranes were then blocked for 1 h at RT in blocking solution, PBS containing 0.1% (v/v) Tween-20 (PBST) and 5% (w/v) non-fat dried milk, and incubated with primary antibodies overnight at 4ºC as follows: ZO-1 (1:500; Zymed Lab, San Francisco, USA), claudin-5 (1:100; Zymed Lab) or occludin (1:250; Zymed Lab). After washing 3×20 min with PBST, the membranes were incubated with alkaline phosphatase-conjugated secondary antibodies (1:20000; Amersham, GE Healthcare Life Science, USA) for 1 h at RT. The assessed proteins were detected using the Enhanced Chemifluorescence (ECF) reagent (Amersham) on a Storm 860 Gel and Blot Imaging System (Amersham, GE Healthcare Life Science, Buckinghamshire, UK). The blots were stripped and reprobed with an antibody against β-actin, which was used as loading control, (1:2000; Sigma-Aldrich, St Louis, MO, USA). Band intensities were quantified using the ImageQuant 5.0 software.

2.3.8. Gelatin gel zymography

Mice were sacrificed by cervical dislocation, brains were quickly removed, placed on an ice-cold dissection disc and the hippocampi were dissected. Brain samples were homogenised in 250 μl lysis buffer (50 mM Tris-HCl, pH 7.4, 0.5% Triton X-100, 1 mM PMSF, 1 mM DTT, and 5 μg/ml CLAP, protease inhibitors) on ice. After centrifugation at 14,000×*g* for 10 min at 4ºC, the supernatant was collected. Total protein concentration of each sample was determined by the Pierce BCA protein assay kit (Thermo Fisher Scientific). MMP-9 activity was assessed by gelatin zymography, as previously described (Asahi et al., 2000) with some modifications. Briefly, protein samples (50 μg) were loaded and separated by 10% acrylamide gel

with 0.1% gelatin (substrate). The gel was placed in renaturing buffer for 30 min and then incubated with developing buffer at 37ºC for 48 h. After incubation, the gel was washed with distilled water for 5 min followed by staining with 0.5% Commassie Blue R-250 for 30 min. The gel was destained in a solution composed of 20% methanol and 10% acetic acid until white bands appear in a blue background.

2.3.9. Immunohistochemistry

Mice were anaesthetised with 100 μl of sodium pentobarbital (25 mg/ml, i.p.; Sigma) and transcardially perfused with 10 ml of 0.01 M PBS (pH 7.4), followed by 20 ml of 4% PFA in 0.01 M PBS (pH 7.4). The brains were removed, post-fixed in 4% PFA solution for 24 h at 4ºC, and then transferred to 20% sucrose in 0.01 M PBS for at least 24 h at 4ºC. Then, brains were cut from the striatum to the hippocampus in coronal sections (30 μm) and the slices were collected in 20% sucrose solution to perform free-floating immunohistochemistry. Slices were rinsed in PBS, blocked with 3% fetal bovine serum (FBS) + 1% Triton X-100 in 0.01 M PBS for 30 min at RT, and incubated with anti-MMP-9 antibody (1:1000; Abcam, Cambridge, UK). For double-labelling of MMP-9 and CD11b, GFAP or NeuN, slices were incubated with anti-CD11b (1:500; AbD Serotec, Oxford, UK), anti-glial fibrillary acidic protein (GFAP) conjugated to Cy3 (1:500; Sigma-Aldrich) or anti-NeuN (1:100; Chemicon-Millipore, Madrid, Spain) antibodies. The slices were then incubated with Alexa Fluor 488 or Alexa Fluor 568 secondary antibodies (1:200, Invitrogen, Inchinnan Business Park, UK), for 90 min at RT. Afterwards, slices were washed, incubated with 10 μg/ml Hoechst 33342 (in PBS containing 0.25% BSA)

for 10 min at RT in the dark, and mounted with Dako fluorescence medium (Dako North America). Images were recorded using an LSM 510 Meta Confocal microscope (Carl Zeiss, Oberkochen, Germany).

2.3.10. Statistical analysis

Statistics were performed using one- or two-way ANOVA, followed by Dunnett's or Bonferroni's post-test, and Student's *t*-test, as indicated in the figure legends. Results are expressed as mean ± SEM, and the level of $p<0.05$ was accepted as statistically significant.

2.4. Results

2.4.1. Time course changes of METH and AMPH levels in the plasma and brain

Since the present study aims to clarify the effect of METH on BBB, we first characterised our experimental model regarding the levels of METH and AMPH in the plasma and brain at different time points (1 h, 4 h, 8 h, 24 h, 48 h and 72 h) after METH administration (30 mg/kg). Regarding blood levels, we found that METH reached its highest levels at 1 h after the administration (5584.00±717.00 ng/ml; Fig. 2.1A, $p<0.001$). After 4 h and 8 h, the levels of METH decreased to 357.90±38.89 ng/ml ($p<0.001$) and 59.47±35.15 ng/ml, respectively (Fig. 2.1A). Moreover, at 24 h, 48 h and 72 h post-drug injection, the levels of METH detected in the plasma were residual (4.07±0.97, 0.68±0.19 and 0.53±0.28 ng/ml, respectively; Fig. 2.1A).

Regarding AMPH levels, 1 h after METH administration we detected 780.70±50.58 ng/ml of AMPH in the plasma, which demonstrates that METH was already metabolised (Fig. 2.1B, $p<0.001$). After 4 h the AMPH levels were still significantly increased (156.30±26.15 ng/ml, $p<0.001$), whereas at 8 h the levels decreased to 18.93±13.32 ng/ml (Fig. 2.1B). Similarly as observed in Fig. 2.1A for METH, at 24 h, 48 h and 72 h after drug injection the AMPH levels were only vestigial.

Regarding brain levels, we concluded that the drug rapidly reached the brain because 1 h after administration it was possible to detect 32335.00±533.90 ng/g of METH (Fig. 2.1C, $p<0.001$). After 4 h, the levels of METH were still significantly increased when compared to the control (2179.00±178.40, $p<0.001$), whereas after 8 h, 24 h, 48 h and 72 h the levels were not statistically different from control (318.30±190.40, 12.70±6.95, 5.25±1.58 and 4.63±2.92 ng/g, respectively; Fig. 2.1C). AMPH was also detected in the brain, and its levels were significantly increased, comparing to control, after 1 h (3461.00±459.10 ng/g, $p<0.001$) and 4 h (949.10±88.77 ng/g, $p<0.01$) of METH administration (Fig. 2.1D). At 8 h the AMPH levels were 103.10±64.63 ng/g, whereas after 24 h, 48 h and 72 h its levels were vestigial in brain samples.

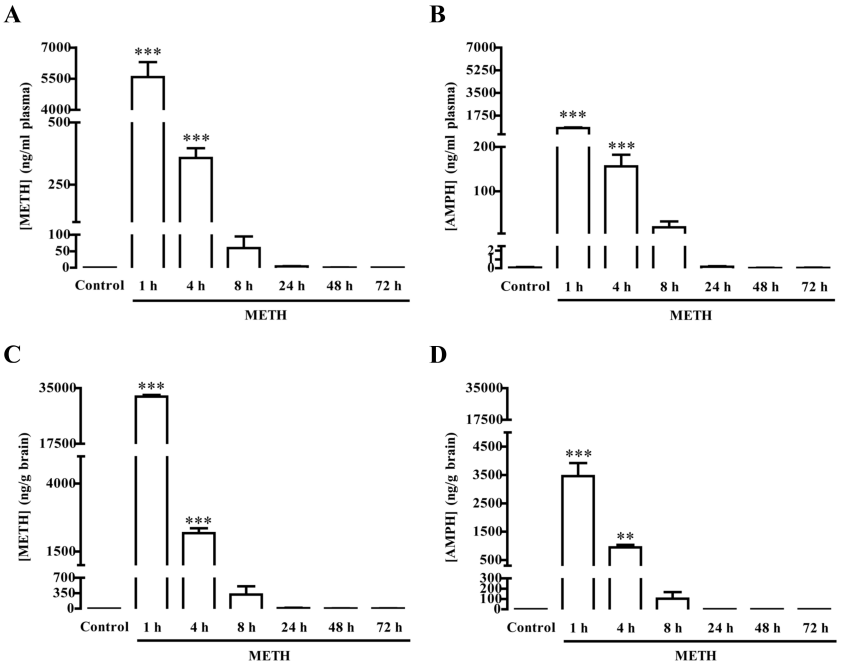

Fig. 2.1. Quantification of methamphetamine (METH; A, C) and its metabolite amphetamine (AMPH; B, D) by liquid chromatography-tandem mass spectrometry in the plasma (A, B) and in the brain (C, D). The levels of both drugs were significantly increased in both plasma and brain at 1 h and 4 h after an acute dose of METH (30 mg/kg, i.p.). The results are expressed as mean ± SEM (n=3-4). ***p*<0.01, ****p*<0.001, significantly different when compared to control (saline) using Dunnett's multiple comparison test.

2.4.2. METH increases Evans blue leakage in the right and left brain hemispheres

Evans blue (EB) is a non-toxic dye that binds to serum albumin. Under normal physiological conditions this complex does not cross the BBB and so, the leakage of albumin into the brain tissue only occurs when there is an increase in the permeability of blood vessels. Due to these properties,

the conjugate of EB dye-albumin is widely used to study the integrity of BBB (Sharma and Ali, 2006; Kiyatkin et al, 2007; Manaenko et al., 2011). In the present study, we observed that 1 h after METH administration the levels of EB detected in the right (2.15±0.60 μg/g) and left hemispheres (2.04±0.58 μg/g) were not statistically different from the values obtained in both hemispheres from control animals (1.56±0.30 and 1.41±0.44 μg/g, right and left hemispheres, respectively; Fig. 2.2A). However, a significant increase in the leakage of EB was detected 24 h after METH injection (7.34±0.74 and 7.42±0.87 μg/g, right and left hemispheres, respectively; $p<0.001$), indicating a disruption of barrier integrity at this time point (Fig. 2.2A). In accordance with these findings, the brains of the mice sacrificed 24 h after METH administration have a blue colour (Fig. 2.2C), which clearly indicates EB extravasation. In contrast, at 72 h post-administration no differences were found relatively to control (1.77±0.24 and 1.77±0.24 μg/g, right and left hemispheres, respectively), which suggests a recovery of the BBB permeability (Fig. 2.2A). Moreover, despite our focus in this study was to compare potential changes induced by METH in the hippocampus, frontal cortex and striatum, it was also possible to observe a blue colour in the posterior cortex at 24 h after METH injection (Fig. 2.2C), as well as an increase in EB leakage in the cerebellum, but only at 24 h after METH administration (control: 2.02±0.29; METH: 13.16±1.44 μg/g; Fig. 2.2B).

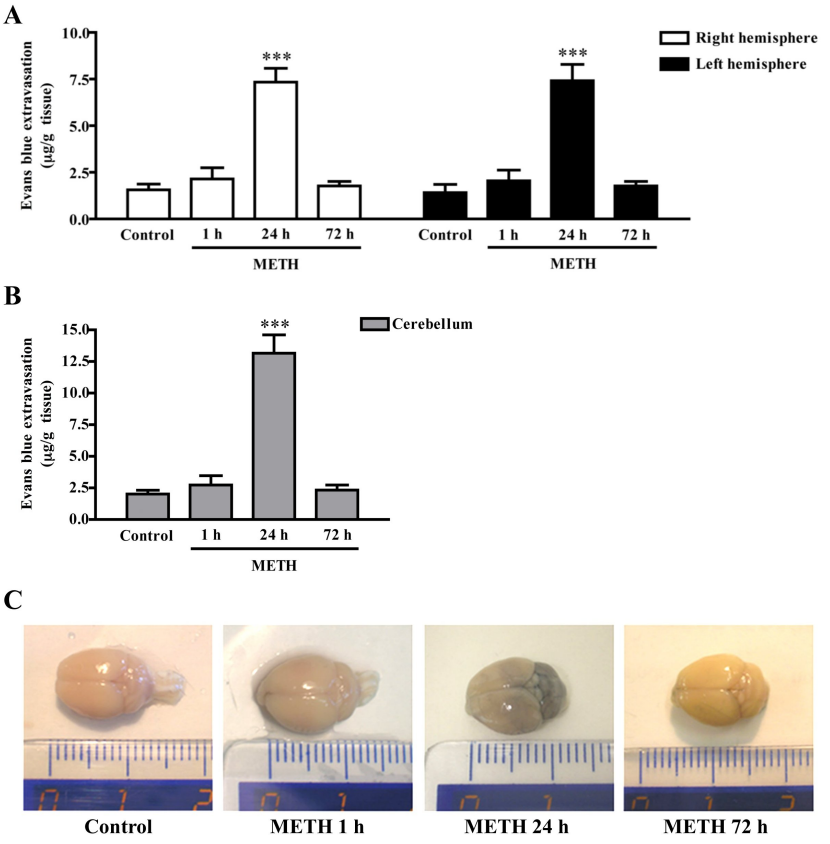

Fig. 2.2. Methamphetamine (METH) induces a transient increase in blood-brain barrier (BBB) permeability. Quantification of Evans blue dye extravasation in the (A) right and left hemispheres, and (B) cerebellum at 1 h, 24 h and 72 h after an acute high dose of METH (30 mg/kg; i.p.). (C) Representative images of mice brains, where the Evans blue leakage (blue colour) is evident only at 24 h following METH injection, without a significant effect at 1 h or 72 h. The results are expressed as mean ± SEM (n=3-4). ****p*<0.001, significantly different when compared to control (saline), 1 h and 72 h post-METH, using Bonferroni's multiple comparison test.

2.4.3. Hippocampus, frontal cortex and striatum are differently affected by METH

METH treatment causes neuronal cell death in several brain regions, including frontal cortex, striatum and hippocampus (Deng et al., 2001; Dietrich, 2009). Thompson and collaborators (2004) also demonstrated that human subjects who have used METH chronically presented severe grey-matter deficits in the cortex and a reduction in hippocampal volume. Thus, since we had observed an increase in the permeability of BBB at 24 h after METH administration, we then analysed different brain regions at this time point, by fluorescence microscopy and EB quantification, to clarify if they were differently affected. Interestingly, the hippocampus (Fig. 2.3) revealed to be the only brain region affected by METH, since at 24 h post-administration the EB extravasation was evident in all hippocampal subregions analysed (DG, CA3 and CA1) (Fig. 2.3A), whereas in both frontal cortex and striatum no EB leakage was detected at 24 h post-METH injection (Fig. 2.3A). Accordingly, we detected a significant increase in EB extravasation in the hippocampus (266.50±26.01% of control, $p<0.001$; Fig. 2.3B), while no differences in the frontal cortex and striatum were detected (83.64±20.62% and 109.70±16.26% of control, respectively; Fig. 2.3B).

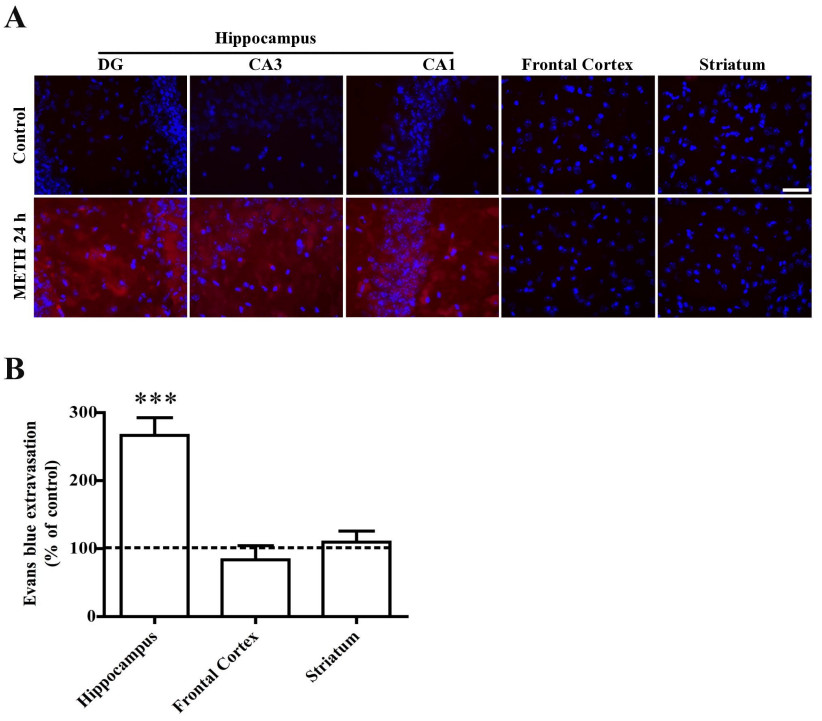

Fig. 2.3. Evans blue (EB) extravasation in the hippocampus at 24 h after methamphetamine (METH) administration. (A) Fluorescence images show the presence of EB (red) in the hippocampus demonstrating that METH induces an increase in BBB permeability in this brain region, and not in the frontal cortex and striatum. Also, no significant differences were observed among different hippocampal subregions, dentate gyrus (DG), cornu ammonis field 3 (CA3) and cornu ammonis field 1 (CA1). Total brain sections were also stained with Hoechst 33342 (blue), a nuclear marker, for visualisation of cellular organization. Scale bar = 50 μm. (B) The quantification of EB dye extravasation in the hippocampus, frontal cortex and striatum at 24 h after an acute high dose of METH (30 mg/kg; i.p.) shows an increase in BBB permeability, but only in the hippocampus. The results are expressed as mean ± SEM (n=3-7). ****p*<0.001, significantly different when compared to control (saline) using Bonferroni's multiple comparison test.

2.4.4. METH induces alterations in the hippocampal tight junction protein levels

TJ proteins confer low paracellular permeability and high electrical resistance to the BBB (Bazzoni and Dejana, 2004). In many CNS diseases, as multiple sclerosis and encephalitis, the alteration in the content of TJ proteins, like ZO-1, claudins and occludin, is linked to the impairment of the BBB and to the increase in its permeability (Forster, 2008; Petty and Lo, 2002; Zlokovic, 2008). Therefore, we analysed the protein levels of ZO-1, claudin-5 and occludin in the hippocampus, frontal cortex and striatum to clarify if alterations in the levels of these tight junction proteins could be correlated with the increase in the BBB permeability observed. At 1 h post-METH administration, no changes were observed in the proteins analysed (Fig. 2.4). However, there was a significant decrease in hippocampal ZO-1 protein levels at 24 h after METH-administration (87.14±2.82% of control, $p<0.05$; Fig. 2.5A), but no differences were observed in the frontal cortex and striatum (94.26±2.20% and 88.94±8.71% of control, respectively; Fig. 2.5A). As observed for ZO-1, there was also a decrease in the content of claudin-5 (67.88±5.44% of control, $p<0.01$; Fig. 2.5B) and occludin (75.78±1.05% of control, $p<0.01$; Fig. 2.5C) in the hippocampus. No alterations were observed in the frontal cortex and striatum regarding the content of claudin-5 (85.22±3.79% and 97.20±2.93% of control, respectively; Fig. 2.5B) and occludin (95.49±5.18% and 101.06±13.36% of control, respectively; Fig. 2.5C).

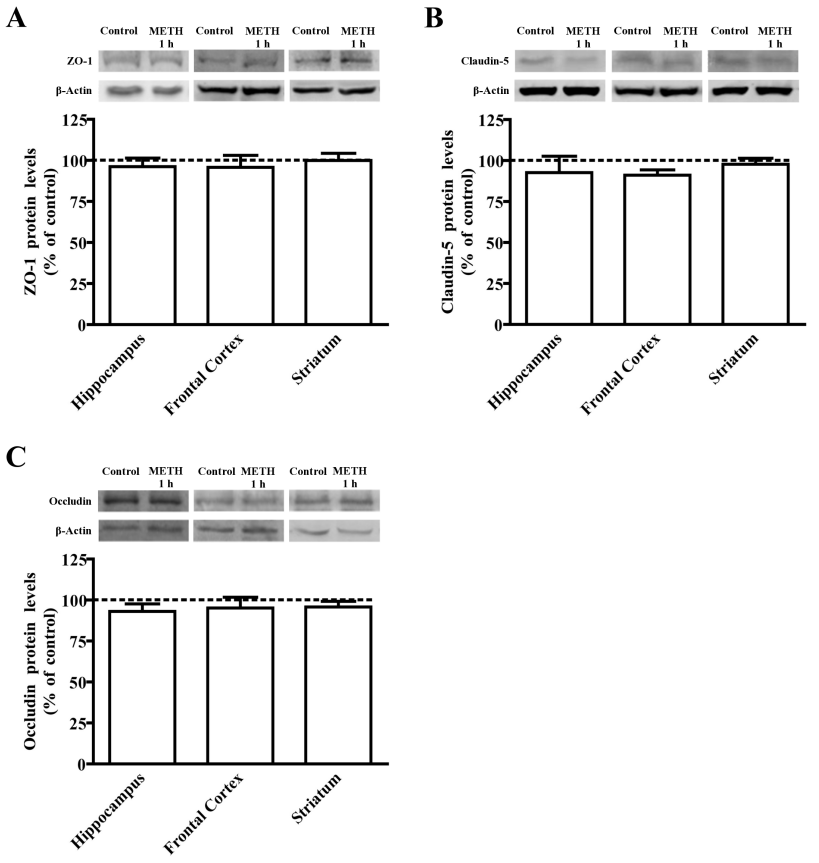

Fig. 2.4. Acute administration of methamphetamine (METH; 30 mg/kg, i.p.) had no effect on protein levels of (A) zonula occludens-1 (ZO-1), (B) claudin-5 and (C) occludin at 1 h post-administration in all the three brain regions analysed. Above the bars, representative western blots for ZO-1 (225 kDa), claudin-5 (24 kDa), occludin (65 kDa) and β-Actin (42 kDa) are shown.

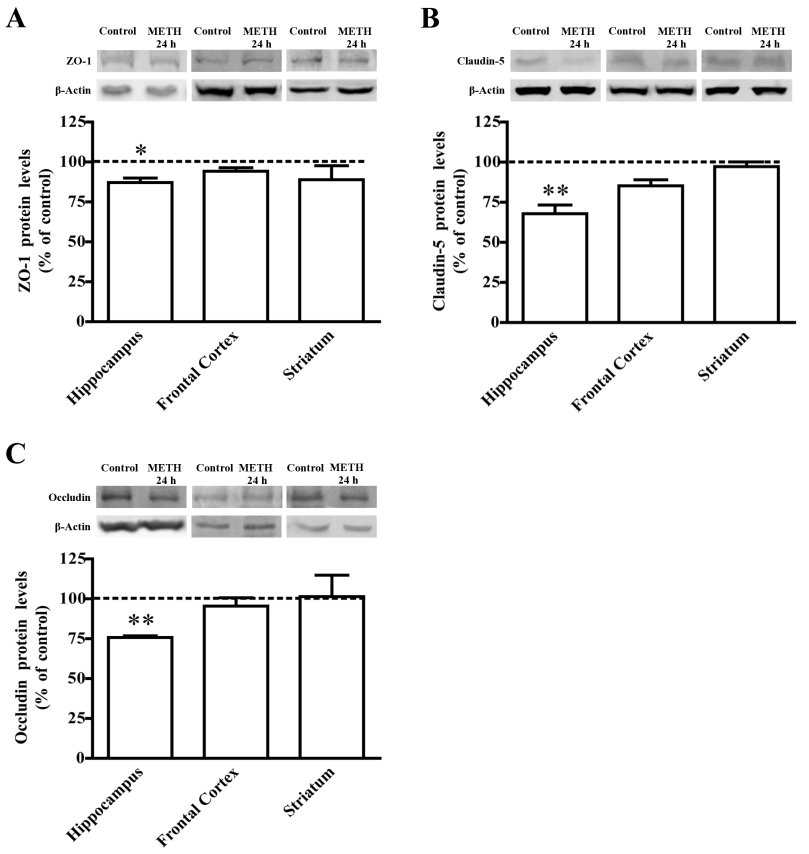

Fig. 2.5. Acute administration of methamphetamine (METH) decreases the protein levels of zonula occludens-1 (ZO-1), claudin-5 and occludin in the hippocampus. Quantification of (A) ZO-1 (225 kDa), (B) claudin-5 (24 kDa) and (C) occludin (65 kDa) protein levels in the hippocampus, frontal cortex and striatum at 24 h after METH administration (30 mg/kg, i.p.). Above the bars, representative western blots for ZO-1, claudin-5, occludin and β-Actin (42 kDa) are shown. The results are expressed as mean ± SEM (n=3-7). *p<0.05, **p<0.01, significantly different when compared to control (saline) using Bonferroni's multiple comparison test.

2.4.5. METH increases the activity and immunoreactivity of MMP-9

Besides TJs, there are other players, such as the MMPs, that can contribute to the impairment of the BBB, not only because they can degrade the neurovascular matrix, but also because they can degrade the TJ proteins. Previous studies showed that some MMP inhibitors are able to block the proteolysis of occludin in endothelial cells (Bojarski et al., 2004; Lohmann et al., 2004; Wachtel et al., 1999). Since we found that at 24 h post-METH administration there was an increase in BBB permeability and a decrease in TJ protein levels in the hippocampus, the effect of METH on the activity and immunoreactivity of MMP-9 was investigated only in this brain region and at this time point. In gelatine zymography analysis (Fig. 2.6), we detected the latent (105 kDa) and the active (97 kDa) MMP-9, and we found that, after METH treatment, the active form of MMP-9 in the hippocampus was increased (1.15±0.01 fold increase, $p<0.01$; Fig. 2.6).

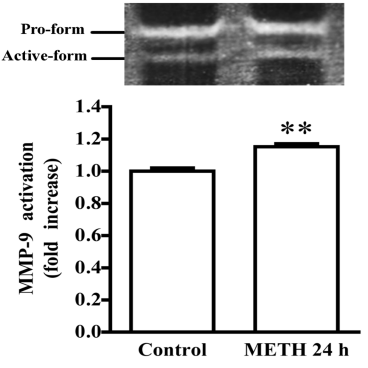

Fig. 2.6. Methamphetamine (METH) increases matrix metalloproteinase-9 (MMP-9) activity in the hippocampus. The relative activation of MMP-9 was calculated by dividing active MMP-9 proteolysis by total lysis (latent and active forms), and it shows that MMP-9 gelatinolytic activity was increased in the hippocampus at 24 h after METH injection (30 mg/kg, i.p.), when compared to the control. The results are expressed as mean ± SEM (n=3). $^{**}p< 0.01$, significantly different when compared to control (saline) using Student´s t-test.

We then analysed the immunoreactivity of MMP-9 in the hippocampus by immunohistochemistry, and we observed that at 1 h post-METH injection there were no changes in the MMP-9 immunoreactivity, whereas there was a significant increase in the MMP-9 immunoreactivity after 24 h (Fig. 2.7). Also, we observed a co-localization of MMP-9 with Hoechst, a nuclear marker, showing that MMP-9 is localised within the nucleus of cells (Fig. 2.7). Interestingly, this increase in MMP-9 immunoreactivity induced by METH was prevented by the pre-treatment with BB-94, a MMP inhibitor (Fig. 2.7). Moreover, at 24 h after METH injection, the MMP-9 immunoreactivity was similar to the control in the frontal cortex (Fig. 2.8A) and striatum (Fig. 2.8B), showing that the changes in MMP-9 expression occur specifically in the hippocampus. Due to the fact that several cell types could be the source of MMP-9 (Agrawal et al., 2008), we also performed double labelling to identify the cells that were expressing MMP-9. We concluded that MMP-9 did not co-localise with microglia (Fig. 2.9A) and astrocytic cells (Fig. 2.9B) but, in contrast, the double labelling with NeuN, a neuronal marker, showed that MMP-9 co-localised with the majority of neurons (Fig. 2.9C), indicating that after METH insult MMP-9 is expressed mainly by this cell type. Interestingly, by inhibiting MMP-9 with BB-94 it was possible to prevent the increase in permeability induced by METH in the hippocampus after 24 h (Fig. 2.10).

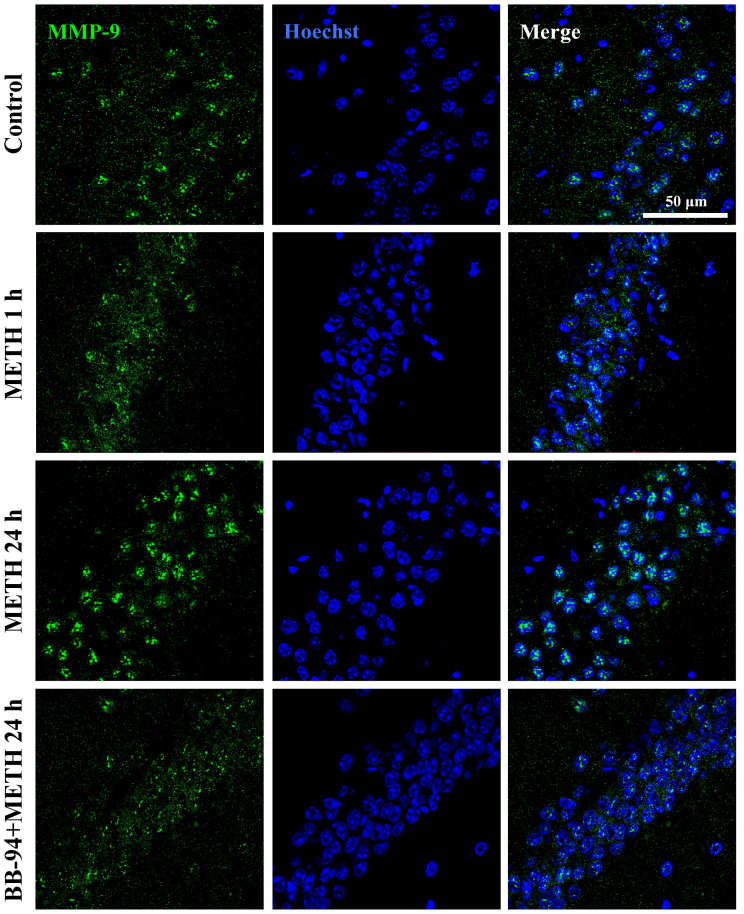

Fig. 2.7. The immunoreactivity of matrix metalloproteinase-9 (MMP-9) increases in the hippocampus at 24 h post-methamphetamine (METH) administration. Immunofluorescent labelling for MMP-9 (green) demonstrates an increase in its immunoreactivity at 24 h following METH injection, when compared to control (saline), without changes at 1 h. The pre-treatment with BB-94, a MMP inhibitor, prevented the METH-induced increase in MMP-9 immunoreactivity at 24 h. Total brain sections were also stained with Hoechst 33342 (blue) to visualise cellular organisation. Co-localisation of Hoechst fluorescence with MMP-9 immunoreactivity shows that MMP-9 is mainly localised within the nucleus. Scale bar = 50 µm. Representative images were chosen from the hippocampal subregion cornu ammonis field 1 (CA1) and were recorded using a confocal microscope.

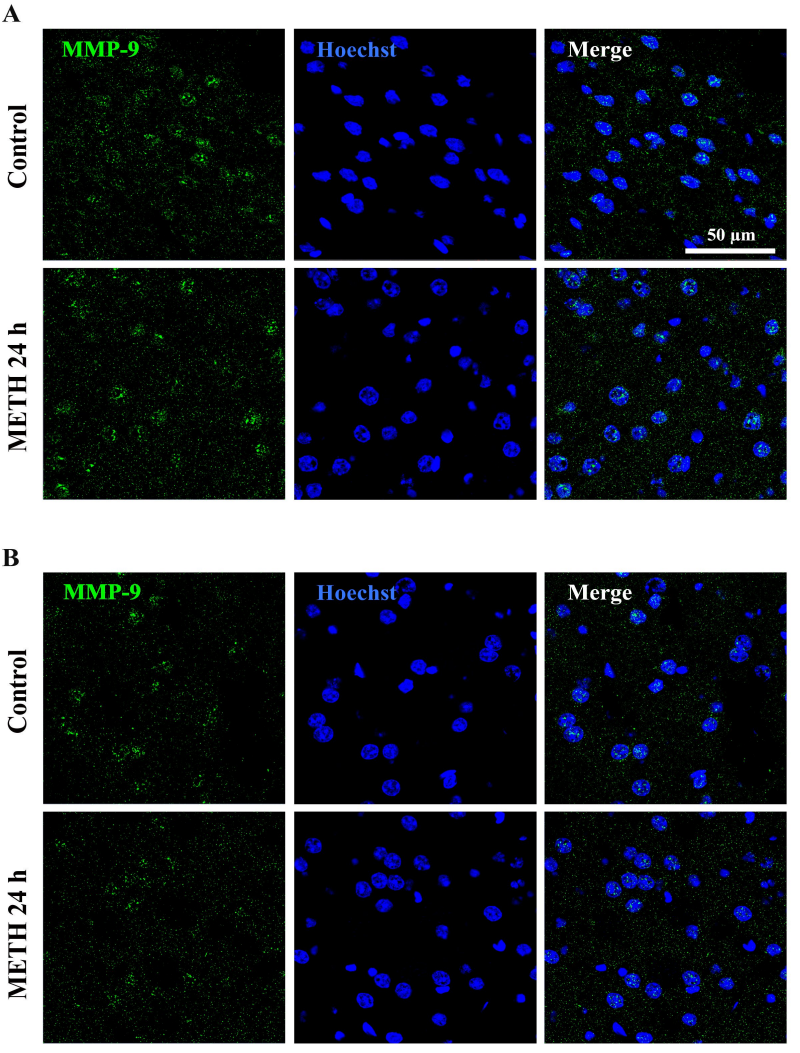

Fig. 2.8. Methamphetamine (METH) does not change the immunoreactivity of matrix metalloproteinase-9 (MMP-9) in the frontal cortex and striatum. Immunofluorescent labelling of MMP-9 (green) demonstrates that there were no changes in MMP-9 immunoreactivity at 24 h following METH injection (30 mg/kg, i.p.), when compared to the control (saline) in both (A) frontal cortex and (B) striatum. Total brain sections were also stained with Hoechst 33342 (blue) for nuclei staining. Representative images were recorded using a confocal microscope. Scale bar = 50 µm.

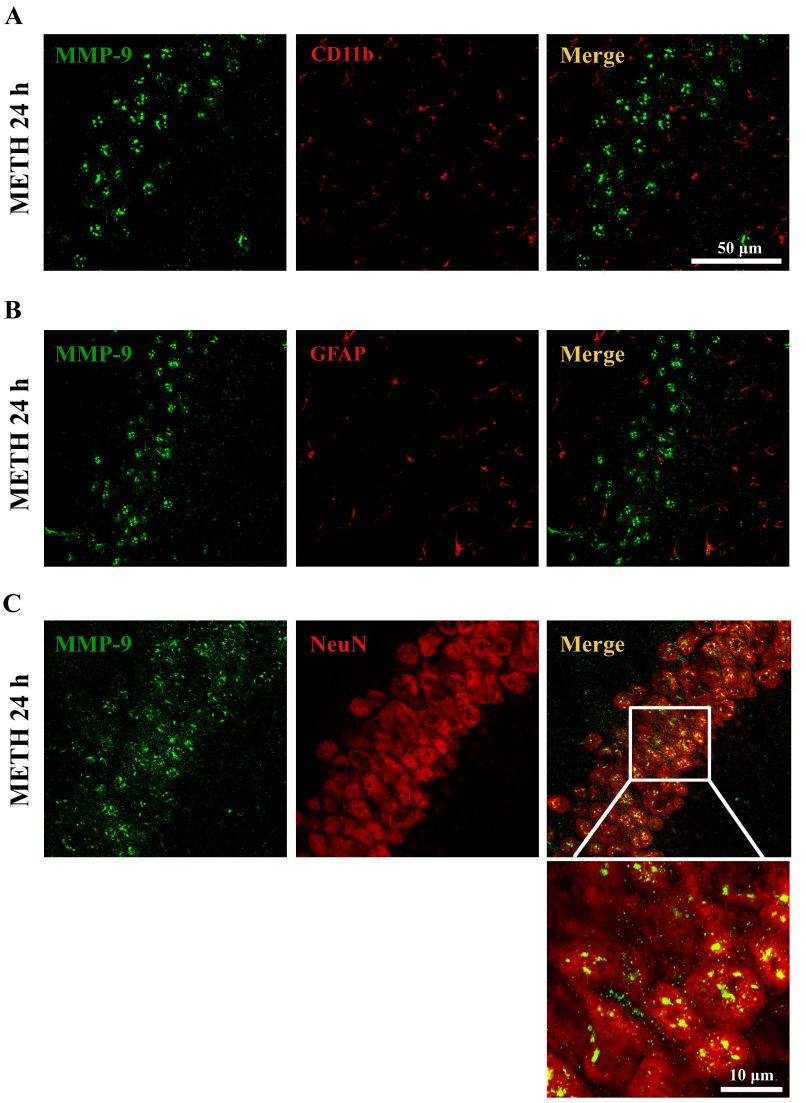

Fig. 2.9. Neurons are the main source of matrix metalloproteinase-9 (MMP-9) in the hippocampus. Images of the double-labelling of MMP-9 with (A) CD11b, (B) glial fibrillary acidic protein (GFAP), and (C) NeuN, at 24 h after METH administration. Scale bar = 50 µm. Representative images were chosen from the hippocampal subregion cornu ammonis field 1 (CA1) and were recorded using a confocal microscope. Small scale bar = 10 µm.

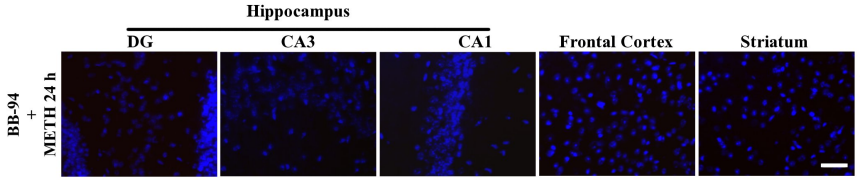

Fig. 2.10. BB-94, a matrix metalloproteinase inhibitor, prevents the methamphetamine (METH)-induced increase in Evans blue extravasation in the hippocampus after 24 h. Total brain sections were stained with Hoechst 33342 (blue), a nuclear marker, for visualisation of cellular organization. Scale bar = 50 μm.

2.5. Discussion

METH is a drug of abuse that causes several brain abnormalities (Thomas et al., 2004; Thomas and Kuhn, 2005a). However, the molecular and cellular mechanisms underlying its effects remain unclear. This drug is a lipophilic molecule and a weak base, with low molecular weight and low protein binding capacity, allowing an easy diffusion across plasma membranes and lipid layers (de la Torre et al., 2004). Due to its characteristics, rare are the studies where the drug levels that reach the brain were evaluated. Nevertheless, Melega and co-workers (1995) assessed plasma and brain kinetics of AMPH and METH from 5 to 60 min after administration (1 and 5 mg/kg, i.v.), and concluded that a dose-dependent increase in AMPH and METH plasma levels resulted in a proportional increase in striatum levels that were also equivalent for both drugs. More recently, METH and AMPH levels were determined in the hippocampus of C57BL/6J mice after one, three or four injections of 5 mg/kg METH, but no differences were detected among the different METH injection protocols for both METH and AMPH (Ladenheim et al., 2000). In the

present study, we went a step further by characterising the time-course changes in the levels of METH and AMPH in the plasma, and particularly the levels that reached the brain, in an animal model of METH intoxication. We concluded that, within 1 h, METH diffused to the circulation and rapidly reached the brain tissue by crossing the BBB. Moreover, 4 h after the administration, the levels of METH and AMPH in plasma and brain had decreased, but were still significantly increased compared to the control, indicating that METH metabolisation was occurring.

Once in the brain, METH leads to several abnormalities (Thomas et al., 2004; Thomas and Kuhn, 2005a). Very recently, Tobias and collaborators (2010) demonstrated that METH abusers show microstrutural abnormalities in white matter of the prefrontal cortex, in the genu of the corpus callosum, and in the hippocampus, which were associated with psychiatric symptoms. Moreover, METH-induced neurotoxicity can be caused by oxidative stress, mitochondrial dysfunction, excitotoxicity and inflammation (Quinton and Yamamoto, 2006; Yamamoto et al., 2010; Yamamoto and Raudensky, 2008). Despite the well documented harmful effects of METH in the brain, the impact of this drug on the BBB has been overlooked. Only recently, Sharma and Ali (2006) demonstrated that an acute high dose of METH (40 mg/kg) increases BBB permeability in the mouse cerebral cortex, as well as in the medial and ventral amygdala, hippocampus (Bowyer and Ali, 2006) and caudate-putamen (Bowyer et al., 2008), which was correlated with severe hyperthermia and extensive seizure activity. Moreover, in rats injected with a single dose of METH (9 mg/kg), the EB leakage observed in the nucleus accumbens was aggravated by brain hyperthermia (Kiyatkin et al., 2007). Here, we clearly

show that an acute high dose of METH increased BBB permeability after 24 h. Interestingly, among the three brain regions analysed, this effect was observed only in the hippocampus. Nevertheless, the reasons for the highest susceptibility of the hippocampus in our model remains to be further investigated. Also, a new finding was the transient increase of BBB permeability since at 72 h post-METH administration no EB leakage was detected. Additionally, mice did not develop seizures after METH administration, which suggest that seizures are not a prerequisite to increase BBB permeability in our animal model. The apparent contradiction between our and other results (Bowyer and Ali, 2006; Bowyer et al., 2008) can be explained by the use of different doses and different rodent species and strains.

It has been clearly shown that METH damages striatal dopaminergic terminals that seems to be preceded by microglia activation (Thomas et al., 2004; Thomas and Kuhn, 2005a), as well as by a significant increase in the reactivity of astrocytes in the striatum, cortex and hippocampus (Narita et al., 2008; Pubill et al., 2003; Simões et al., 2007). Indeed, we have also demonstrated that an acute high dose of METH induces astrogliosis, microglial activation and alterations in the tumour necrosis factor system in the hippocampus, without inducing cell death, only neuronal dysfunction (Gonçalves et al., 2010). Moreover, significant alterations in the rat hippocampal glutamatergic system were shown after administration of an acute high dose of METH (Simões et al., 2007). Thus, we can hypothesise that these events can be responsible, at least in part, for the specific increase of BBB permeability in the hippocampus shown in the present study. In fact, the neuroinflammatory events are accompanied by microglial activation, astrogliosis, and production of pro-inflammatory

cytokines, reactive oxygen species, and nitric oxide (Glass et al., 2010) that can lead to the disruption of the BBB (de Vries et al., 1996; Gloor et al., 1997; Pun et al., 2009; Thiel and Audus, 2001). Zhao and collaborators (2007) demonstrated that the increase in BBB permeability observed in 1-methyl-4-phenyl-1,2,3,6-tetrahydropyridine (MPTP)-treated mice or in tumour necrosis factor-alpha (TNF-α) knockout mice was attenuated by minocycline, an inhibitor of microglia activation. Regarding human studies, Thompson and collaborators (2004) showed for the first time the profile of structural deficits in the human brain associated with chronic METH abuse. Specifically, cortical maps revealed severe grey-matter deficits in the cingulate, limbic, and paralimbic cortices of METH abusers, and on average, these patients had 7.8% smaller hippocampal volumes than control subjects, and significant white-matter hypertrophy. These results suggest that chronic METH abuse causes a selective pattern of cerebral deterioration that contributes to impaired memory performance. Several explanations were raised for this selective damage, such as neuropil reduction, cell death and gliosis. In this study, we demonstrated that BBB function in the hippocampus is specifically impaired by METH, making this brain region highly susceptible to injury, which may justify the cognitive deficits showed by METH users.

In an attempt to clarify the mechanisms underlying the increased BBB permeability observed at 24 h after METH administration, we investigated potential changes in TJ proteins and MMPs. The TJ complex is the main responsible for the restriction of the paracellular transport of molecules across the BBB (Persidsky et al., 2006; Romero et al., 2003). It is composed by the transmembrane proteins occludin, claudins, and junctional adhesion molecules (JAMs) that in turn are connected to the actin cytoskeleton by

the intracellular accessory proteins ZO-1, -2 and -3 (Ballabh et al., 2004; Bazzoni and Dejana, 2004; Persidsky et al., 2006; Wolburg et al., 2009). The decrease or alteration in the arrangement of TJs lead to BBB disruption, a feature of many CNS pathologies like Parkinson's (Carvey et al., 2005; Drozdzik et al., 2003) and Alzheimer's disease, ischemic stroke (Lo et al., 2003; Sandoval and Witt, 2008), multiple sclerosis (Correale and Villa, 2007; McQuaid et al., 2009), encephalitis (Tunkel and Scheld, 1993), and AIDS-related dementia (Kanmogne et al., 2007). However, the alterations occurring in TJ and their contribution for brain dysfunction induced by drugs of abuse have been less explored. In accordance with the EB results, we also observed a decrease in the TJ proteins ZO-1, claudin-5 and occludin at 24 h post-METH administration only in the hippocampus, whereas at 1 h post-METH neither EB extravasation nor decrease in the TJ protein levels were observed. This correlation shows that the decrease in the TJ protein expression could be one of the causes of the increase in the permeability observed only in this brain region. Also, Ramirez and collaborators (2009) demonstrated that human brain endothelial cells treated with METH show low immunostaining and gap formation for occludin and claudin-5, as well as decrease in their protein expression. Protein phosphorylation can also interfere with the junctional integrity (Aijaz et al., 2006). A study relating the combination effect of METH and the viral protein gp120 on TJ proteins demonstrated that the treatment of human brain microvascular endothelial cells with gp120 alone decreased ZO-1, JAM-2 and claudin-3 gene expression, but had no effect in claudin-5 and occludin gene expression. However, a combination of METH and gp120 induced a higher decrease in the ZO-1, JAM-2, claudin-3, and claudin-5 levels while a significant increase in occludin was observed

(Mahajan et al., 2008). More recently, Banerjee and collaborators (2010) showed that repeated administrations of METH (10 mg/kg) potentiated the oxidative-stress induced by the viral proteins Tat and gp120. This combination of Tat with gp120 and METH also increased the BBB permeability and decreased the protein expression of occludin and ZO-1. All these changes were attenuated by the pre-treatment with a thiol antioxidant, suggesting a role of oxidative stress in the alteration of BBB permeability (Banerjee et al., 2010).

Besides TJ proteins, we also hypothesised that MMP-9 could be a key player in this process. The MMPs constitute a family of proteolytic enzymes of more than 20 members that require the binding of Zn^{2+} for their enzymatic activity (Yong, 2005). MMPs are involved in the remodelling and cleavage of the extracellular matrix, which have been implicated in the regulation of synaptic plasticity, and learning and memory (Agrawal et al., 2008). Moreover, the MMPs can be one of the causes of BBB disruption, since they can degrade the extracellular matrix of the basal membrane and also the TJ proteins (Bojarski et al., 2004; Lohmann et al., 2004; Wachtel et al., 1999). Based on these multiple evidence, we analysed the activity and expression of MMP-9 in the hippocampus, and we observed an increase in its activity and immunoreactivity in this brain region at 24 h post-METH injection. Accordingly, Liu and collaborators (2008) demonstrated that METH (10 and 40 mg/kg) increases the gene expression of MMP-9 in whole mouse brain (Liu et al., 2008), and rats treated repeatedly with METH (2 mg/kg) showed an increase in MMP-2 and -9 protein levels and activity in the nucleus accumbens and frontal cortex (Mizoguchi et al., 2007b). Different MMPs can be produced depending on the stimulus and cell type (Agrawal et al., 2008). Within the

hippocampus, MMP-9 is preferentially expressed by granular and pyramidal neurons (Szklarczyk et al., 2002). Thus, we also demonstrated that MMP-9 co-localised with neurons in the hippocampus. This increase in the expression and activity of MMP-9 could lead to the degradation of ZO-1, claudin-5 and occludin in the hippocampus, which can be responsible for the opening of the BBB observed in this brain region. In fact, both the inhibition of MMP-9 and the deletion of MMP-9 gene attenuate the BBB disruption (Rosenberg et al., 1998; Svedin et al., 2007). In our study, METH induced an increase in hippocampal MMP-9 immunoreactivity and activity after 24 h, which was correlated with the decrease in TJ protein levels and BBB disruption observed at the same time point and only in the hippocampus. Moreover, we observed that METH-induced increase in MMP-9 immunoreactivity and Evans blue leakage in the hippocampus were prevented by BB-94, a MMP inhibitor. These observations suggest that the increase in MMP-9 expression and activity contribute for the BBB breakdown induced by METH, and so, the inhibition of MMP-9 could be used as a target in order to prevent or minimise the BBB impairment caused by the consumption of this drug of abuse.

In conclusion, in this study we demonstrate that an acute high dose of METH induces a transient increase in the BBB permeability in the hippocampus. Moreover, our results suggest that the BBB breakdown is caused by the downregulation of the TJ proteins, namely ZO-1, claudin-5 and occludin, which may be also correlated with the increase in MMP-9 activity and expression by hippocampal neurons.

According with our and other recent results, we can speculate about the "dark and the bright side" of the effect of METH on BBB. Indeed, it is

obvious that the increase of BBB permeability by METH increases the probability of brain infection, including by HIV-1 since HIV-infected leukocytes can easily enter the brain under such conditions (Toborek et al., 2005). On the other hand, the transient opening of BBB induced by METH can be very useful as a therapeutic approach to allow the entry of drugs that do not cross the BBB under physiological conditions, in order to treat several brain diseases, such as chronic myelogenous leukaemia and glioblastoma (Kast, 2009; Kast and Focosi, 2010). In any case, it is of high importance to fully characterise the impact of this drug of abuse in the BBB and the present study is a step forward in the understanding of the BBB dysfunction induced by METH.

Chapter 3

Methamphetamine-induced nitric oxide promotes vesicular transport in blood-brain barrier endothelial cells

3.1. Abstract

Methamphetamine's (METH) neurotoxicity is thought to be in part due to its ability to induce blood-brain barrier (BBB) dysfunction. Here, we investigated the effect of METH on barrier properties of cultured rat primary brain microvascular endothelial cells (BMVECs). It was possible to conclude that transendothelial flux doubled in response to METH (1 μM), irrespective of the size of tracer used. At the same time, transendothelial electrical resistance was unchanged as was the junctional distribution of the adherens or tight junction proteins VE-cadherin, occludin, claudin-5 or zonula occludens-1, suggesting that METH promoted vesicular but not junctional transport. Indeed, METH significantly increased the uptake of horseradish peroxidase into vesicular structures. METH also enhanced transendothelial migration of lymphocytes indicating that the endothelial barrier against both molecules and cells was compromised. Importantly, barrier breakdown was only observed in response to METH at low micromolar concentrations. Moreover, the BMVEC response to METH (1 μM) involved rapid activation of endothelial nitric oxide synthase and its inhibition abrogated METH-induced permeability and lymphocyte migration, indicating that nitric oxide was a key mediator of BBB disruption in response to METH. This study underlines the key role of nitric oxide in BBB function and describes a novel mechanism of drug-induced fluid-phase transcytosis at the BBB.

3.2. Introduction

The BBB regulates the exchange of nutrients, waste and immune cells between the blood and the nervous tissue of the central nervous system (CNS) and is the most important component preserving CNS homeostasis and neuronal function (Abbott et al., 2010). Barrier function is epitomised by the restriction of ionic currents across the BBB, with electrical resistance reaching 1500-2000 $\Omega.cm^2$ *in vivo* (Butt et al., 1990). The barrier properties of the BBB are essentially conferred by the endothelial cells (ECs) of the brain capillary network. However, associated pericytes, astrocytes and the basement membrane also play an additional regulatory and structural role. Many BBB mechanisms can be modelled *in vitro* using monocultures of brain microvascular endothelial cells (BMVECs) (Perriere et al., 2007; Roux and Couraud, 2005). Importantly, such BMVEC models retain the features that render the BBB such a formidable barrier, namely a full complement of tight junctions (TJs), lack of fenestrations and low fluid-phase endocytosis (pinocytosis) (Abbott et al., 2010). At the healthy BBB, molecule transport in and out of the CNS is carried out by carrier-mediated transport systems or receptor- and adsorptive-mediated transcytosis. In certain pathological conditions, molecules can also cross the BBB endothelium non-specifically *via* a paracellular pathway. Indeed, BBB dysfunction involving transient or even chronic opening of TJs contributes to the pathogenesis of many diverse CNS pathologies, such as epilepsy, Parkinson's and Alzheimer's disease, and multiple sclerosis (Forster, 2008; Zlokovic, 2008). Interestingly, fluid-phase endocytosis or (macro)pinocytosis, which rarely occurs in the healthy BBB, has been reported to be enhanced in BBB ECs in response to hypoxic or ischemic

conditions (Kaur and Ling, 2008), indicating that the non-specific transport of molecules across the BBB in pathological conditions can also occur *via* the transcellular pathway.

Methamphetamine (METH) is a highly addictive psychostimulant with neurotoxic features. Like other amphetamines and because of its similarity to dopamine, METH causes monoamine release at neuronal synapses, primarily through the inhibition of plasmalemmal transporters such as the dopamine or the serotonin transporters (Cruickshank and Dyer, 2009). METH also causes long-term damage to monoaminergic nerve terminals by its ability to induce excitotoxicity, mitochondrial dysfunction and to increase the production of reactive oxygen and nitrogen species (ROS and RNS, respectively) (Quinton and Yamamoto, 2006). Because of its small size and lipophilicity, METH readily crosses the BBB by non-specific diffusion. In addition, METH can induce BBB dysfunction in rodents (Kiyatkin et al., 2007; Sharma and Ali, 2006), in particular in the limbic region (Bowyer and Ali, 2006; Martins et al., 2011). Thus, it is now assumed that, in addition to direct damage of monoaminergic nerve terminals, the deregulation of the BBB in these brain areas potentially contributes to widespread METH-induced neurotoxicity.

Nitric oxide synthases (NOS) convert L-arginine to produce the second messenger nitric oxide (NO). Two NOS isoforms exist in ECs: endothelial NOS (eNOS), which is expressed constitutively, and inducible NOS (iNOS), which is synthesised and utilized during long-term adaptation of the vasculature (Michel and Feron, 1997). In vascular ECs, eNOS regulates many key functions including angiogenesis, inflammatory and anti-inflammatory processes, and is the main responsible among all the molecules of the NOS system that regulates barrier function and

permeability (Fukumura et al., 2001; Schubert et al., 2002). The activity of eNOS is primarily regulated by reversible phosphorylation in response to various stimuli including VEGF, insulin or shear stress, and phosphorylation on S1177 is considered to be a reliable indicator of its activation status (Fleming, 2010). The activation and activity of eNOS is also intimately linked to that of caveolin-1 and caveolae and thus to fluid-phase endocytosis (Simionescu et al., 2009).

The purpose of the present study was to investigate the effect of METH in a system of primary BMVECs with very well-preserved TJs and barrier function. BMVEC permeability and the underlying mechanism were evaluated in response to METH exposure. Since nitric oxide production may play an important role in METH-induced monoaminergic neurotoxicity (Imam et al., 2000), we tested the role of eNOS in the METH-induced EC response. Given that pathophysiological BBB breakdown is often associated with enhanced leukocyte infiltration, alterations to lymphocyte migration were also studied.

3.3. Material and methods

3.3.1. Materials

Unless otherwise stated all materials were from Sigma. METH was provided by Drs Nuno Milhazes (Institute of Health Sciences-North, Gandra PRD, Portugal) and Fernanda Borges (Faculty of Sciences, University of Oporto, Portugal).

3.3.2. Brain microvascular endothelial cells (BMVECs)

Microvessels were isolated from brains of 6-8 week-old female Lewis rats (Abbott et al., 1992). The brains were removed and put into working buffer [Ca^{2+}- and Mg^{2+}-free Hanks's balanced saline solution (HBSS), buffered with 10 mM HEPES, containing 100 U/ml penicillin and 100 μg/ml streptomycin, with 0.5% bovine serum albumin (BSA)]. Cortices were isolated by removing cerebellum, striatum, optic nerves and brain white matter. Outer vessels and meninges were removed by rolling the cortices on dry lint. Brain material was then transferred to fresh working buffer and chopped with a scalpel into pieces of about 1-2 mm^3. The suspension was centrifuged at 600×*g*, at 4ºC for 5 min, and the pellet (from three brains) resuspended in 15 ml of digest medium [1 mg/ml collagenase/dispase, 20 units/ml DNAse I (deoxyribonuclear-5'oligonucleotideo-hydrolase) and 0.147 μg/ml TLCK (tosyl-lysine-chloromethyl-ketone) in Ca^{2+}- and Mg^{2+}-free HBSS containing 10 mM HEPES, 100 U/ml penicillin and 100 μg/ml streptomycin]. The cells were digested for 1 h at 37ºC, and the suspension was agitated gently every 15 min. After the digestion, the suspension was triturated with a Pasteur pipette and then centrifuged at 600×*g* for 5 min. The pellet was resuspended in 20 ml of 22% (w/v) BSA in PBS, and then centrifuged for 20 min at 1,000×*g*. After centrifugation, the top layers were poured off, and the capillary pellet was resuspended in working buffer and centrifuged for 5 min at 600×*g*. The pellet was then resuspended in 5 ml of digestion medium and incubated for 2h30 at 37ºC. After the incubation, the enzyme digest was centrifuged at 600×*g* for 5 min, the pellet was resuspended in 1 ml of working buffer and layered onto the pre-equilibrated 50% Percoll

gradient, and then centrifuged at 1,000×*g* for 20 min. The capillary fragments were then removed using a Pasteur pipette, suspended in working buffer and centrifuged at 600×*g* for 5 min. Microvessels were seeded onto collagen IV/fibronectin-coated tissue culture ware or 12-mm Costar Transwells (3460) at high density (vessels from 6 rat brains per 40 cm^2). Cells were grown in EGM2-MV (Lonza, Wokingham, United Kingdom) [with 5 μg/ml puromycin during the first 3 days (Perriere et al., 2007)] for 2 to 3 weeks until their transendothelial electric resistance (TEER) plateaued at values above 200 $\Omega.cm^2$. The immortalized Lewis rat cell line GPNT, which maintains many of the signalling and metabolic features of primary BMVECs, but not tight junctions and well-developed barrier properties (Martinelli et al., 2009; Roux and Couraud, 2005), was maintained in Ham's F10 supplemented with 10% fetal calf serum, 2 ng/ml bFGF, 100 U/ml penicillin and 100 μg/ml streptomycin.

3.3.3. Transendothelial flux

Fluorescein (FITC) or rhodamine B isothiocyanate (RITC)-dextran of 4, 70 or 250 kDa was added at 1 mg/ml to the apical side of BMVEC grown on 12-mm Transwell filters. Samples (50 μl) were removed from the basal chamber (and replaced by fresh medium) at 20-30 min intervals for 120 min before and after addition of METH and/or L-NG-Nitroarginine methyl ester (L-NAME). Fluorescence of samples was measured in a FLUOstar OPTIMA microplate reader (BMG LABTECH, Aylesbury, UK), plotted against time and permeability changes were determined from linear slope changes before and after addition of compounds.

3.3.4. Transendothelial electrical resistance (TEER)

TEER of primary brain EC monolayers was measured using STX-2 chopstick electrodes connected to an EVOM epithelial voltohmmeter (World Precision Instruments, Herts, UK). Real time TEER changes during METH treatment were monitored by impedance spectroscopy using a 1600R ECIS system (Applied Biophysics, Troy, NY, USA). For this, ECs were seeded on collagen type IV/fibronectin-coated 8W10E electrode arrays (Applied Biophysics). Impedance was measured at 4000 Hz and 10-min intervals. After the cells reached stable impedance, the ECs were either left untreated or treated with 1 or 50 μM METH, and the readings were acquired continuously for 4 h. Results were normalised and averaged from at least 3 independent experiments.

3.3.5. Immunocytochemistry

Confluent BMVEC were either left untreated or treated with 1 μM METH for 2 or 6 h. ECs were then fixed in 80% methanol, 3.2% formaldehyde, 0.05 M HEPES, pH 7.4 (-20ºC) for 5 min. After rinsing once with PBS and blocking (0.25% BSA in PBS) for 10 min, cells were incubated with primary antibodies at 37ºC for 1 h as follows: affinity purified anti-vascular endothelial cadherin (VEC) (1:50), anti-claudin-5 (1:100), occludin (1:50) and zonula occludens (ZO)-1 (1:50) (Zymed Lab, San Francisco, CA, USA). After washing twice with blocking solution, cells were incubated for 40 min at 37ºC with Cy3-conjugated anti-mouse (1:100; Jackson Immunoresearch Laboratories, West Grove, PA, USA) or fluorescein-conjugated anti-rabbit secondary antibodies (1:30; CAPPEL, MP Biomedicals LLC, Illkirch, France). Immunostained preparations were

mounted using Moviol 4-88 and analyzed on a confocal laser-scanning microscopy LSM 700 system (Carl Zeiss, Hertfordshire, UK). Series of overlapping 0.35 μm sections spanning the entire cell thickness were recorded.

3.3.6. Horseradish peroxidase transport

Horseradish peroxidase (HRP, 10 mg/ml) was added with or without 1 μM METH to the apical side of confluent primary BMVECs grown on 12-mm Costar Transwells filters. After 1 h cells were washed 3 times with warm HBSS containing Ca^{2+} and Mg^{2+} and new medium was added. Samples (100 μl) were removed from the basal chamber (and replaced by fresh medium) at 30-min intervals for 120 min. Samples were reacted with 100 μl of 1 mg/ml o-phenylenediamine and 1 μl/ml of 30% hydrogen peroxide and, after colour appearance, stopped with 100 μl of 1 N HCl. Absorbance of each sample was measured in a FLUOstar OPTIMA microplate reader (BMG LABTECH, Aylesbury, UK). HRP activity was plotted against time and rates determined by linear regression.

3.3.7. Electron microscopy

Primary ECs were grown to confluence on collagen type IV/fibronectin-coated polycarbonate filters. HRP (10 mg/ml) was added to the apical side of cells, and cells were either left untreated or treated with METH (1 μM). Where indicated, ECs were preincubated with L-NAME (1 mM, 1 h) before HRP and METH addition. After 1 h of incubation, monolayers were washed with Dulbecco's phosphate-buffered saline (DPBS) and then

fixed in 2% paraformaldehyde, 2% glutaraldehyde, in 0.05 M cacodylate buffer for 30 min. For the diaminobenzide (DAB) reaction, cells were incubated with 3% DAB, 30% hydrogen peroxide and imidazole in the dark for 30 min at RT. Cells were then incubated with 1.5% potassium ferricyanide, 1% osmium tetroxide for 1 h in the dark at 4°C, followed by a dehydration step, and finally embedded in Epon resin. The specimens were sectioned at 70 nm with no post-staining and visualised on a JEOL 1010 transmission electron microscope. The area and number of HRP-containing structures from METH treated-cells were normalised to the control values from non-treated cells, and represented as average per 1000 μm^2 of cytoplasm.

3.3.8. Western blot analysis

Primary or GPNT ECs were grown on collagen I-coated 35-mm dishes, and, at confluence, cultured in serum-free medium overnight. Cells were treated as detailed in the figures legends and then lysed in boiling 50 mM Tris/Cl, pH 6.8, 2% SDS, 10% glycerol, 100 mM DTT, 100 nM calyculin A (100 µl / 35-mm dish). Samples were subjected to SDS-PAGE and transferred to nitrocellulose by semidry electrotransfer. The membranes were then blocked for 2 h at RT in blocking solution [0.05 M tris buffered saline (TBS; pH 7.5) containing 5% BSA, 0.1% (v/v) Tween-20 and 0.1% (v/v) Triton X-100], and incubated with anti-phospho-eNOS (Ser1177) (1:1000; Cell Signaling Technology, Beverly, MA) overnight at 4ºC. Membranes were washed 3×10 min with TBS containing 0.1% BSA, 0.1% Tween-20 and 0.1% Triton X-100 before 1 h incubation with an ECL anti-rabbit IgG HRP secondary antibody (1:5000; GE Healthcare Life Science,

Buckinghamshire, UK). After washing 3×10 min in PBS containing 0.1% Tween-20 and 0.1% Triton X-100, membranes were developed using the ECL reagents (Roche Diagnostics, Burguess Hill, UK) according to the manufacturer's instructions and exposed to x-ray film. The blots were stripped and reprobed with an antibody against total eNOS (49G3) (1:1000; Cell Signaling Technology, Beverly, MA). Protein bands were evaluated by densitometric quantification using the ImageJ software.

3.3.9. Transendothelial lymphocyte migration

For migration assays, myelin basic protein (MBP)-specific rat T lymphocyte lines were used (established from Lewis rat lymph nodes). T-cells were cultured overnight at 1.5×10^6/ml in RPMI-1640 supplemented with 10% FCS, 100 U/ml penicillin, 100 μg/ml streptomycin, 1 mM sodium pyruvate, 1 mM nonessential amino acids, 2 mM L-Glu, and 50 μM β-mercaptoethanol in the presence of recombinant IL-2 (50 U/ml). Primary or GPNT BMVECs were grown to confluence in collagen I-coated 96-well plates, and treated as indicated in figure legends. ECs were washed extensively and then, 2×10^5 T-cells were added and allowed to migrate for 1 to 4 h. After the incubation, the migration and adhesion rates were determined by time-lapse video microscopy as described previously by Adamson et al (1999). Briefly, the cell cultures were placed on the stage of a phase-contrast inverted microscope, housed in a temperature controlled (37ºC) and 5% CO_2 gassed chamber, and recorded for 5 min using a camera linked to a time-lapse video recorder. Lymphocytes were identified and counted. Lymphocytes on the surface of the monolayer were identified by their highly refractive morphology (phase-bright) and

rounded or partially spread appearance, while cells that had migrated through the monolayer were phase-dark, higly attenuated, and moved slowly under de EC monolayer. Migration data was collected from multiple experiments, each representing a minimum of six wells.

3.3.10. MTT reduction assay

The 3-(4,5-dimethylthiazol-2-yl)-2,5-diphenyltetrazolium bromide (MTT) assay is a colorimetric assay that gives an indication of the cell viability. MTT is a yellow tetrazole that is reduced to purple formazan in living cells (Mosmann, 1983). Confluent GPNT ECs were treated with increasing concentrations of METH. After treatment, MTT (0.5 mg/ml) was added to each well. After 3 h of incubation (until the formation of crystals), 100 µl of the solution composed of 50% dimethylformamide and 50 mg/ml sodium dodecyl sulfate was added. The cells were kept at 37ºC overnight until all crystals dissolved. Absorbance of each well was measured in a Safire microplate reader (Tecan, Reading, UK) at 570 nm (reference filter at 620 nm).

3.3.11. Statistical analysis

Statistics were performed using one-way ANOVA, followed by Dunnett's or Bonferroni's post-test, and Student's *t*-test, as indicated in the figure legends. Data are presented as mean ± SEM, and the level of $p<0.05$ was accepted as statistically significant.

3.4. Results

3.4.1. METH-induced increase in macromolecular flux across EC monolayers is mediated by eNOS

To investigate cellular and molecular mechanisms underlying METH-induced changes of the BBB we studied the response of BMVECs to METH *in vitro*. Unless stated otherwise, freshly prepared primary rat BMVEC (Perriere et al., 2007) were used. These cells retained many characteristics of the intact BBB such as the expression of continuous adherens and tight junctions (see Fig. 3.3), low permeability to macromolecules ($0.113\pm0.016 \times 10^{-3}$ cm/min for 4 kDa FITC-dextran, n=11), and high transendothelial electrical resistance (TEER = 345 ± 30 $\Omega.cm^2$). For this study, only BMVEC monolayers, which displayed a TEER of at least 200 $\Omega.cm^2$, were used. The blood concentrations of METH in drug abusers are in the low micromolar range, with a medium concentration of 1.25 μM (Melega et al., 2007). Based on this, macromolecular flux of fluorescent dextrans across primary BMVEC monolayers was measured in the absence or presence of 1 μM METH. Treatment with METH resulted in a 2.07 ± 0.31 fold increase ($p<0.01$) of 4 kDa FITC-dextran flux (Fig. 3.1A). Interestingly, this increase remained unchanged even when the flux of considerable larger tracers, 70 kDa RITC- and 250 kDa FITC-dextrans (2.29 ± 0.39 and 2.11 ± 0.12 fold increase, respectively; $p<0.01$), was assessed (Fig. 3.1B and C, respectively). The effect of METH on endothelial electrical barrier properties was also measured by impedance spectroscopy. Impedance (and consequently the TEER) of primary rat BMVEC monolayers was not altered by the exposure to 1 μM METH (Fig. 3.1D), whereas lysophosphatidic acid (10

μM LPA) produced a strong and transient opening of the ionic barrier (Fig. 3.1D). Taken together, this suggested that junctional transport, which is size-selective and usually involves concomitant changes in TEER (Steed et al., 2010), was not affected by exposure to METH.

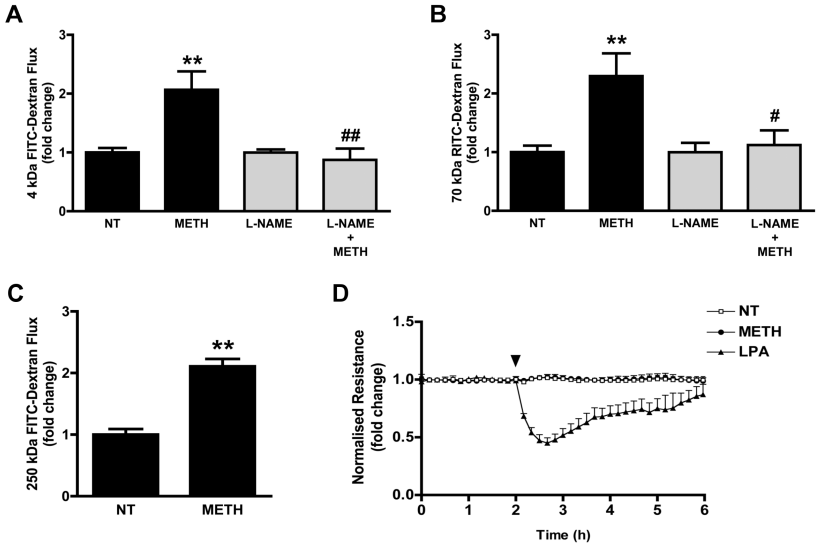

Fig. 3.1. Methamphetamine (METH)-induced increase in barrier permeability in primary brain microvascular endothelial cells (BMVECs). (A-C) Macromolecular flux across primary BMVEC was assessed using (A) 4 kDa fluorescein isothiocyanate (FITC)-dextran, (B) 70 kDa rhodamine B isothiocyanate (RITC)-dextran or (C) 250 kDa FITC-dextran. Flux was determined before and after the addition of METH (1 μM). Where indicated the cells were pre-treated with L-NAME (1 mM, 1 h) (grey bars). (**D**) Transendothelial electrical resistance (TEER) of confluent BMVECs monolayers, grown on gold electrodes, was measured by impedance spectroscopy before and after the addition (arrowhead) of 1 μM METH or 10 μM lysophosphatidic acid (LPA). All results shown are means ± SEM of at least three independent experiments. Note that only positive SEM are shown. $^{**}p<0.01$, Dunnett's post test vs untreated cells (NT); $^{\#}p<0.05$, $^{\#\#}p<0.01$, Bonferroni's post test vs METH.

Since eNOS activation is functionally linked to endothelial permeability (Fukumura et al., 2001; Schubert et al., 2002), we further investigated whether eNOS inhibition attenuated the effects of METH in BMVECs permeability. Pre-treatment of primary BMVEC with L-NAME (1 mM) completely inhibited the METH-induced increase of macromolecular flux to 4 kDa FITC- and 70 kDa RITC-dextrans (0.87±0.19 and 1.12±0.25 fold increase; Fig. 3.1A and B, grey columns, respectively). Activation of eNOS was also determined by measuring phosphorylation on S1177. Exposure of primary BMVECs to 1 μM METH induced eNOS S1177 phosphorylation (Fig. 3.2A). Levels of eNOS phosphorylation increased significantly within 30 min of METH exposure (1.44±0.13 fold increase; $p<0.05$), plateaued after 1 h, and persisted for at least 2 h (1.69±0.09 and 1.63±0.15 fold increase, respectively; $p<0.01$). We observed a similar response to METH in the GPNT BMVEC cell line, indicating that the biochemical response to METH was preserved even after EC immortalisation (Fig. 3.2B). In GPNT ECs, the levels of eNOS phosphorylation increased significantly within 15 min of METH exposure (1.51±0.15 fold increase; $p<0.05$), plateaued after 30 min, and persisted for at least 1 h (1.72±0.22 and 1.75±0.07 fold increase, respectively; $p<0.01$). Taken together, these data indicated that eNOS activation and the consequent NO production was involved in METH-induced increase in permeability.

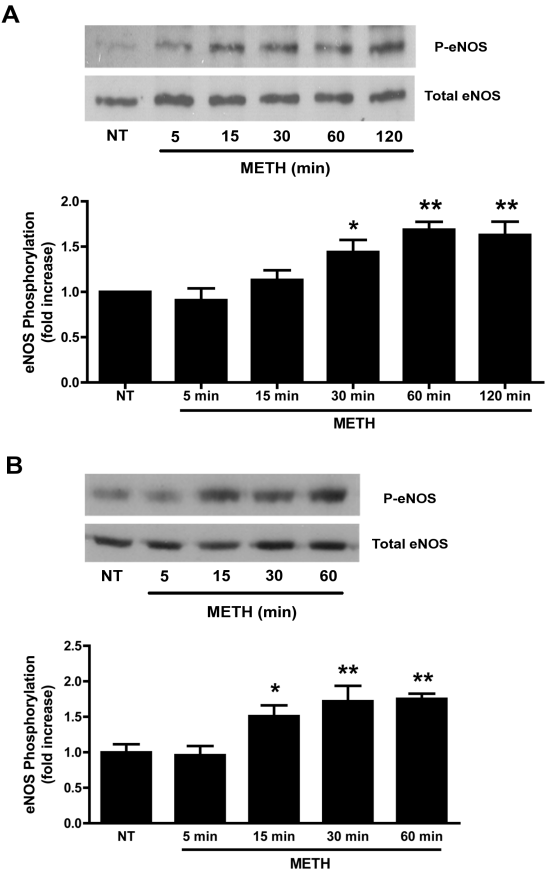

Fig. 3.2. Methamphetamine (METH) activates endothelial nitric oxide synthase (eNOS) in brain microvascular endothelial cells (BMVECs). (**A**) Primary BMVECs were either left untreated (NT) or treated with METH (1 μM) for the indicated times. Total protein extracts (ca. 50 μg) were analysed by immunoblotting with an anti-phospho (P)-S1177 eNOS antibody. The blot was subsequently stripped and probed for total eNOS. (**B**) As in A, except that GPNT BMVECs were used. Densitometric quantification (normalised means ± SEM) of three independent experiments is shown in the bottom panel. *p<0.05, **p<0.01 (Dunnett's post test vs NT).

3.4.2. Endothelial junction organisation in response to METH treatment

We examined the effect of METH on the organisation of some of the major junction proteins in BMVEC by immunocytochemistry followed by confocal microscopy (Fig. 3.3). In unstimulated cells, staining of VE-cadherin (VEC), occludin and zonula occludens-1 (ZO-1) was restricted to areas of cell-cell interaction and surrounded the entirety of each cell in uninterrupted fashion (Fig. 3.3A). Claudin-5 immunostaining was very similar but could also be detected on apical membranes. Treatment with 1 μM METH for 2 or 6 h did not disrupt the continuity of any junction staining. For VEC and occludin, additional staining was observed in parajunctional areas (Fig. 3.3A and B). Diffuse parajunctional VEC staining, which in unstimulated cells was only seen in tricellular areas and which is thought to represent junctional flow (Kametani and Takeichi, 2007), was frequently found along long stretches of bicellular junction areas in METH-treated cells. In the case of occludin, the METH-induced parajunctional staining was less diffuse but very punctate in appearance and primarily found in tricellular areas. At least in the case of METH-induced parajunctional VEC accumulation, staining accumulated in an area clearly distinct of the intact junctional strand (as identified by claudin-5 staining) (Fig. 3.3C). Collectively, our data indicated that METH did not induce global changes to interendothelial junctions but may have enhanced the flow/turnover of certain junctional proteins.

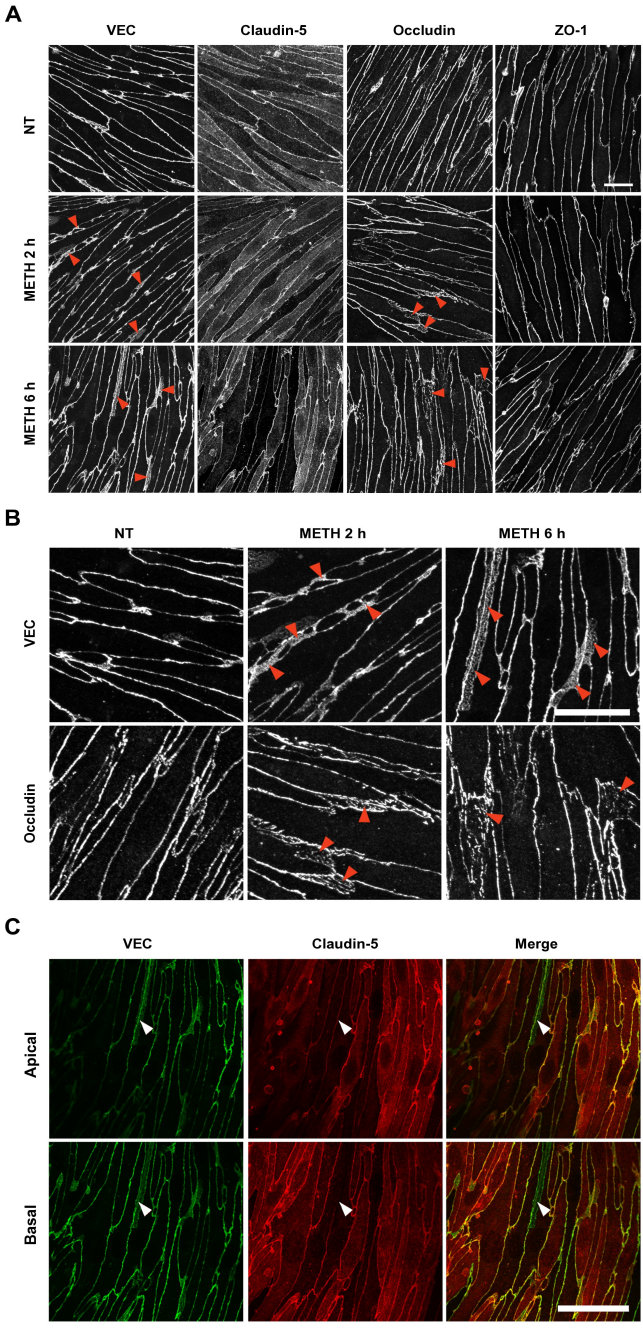
A
VEC
Claudin-5
Occludin
ZO-1
NT
METH 2 h
METH 6 h
B
NT
METH 2 h
METH 6 h
VEC
Occludin
C
VEC
Claudin-5
Merge
Apical
Basal

Fig. 3.3. Effect of methamphetamine (METH) on the organisation of the interendothelial junctions. (**A-C**) Primary brain microvascular endothelial cells (BMVECs) were either left untreated (NT) or treated with METH (1 μM) for 2 or 6 h. Subsequently, cells were fixed and stained for vascular endothelial cadherin (VEC), claudin-5, occludin and zonula occludens (ZO)-1, and then analysed by confocal microscopy. Shown are representative projections of overlapping 0.35 μm sections spanning the entire cell thickness. METH exposure did not disrupt the continuity of any junction staining. However, additional VEC and occludin staining was also observed at parajunctional areas in METH-treated cells (red arrowheads). Enlarged regions of the staining for VEC and occludin are shown in (B). (C) Shows apical and basal sections of BMVEC treated with METH for 6 h and stained for VEC and claudin-5. White arrowheads depict an uninterrupted interendothelial junction (as determined by the claudin-5 staining), which was also intact as judged by VEC staining. Additional diffuse VEC staining could be found in areas basal to the junction. Scale bars = 20 μm.

3.4.3. METH promotes endocytosis in BMVECs

METH-induced permeability in ECs was not paracellular, since permeability occurred without changes in TEER and without significant alterations in the structure of the junctions. Thus, we investigated whether the increased macromolecular flux was due to transcytosis. To test this, unidirectional, non-junctional HRP flux was measured. For this, BMVEC were allowed to take up apically presented HRP for 1 h in the absence or presence of METH. Then, all extracellular HRP was washed off before comparing basal HRP efflux rates. As shown in Fig. 3.4A, HRP efflux was increased 1.77±0.11 fold ($p<0.001$) in the BMVEC treated with 1 μM METH, which was a similar increase as seen for METH-induced continuous apical-to-basal dextran flux. HRP-treated cells were further analysed by electron microscopy (EM). DAB staining revealed the presence of HRP-containing vesicular structures in all cells (Fig. 3.4B). HRP was detected in large structures with a diameter of at least 150 nm (morphologically resembling lysosomes), and much smaller vesicles.

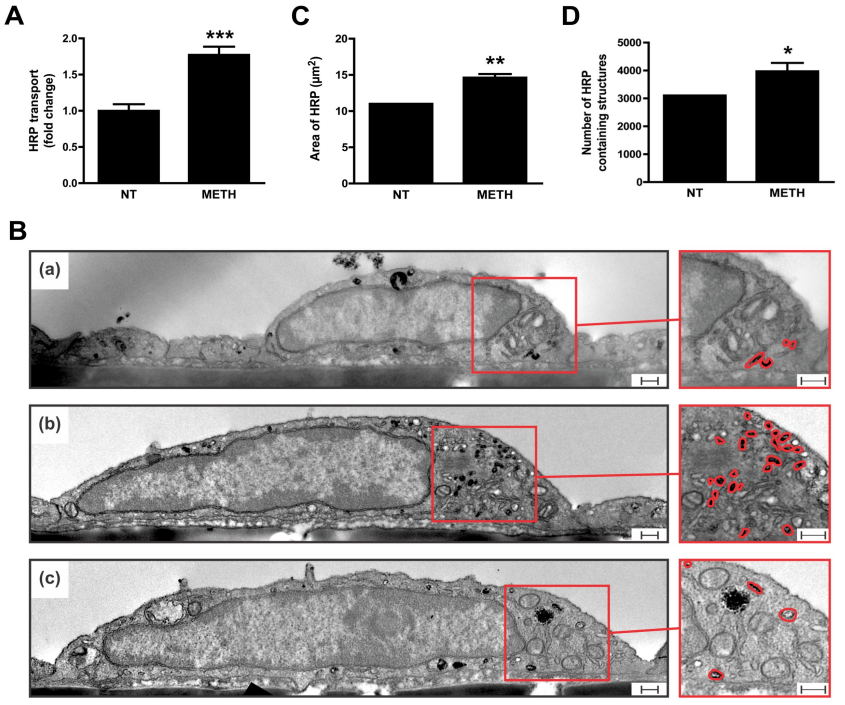

Fig. 3.4. Methamphetamine (METH) enhances transcytosis in brain microvascular endothelial cells (BMVECs). (A) Primary rat BMVECs were either left untreated (NT) or treated with METH (1 μM) for 1 h in the presence of horseradish peroxidase (HRP) on the apical side of cells. HRP was then removed and the rate of its transport to the basal side determined and compared. (**B-D**) Uptake of HRP by primary BMVECs visualised using transmission electron microscopy (EM). Cells were either [B(a)] left untreated or [B(b and c)] treated with METH (1 μM) and incubated with HRP in the apical media for 1 h before fixing and processing for HRP visualisation (using DAB) and transmission EM. [B(c)] Additional pre-treatment with L-NAME (1 mM, 1 h) prevented METH-induced accumulation of HRP-containing structures. Shown are representative images in which electron dense DAB reaction products revealed the presence of HRP-containing compartments. Scale bar = 250 nm. Densitometric quantification of the (C) area of DAB staining or (D) number of DAB-positive vesicles per 1000 μm² of cytoplasm, showing a significant increase with METH treatment. The results are expressed as mean ± SEM of at least three independent experiments. *p<0.05, **p<0.01, ***p<0.001 (Student's t-test), significant when compared to NT.

METH treatment did not affect HRP uptake into the large vesicular structures but significantly increased HRP in small vesicles [Fig. 3.4B(b)]. In fact, the area of such DAB staining increased nearly 1.5-fold (14.63±0.49 μm²; $p<0.01$; Fig. 3.4C). This was at least in part due to a significantly higher number of DAB-positive vesicles (3972±299; $p<0.05$; Fig. 3.4D). Transcytosis in ECs occurs mainly *via* caveolae (Predescu et al., 2007), and eNOS activation is also functionally linked to caveolae (Maniatis et al., 2006). In fact, L-NAME prevented the accumulation of HRP-positive vesicles in response to METH [Fig. 3.4B(c)], which is in accordance with the previous permeability results (Fig. 3.1A and B, grey columns). In addition, transmission EM revealed numerous plasma membrane invaginations reminiscent of caveolae but not HRP-positive clathrin-coated vesicles (Fig. 3.5). Collectively, these data demonstrated that METH-induced permeability in BMVECs was mediated by fluid-phase transcytosis, and that eNOS activation was involved in this process.

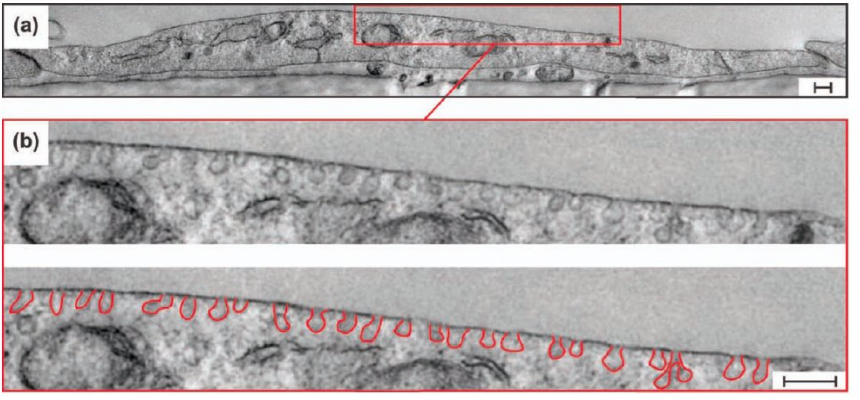

Fig. 3.5. Plasmalemmal caveolar structures in primary brain microvascular endothelial cells (BMVECs). Primary rat BMVECs were fixed and processed for transmission EM. (a) Shown is a representative image [and a magnified section in (b)], which demonstrated the presence of caveolar structures (outlined in red) on the apical plasma membrane. Scale bars = 200 nm.

3.4.4. Enhanced lymphocyte transendothelial migration (TEM) following METH treatment is mediated by eNOS activation

The BBB not only forms a formidable regulated barrier to blood borne molecules but also to immune and cancer cells (Weil et al., 2005; Greenwood et al., 2011). Thus, we analysed the effect of METH on lymphocyte TEM across primary BMVEC monolayers. Pre-treatment with 1 μM METH for 30 min or 2 h resulted in a significant increase in the number of T-cells that migrated across primary ECs (184.30±4.79 and 177.77±9.97% of control, respectively; $p<0.01$; Fig. 3.6A). Similarly, exposure of immortalised GPNT ECs to 1 μM METH for 30 min also enhanced TEM of T-cells (153.93±7.84% of control; $p<0.01$; Fig. 3.6B). Moreover, we concluded that eNOS activation is involved in lymphocyte TEM (Martinelli et al., 2009). In fact, pre-treatment of primary BMVEC with L-NAME also prevented enhanced lymphocyte TEM in response to METH (100.75±15.85% of control; Fig. 3.6A). This suggested that METH induced dysfunction of the endothelial barrier against cells and molecules alike, and eNOS activation was central to METH-induced barrier impairment.

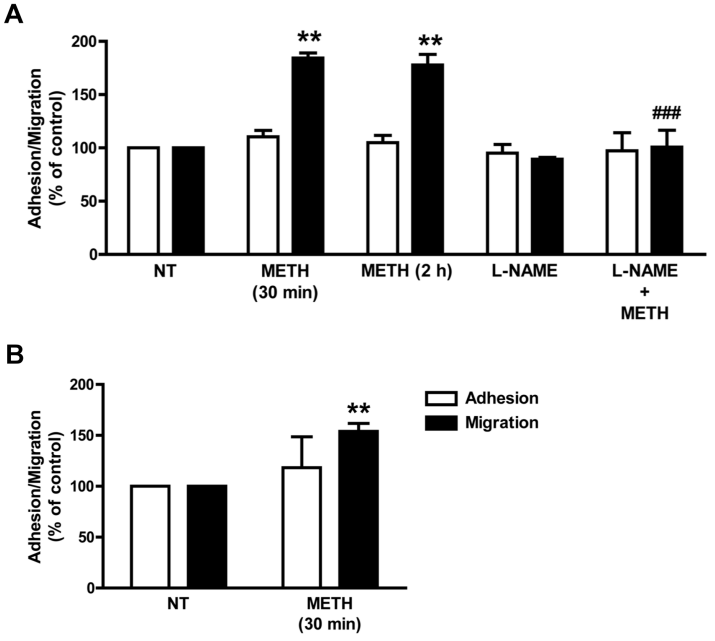

Fig. 3.6. Methamphetamine (METH) enhances transendothelial lymphocyte migration. (**A**) Primary brain microvascular endothelial cells (BMVECs) were either left untreated (NT) or treated with METH (1 μM) for the indicated times. Cells were then washed before myelin basic protein (MBP)-specific rat lymphocytes were added and allowed to adhere and migrate for 4 h. Pre-incubation with L-NAME (1 mM, 1 h) prevented the increase in migration induced by exposure to METH for 30 min. Shown are adhesion (white bars) and migration rates (black bars) as % of control cells (NT) (mean ± SEM of six replicates from at least three independent experiments). $^{**}p<0.01$, Dunnett's post test vs NT; $^{\#\#\#}p<0.001$, Bonferroni's post test vs METH 30 min. (**B**) As in A, except that lymphocytes were allowed to adhere and migrate across GPNT BMVECs for 1 h. $^{**}p<0.01$, Student's t-test vs NT.

3.4.5. Absence of effects following exposure to higher METH concentrations

We also tested the effect of higher METH concentrations in our model systems. Importantly, the treatment with METH at concentrations of up to 100 μM for 24 h did not affect GPNT ECs viability (Fig. 3.7).

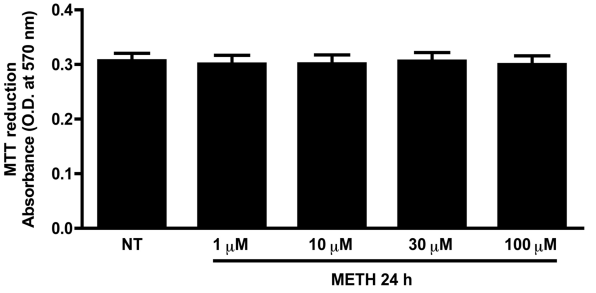

Fig. 3.7. Effect of methamphetamine (METH) on cell viability. GPNT endothelial cells (ECs) were either left untreated (NT) or treated with the indicated concentrations of METH during 24 h. The results are expressed as means ± SEM of four replicates from three independent experiments.

Moreover, ECs were exposed to METH at concentrations varying between 1 and 100 μM, and 1 h later, eNOS activation was measured. We observed that only exposure to METH at 1 μM led to eNOS activation (1.89±0.09 fold increase; $p<0.01$; Fig. 3.8A). In view of the central role of eNOS in METH–induced barrier dysfunction, these results suggested that higher METH concentrations might not affect barrier properties of BBB ECs *in vitro*. Indeed, when permeability changes across primary BMVECs were assessed in response to 50 μM METH, we found no effect on macromolecular flux to 4 kDa FITC- and 70 kDa RITC-dextrans

(0.94±0.07 and 1.08±0.14 fold increase; Fig. 3.8B and C, respectively) or TEER (Fig. 3.8D). Furthermore, a higher concentration of METH (50 μM) did not affect lymphocytes TEM either (104.44±8.79% of control; Fig. 3.8E). Collectively, these data suggest that, in our BBB *in vitro* models, METH concentrations higher than 1 μM do not affect eNOS activity, EC permeability or lymphocyte TEM.

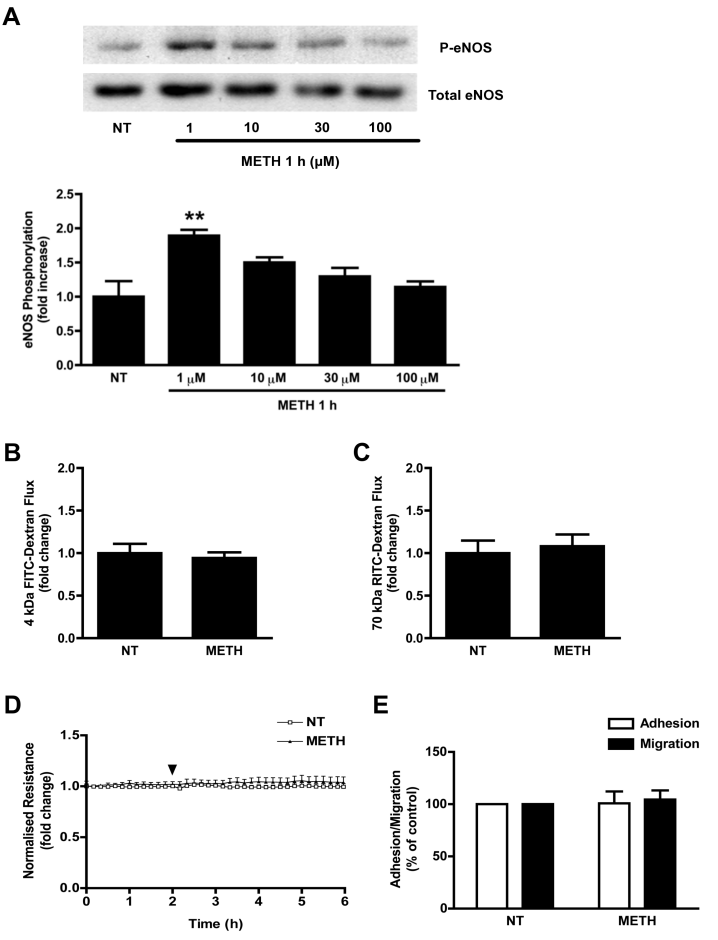

Fig. 3.8. Effect of higher methamphetamine (METH) concentrations in brain microvascular endothelial cells (BMVECs). (**A**) Quantification of eNOS protein levels in GPNT BMVECs that were either left untreated (NT) or treated with METH during 1 h with the indicated METH concentrations. Above the bars, representative western blots for phospho(P)-eNOS (140 kDa) and total eNOS (140 kDa) are shown. $^{**}p<0.01$, Dunnett´s post test vs NT. (**B, C**) Changes in flux of (B) 4 kDa FITC-dextran or (C) 70 kDa RITC-dextran across primary BMVECs in response to 50 μM METH. (**D**) Transendothelial electric resistance (TEER) was measured in monolayers of primary BMVECs in response to 50 μM METH. (**E**) GPNT ECs were either left untreated or treated with METH (50 μM, 30 min) before lymphocyte adhesion (white) and migration (black) was determined.

3.5. Discussion

METH directly damages dopaminergic and serotonergic nerve terminals, but also induces BBB dysfunction, which is thought to contribute to its neurotoxicity (Silva et al., 2010). It is conceivable that BBB dysfunction is an indirect result of pathophysiological changes following METH administration, such as hyperthermia and seizures (Kiyatkin et al., 2007). In the present study and in agreement with a previous published work (Ramirez et al., 2009), we demonstrate that METH acts directly on cultured primary BMVEC to compromise their barrier properties. In addition, we provide mechanistic evidence that barrier breakdown was due to eNOS activation and enhanced transcytosis.

For our study, we have used primary rat BMVEC as a system of high reproducibility and statistical robustness. We introduced modifications to standard isolation procedures, namely selection with puromycin (Perriere et al., 2007) and direct seeding at high density (extensive growth periods of BMVEC lead to loss of TJ proteins), to generate monocultures of high purity and unmatched barrier properties as assessed by TJ protein expression and TEER. Exposure of these cells to METH did not affect interendothelial junction integrity. Despite mild changes to the staining pattern of VEC and occludin, which suggested altered protein turnover, the lateral continuity of all assessed junction proteins remained unchanged following METH exposure. In agreement, changes in TEER, considered a robust readout for junction opening (Steed et al., 2010), were not observed in response to METH. Rather than enhanced paracellular permeability, we found clear evidence for enhanced transcytosis in response to METH. Dextrans of varying size and HRP were transported at equally enhanced

rate, suggesting that fluid-phase transcytosis was operational (Hawkins and Egleton, 2008). Accordingly, electron microscopy showed numerous plasma membrane invaginations similar to caveolae. This is in line with the notion that caveolae are the principal vesicular structure for transcytosis in ECs (Predescu et al., 2007; Simionescu et al., 2009). Significantly, METH also induces fluid-phase endocytosis in cultured neurons (Nara et al., 2010), suggesting that this response may not be restricted to ECs. Non-specific fluid-phase transcytosis is rarely observed in the healthy BBB endothelium (Abbott et al., 2010), but has been associated with hypertension, hypoxia and ischemia, although effector mechanisms are unknown (Cipolla et al., 2004; Kaur and Ling, 2008). Here we provide the first evidence that fluid-phase transcytosis across BMVEC can be directly enhanced by a small molecule, namely METH.

BBB dysfunction often results in increased leukocyte TEM. Exposure to METH enhanced lymphocyte TEM, in agreement with reports using a low barrier BMVEC line and monocytes (Ramirez et al., 2009; Park et al., 2012). Leukocyte TEM utilises both paracellular and transcellular pathways (Muller, 2011). Since the effective dose of METH left endothelial junctions intact and increased vesicular transport in primary BMVECs, it appears likely that transcellular TEM was enhanced. Vesiculo-vacuolar organelles (VVOs), which form channels for the passage of macromolecules and are responsible for enhanced permeability in the tumour vasculature, were initially suggested as possible endothelial structures that could mediate transcellular migration (Hordijk, 2006). Subsequently, Muller and co-workers showed that the lateral border recycling compartment (LBRC), a membrane reticulum involved in membrane and junction protein trafficking in cell border areas of ECs, is implicated in regulating both

transcellular and paracellular TEM (Muller, 2011). As judged by transmission EM, METH typically induced HRP uptake into large groups of juxtapositional vesicular structures, which were restricted to a single area of the cell (as illustrated in Fig. 3.4B). Since images were derived from 70 nm thick sections it was impossible to determine whether HRP was taken up into isolated vesicles or a reticulum similar or identical to the LBRC. Thus, METH may influence membrane availability and/or dynamics of the LBRC or the VVOs and thus diminish barrier properties to molecules and cells in BMVECs.

Both METH-enhanced transcytosis and TEM were sensitive to pre-treatment with the NOS inhibitor L-NAME. Since effective doses of METH also led to robust eNOS activation and iNOS could not be detected at any time during our experiments, we conclude that eNOS activation and consequent NO production are key factors of METH-induced BBB breakdown. Activation of neuronal NOS and the production of NO and derivatives also occur in METH-stimulated neurons and have been implicated in associated dopaminergic neurotoxicity (Imam et al., 2000), suggesting again that cellular METH targets may be similar in neurons and ECs. In the endothelium, eNOS is instrumental in regulating vascular permeability (Fukumura et al., 2001; Schubert et al., 2002). Activation of eNOS and NO production are also limiting factors of lymphocyte TEM across BMVEC (Martinelli et al., 2009). Thus, by activating eNOS, METH clearly modulated a central regulator of BMVEC barrier function. Most cytotoxicity associated with NO is due to peroxynitrite, the reaction product between NO and the superoxide anion (Pacher et al., 2007). Our study did not address whether barrier breakdown was merely due to NO or rather peroxynitrite. However, acute

microvascular permeability and lymphocyte TEM are mainly dependent on NO but not superoxide production (Martinelli et al., 2009; Duran et al., 2010). Furthermore, we were unable to detect any cytotoxicity in BMVEC in response to METH, suggesting that oxidative stress and peroxynitrite production was not induced.

Typical METH abuse leads to accumulation of the drug in blood plasma at sub or low micromolar concentrations (Cook et al., 1992; Harris et al., 2003; Melega et al., 2007). In primary rat BMVEC, eNOS activation and subsequent barrier breakdown was only observed in response to METH at low micromolar concentrations, suggesting that the BBB is compromised under typical abuse conditions. Higher METH concentrations did not induce eNOS or molecular or cellular barrier dysfunction. This raises the possibility that several targets with different affinities for METH exist in ECs. Alternatively, higher concentrations of METH may induce rapid down regulation of the EC response and render it undetectable. Finally, higher METH concentration may also lead to the activation of another signalling pathway counteracting the primary response described in this report. Indeed, higher concentrations of METH lead to the generation of reactive oxygen species (Fleckenstein et al., 2007; Ramirez et al., 2009; Park et al., 2012), which may subsequently neutralise the bioavailable NO. Nevertheless, it is unclear whether research into the BMVEC response to higher METH concentration is justified since concentrations of METH higher than 30 μM are associated with lethality in humans (Takayasu et al., 1995).

In summary, our results suggest that METH-induced opening of the BBB involves eNOS/NO-mediated transcytosis. Apart from providing important mechanistic insight into METH-induced neurotoxicity, our work

also identifies a potentially novel strategy for drug delivery into the brain. METH has been suggested for such use before (Kast, 2009), but our finding of a link to non-specific fluid-phase transcytosis, which is usually absent at the BBB, increases the significance of potential use for this purpose. To fully assess the possibility of agonist-induced opening of the BBB, future work should focus on identifying the endothelial targets of METH and the structural determinants of METH that are important for BMVEC deregulation. Potentially, this could lead to the design of non-psychostimulant METH derivatives that maintain the capacity to transiently open the BBB without associated toxicity to monoaminergic nerve terminals.

Chapter 4

General Discussion

General Discussion

METH causes several brain abnormalities (Thomas et al., 2004; Thomas and Kuhn, 2005a), but also induces BBB dysfunction, which is thought to contribute to its neurotoxicity (Silva et al., 2010). Since the molecular and cellular mechanisms underlying METH-induced BBB dysfunction remain to be clarified, we first aimed to investigate how METH induces its effects on BBB in an animal model of METH intoxication.

In the present study, we started by characterising the time-course changes in the levels of METH and AMPH in the plasma, and particularly the levels that reached the brain in our animal model, since this has never been addressed before. METH is a lipophilic molecule and a weak base, with low molecular weight and low protein binding capacity, allowing an easy diffusion across plasma membranes and lipid layers (de la Torre et al., 2004). Accordingly, we showed that, within 1 h, METH diffused to the circulation and rapidly reached the brain tissue by crossing the BBB. Furthermore, 4 h after the administration, the levels of METH and AMPH in plasma and brain were still significantly increased.

Analysing the effect of METH on BBB permeability, we found that an acute high dose of METH increased BBB permeability at 24 h. This was a transitory effect since at 72 h post-METH administration no leakage of EB dye was detected. Interestingly, this effect was observed only in the hippocampus, among the three brain regions analysed (hippocampus, frontal cortex and striatum), but the reasons underlying the highest susceptibility of the hippocampus in our model remain to be further investigated. Nevertheless, an acute high dose of METH was shown to induce astrogliosis, microglial activation, alterations in the tumour necrosis

factor system, and neuronal dysfunction in the mice hippocampus (Gonçalves et al., 2010). Also, rats administered with an acute high dose of METH showed significant alterations in the hippocampal glutamatergic system (Simões et al., 2007). Thus, we hypothesise that these events can be responsible, at least in part, for the specific increase of BBB permeability in the hippocampus observed in the present study. In fact, neuroinflammation is characterised by microglial activation, astrogliosis, and production of pro-inflammatory cytokines, ROS, NO, among other events (Glass et al., 2010), which can lead to the disruption of the BBB (de Vries et al., 1996; Gloor et al., 1997; Pun et al., 2009; Thiel and Audus, 2001). Additionally, glutamate and its receptors are also involved in BBB breakdown (Koenig et al., 1992; Mayhan and Didion, 1996; Sharp et al., 2003; Westergren and Johansson, 1992). In human studies, cortical maps revealed severe grey-matter deficits in the cingulate, limbic, and paralimbic cortices of chronic METH abusers, and on average, these patients had 7.8% smaller hippocampal volumes than control subjects, and significant white-matter hypertrophy (Thompson et. al., 2004), suggesting that chronic METH abuse causes a selective pattern of cerebral deterioration that leads to memory impairment. In the present study, we demonstrated that METH specifically impairs the BBB function in the hippocampus, making this brain region highly susceptible to injury, which may justify in part the cognitive deficits showed by METH abusers.

TJ proteins confer the low paracellular permeability characteristic of the BBB, and alterations on the content of the TJs have been linked to the impairment of BBB function (Petty and Lo, 2002). Thus, in order to clarify the mechanisms underlying the observed increase in BBB permeability induced by METH, we investigated whether METH administration could

induce changes in TJ proteins. We detected a decrease in the protein levels of ZO-1, claudin-5 and occludin at 24 h post-METH administration, but only in the hippocampus, which was in accordance with the EB results. Moreover, at 1 h after METH injection neither EB extravasation nor decreases in the TJ protein levels were observed. This correlation suggests that the decrease in the content of TJ proteins might be the cause of the increased BBB permeability observed only in the hippocampus.

MMPs can also contribute to the impairment of BBB by their ability to degrade the neurovascular matrix and also the TJ proteins. Thus, we hypothesised that MMP-9 could be a key player in mediating METH-induced BBB disruption. We observed that METH increased the activity and immunoreactivity of MMP-9 in the hippocampus at 24 h after METH administration. This increase in the expression and activity of MMP-9 correlated with the decrease in TJ protein levels and BBB disruption observed at the same time point. In fact, MMP-9 could lead to the degradation of ZO-1, claudin-5 and occludin in the hippocampus, being responsible for the opening of the BBB observed in this brain region. Moreover, we found that METH-induced increase in MMP-9 immunoreactivity and EB leakage was prevented by pre-treatment with BB-94, a MMP inhibitor, which proves that the increase in MMP-9 expression and activity contributes for the BBB disruption induced by METH. Based on this evidence, we suggest that the inhibition of MMP-9 could be used as a target in order to prevent or minimise the BBB impairment caused by the consumption of high doses of METH.

Besides animal studies, we also aimed to investigate how METH directly affects the BBB. For that, we studied the response of BMVECs to METH *in vitro*. METH concentrations in the blood plasma of drug abusers are

found at sub or low micromolar range. Thus, in this study, rat BMVECs were exposed to a METH concentration (1 μM) that is relevant in the context of METH abuse. We demonstrate that METH increased the macromolecular flux of dextrans of varying size across BMVEC monolayers. However, changes in TEER were not observed in response to METH. In agreement, despite mild changes in the staining pattern of VEC and occludin, which suggested altered protein turnover, the lateral continuity of VEC, occludin, claudin-5 and ZO-1 remained unchanged following METH exposure. This suggested that METH-induced permeability in ECs was not paracellular. In fact, we found that vesicular uptake of HRP by BMVEC was increased in response to METH. With these results, we provide the first evidence that fluid-phase transcytosis across BMVEC can be directly enhanced by METH.

Moreover, BBB impairment is often associated with enhanced leukocyte infiltration. So, alterations to lymphocyte migration were also addressed, and we demonstrated that exposure to METH enhanced lymphocyte TEM across BMVECs. Since METH exposure left endothelial junctions intact and increased vesicular transport in primary BMVECs, it appears likely that transcellular TEM was enhanced. One possible explanation is that METH may influence membrane availability and/or dynamics of the LBRC and thus diminish barrier properties to cells.

In the endothelium, eNOS plays an important role in the regulation of vascular permeability (Fukumura et al., 2001; Schubert et al., 2002). In addition, activation of eNOS and NO production are limiting factors of lymphocyte TEM across BMVEC (Martinelli et al., 2009). Thus, we investigated if eNOS could be a key player in mediating METH effects on BMVECs. We concluded that METH led to robust eNOS activation, and

that METH-enhanced macromolecular flux, transcytosis and TEM were prevented by the NOS inhibitor L-NAME. These results suggest that eNOS activation and consequent NO production are key factors of METH-induced BBB breakdown.

In this study, we also demonstrate that high METH concentrations did not induce eNOS activation or molecular/cellular barrier dysfunction. One explanation for this finding is the possible existence of several targets with different affinities for METH in ECs. Alternatively, higher concentrations of METH may induce rapid down regulation of the EC response and render it undetectable. Another hypothesis is that such concentrations may lead to the activation of other signalling pathway(s) counteracting the primary response described in this report. In fact, higher concentrations of METH lead to the generation of reactive oxygen species (Fleckenstein et al., 2007; Ramirez et al., 2009; Park et al., 2012), which may subsequently neutralise the bioavailable NO. Here, we did not detect any cytotoxicity in BMVEC in response to METH, suggesting that oxidative stress and peroxynitrite production was not induced.

The results obtained *in vitro* appear to contradict those found in animal studies. While in mice, METH administration led to alterations in the TJ proteins and increased paracellular permeability, *in vitro,* the exposure to METH appears to increase fluid-phase transcytosis in ECs without major alterations in TJ proteins. These can be explained, at least in part, by the different experimental models and rodent species used in both studies, as well as the different METH concentrations, since the effects of METH are dose/concentration-dependent. Moreover, in the animal model the alterations in the BBB were detected at 24 h post-METH injection, and the increased activity of MMP-9 (produced by neurons) seemed to be

implicated in those effects. In addition, at 24 h the concentration of METH in the plasma and brain was vestigial, thus, it is likely that BBB disruption results from the interaction/crosstalk between the components of the neurovascular unit with other neuronal cells that culminate in BBB breakdown. *In vitro,* increased fluid-phase transcytosis in EC monolayers was detected within 1 h of exposure to METH (1 μM), and these results demonstrate the direct effect of METH exclusively in ECs, with no influence from other neural cells, which does not happen *in vivo*. Besides, the transcytosis seems to be promoted by NO production by eNOS in the ECs. The effects of NO can vary depending on the expression, activity and localisation of NOS isoforms, as well as concentrations reached in the tissue and duration of NO exposure, and cellular sensitivity to NO (Fukumura et al., 2006). Also, METH increases the expression of both iNOS and nNOS in the mice brain (Deng and Cadet, 1999; Granado et al., 2011; Wu et al., 2006). Thus, *in vivo,* it is plausible to suggest that METH might also induce NO production by induction of iNOS as well as by nNOS activation in other cell types, which can lead to a response and effect on BBB ECs. Taken this, it would be important to evaluate the possible occurrence of fluid-phase transcytosis and NO production in an animal model, using a lower dose of METH.

In summary, the results presented in this study provide a better understanding of the mechanisms underlying METH-induced BBB dysfunction. Using an animal model of METH intoxication, we demonstrate that an acute high dose of METH induces a transient increase in the permeability of the hippocampal BBB. Moreover, our results suggest that the BBB breakdown is caused by the downregulation of the TJ

proteins, namely ZO-1, claudin-5 and occludin, which may be also correlated with the increase in MMP-9 activity and expression by hippocampal neurons. In addition, our *in vitro* studies suggest that METH is also able to increase BBB permeability by enhancing fluid-phase transcytosis and increases lymphocyte TEM. Both effects are suggested to be eNOS/NO-mediated.

Apart from providing important mechanistic insight into METH-induced neurotoxicity, our work also identifies a potentially novel strategy for drug delivery into the brain in order to treat several CNS diseases, such as brain tumours (Kast, 2009; Kast and Focosi, 2010). METH has been suggested for such use before (Kast, 2009), but our finding of a link to non-specific fluid-phase transcytosis, which is rare at the BBB, associated with the transient effect on BBB opening, raises the potential use of METH for this purpose. Still, it is of high importance to fully characterise the effects of this drug in the BBB by identifying its endothelial targets as well as the structural determinants of METH that are involved in BMVEC deregulation. Potentially, this could lead to the design of non-psychostimulant METH derivatives that maintain the capacity to transiently open the BBB without associated neurotoxicity.

Chapter 5

Main Conclusions

Main Conclusions

The main conclusions of the present dissertation are the following:

1. METH increases the BBB permeability at 24 h after drug administration, and this is a transient effect since at 72 h there is no increase in the extravasation of EB dye.

2. Comparing to frontal cortex and striatum, the hippocampus is the most susceptible brain region to METH, since the increase in BBB permeability was observed only in the hippocampus.

3. METH decreased the content of TJ proteins only in the hippocampus at 24 h after drug-injection, which correlates with the increase in the permeability detected only in this brain region and at this time-point.

4. MMP-9 activity and immunoreactivity are increased in the hippocampus at 24 h post-METH administration, suggesting a contribution of MMP-9 to the BBB disruption induced by METH.

5. The increase in MMP-9 immunoreactivity and EB leakage triggered by METH was prevented by BB-94, a MMPs inhibitor, suggesting that a similar strategy could be used to prevent or attenuate the effects of METH consumption on BBB impairment.

6. Relatively low concentrations of METH increase the permeability of monolayers of brain microvascular endothelial cells by promoting fluid-phased transcytosis.

7. METH enhances T-lymphocyte transendothelial migration across brain microvascular endothelial cells.

8. The METH-induced fluid-phased transcytosis on BMVECs and T-lymphocyte TEM are mediated by the activation of eNOS.

Conclusões

As principais conclusões da presente dissertação são as seguintes:

1. A MET aumenta a permeabilidade da BHE às 24 h após a administração, e este efeito é transitório visto que às 72 h não se detectou um aumento no extravasamento do corante azul de Evans.

2. Em comparação com o córtex frontal e o estriado, o hipocampo é a região cerebral mais susceptível à MET, uma vez que o aumento de permeabilidade da BHE foi detectado apenas no hipocampo.

3. A administração de MET diminuiu os níveis das proteínas das junções oclusivas apenas no hipocampo e às 24 h, o que se correlaciona com o aumento da permeabilidade detectado apenas nesta região cerebral e a este tempo.

4. A MET aumenta a actividade e a imunoreactividade da MMP-9 no hipocampo às 24 h após a sua administração, sugerindo uma contribuição da MMP-9 para a disfunção da BHE induzida pela MET.

5. O aumento da imunoreactividade da MMP-9 e o extravasamento do corante azul de Evans induzido pela MET foi prevenido pelo composto BB-94, um inibidor das MMPs, sugerindo que a inibição da MMP-9 pode ser utilizada como uma estratégia para prevenir ou atenuar os efeitos resultantes do consumo de MET na função da BHE.

6. Concentrações relativamente baixas de MET induzem um aumento de permeabilidade em monocamadas de células endoteliais microvasculares cerebrais através da promoção de transcitose de fase-fluida.

7. A MET aumenta a migração transendotelial de linfócitos-T através de monocamadas de células endoteliais microvasculares cerebrais.

8. A transcitose de fase-fluida nas células endoteliais microvasculares cerebrais e a migração transendotelial de linfócitos-T induzidas pela MET são mediadas pela activação da eNOS.

Chapter 6

References

References

Abbott, N.J., 2005. Dynamics of CNS barriers: evolution, differentiation, and modulation. Cell Mol Neurobiol. 25, 5-23.

Abbott, N.J., Hughes, C.C., Revest, P.A., Greenwood, J., 1992. Development and characterisation of a rat brain capillary endothelial culture: towards an in vitro blood-brain barrier. J Cell Sci. 103 (Pt 1), 23-37.

Abbott, N.J., Patabendige, A.A., Dolman, D.E., Yusof, S.R., Begley, D.J., 2010. Structure and function of the blood-brain barrier. Neurobiol Dis. 37, 13-25.

Abbott, N.J., Ronnback, L., Hansson, E., 2006. Astrocyte-endothelial interactions at the blood-brain barrier. Nat Rev Neurosci. 7, 41-53.

Abbruscato, T.J., Davis, T.P., 1999. Protein expression of brain endothelial cell E-cadherin after hypoxia/aglycemia: influence of astrocyte contact. Brain Res. 842, 277-286.

Abbruscato, T.J., Lopez, S.P., Mark, K.S., Hawkins, B.T., Davis, T.P., 2002. Nicotine and cotinine modulate cerebral microvascular permeability and protein expression of ZO-1 through nicotinic acetylcholine receptors expressed on brain endothelial cells. J Pharm Sci. 91, 2525-2538.

Acikgoz, O., Gonenc, S., Kayatekin, B.M., Uysal, N., Pekcetin, C., Semin, I., Gure, A., 1998. Methamphetamine causes lipid peroxidation and an increase in superoxide dismutase activity in the rat striatum. Brain Res. 813, 200-202.

Adamson, P., Etienne, S., Couraud, P.O., Calder, V., Greenwood, J., 1999. Lymphocyte migration through brain endothelial cell monolayers involves signaling through endothelial ICAM-1 via a rho-dependent pathway. J Immunol. 162, 2964-2973.

Aghajanian, A., Wittchen, E.S., Allingham, M.J., Garrett, T.A., Burridge, K., 2008. Endothelial cell junctions and the regulation of vascular permeability and leukocyte transmigration. J Thromb Haemost. 6, 1453-1460.

Agrawal, S.M., Lau, L., Yong, V.W., 2008. MMPs in the central nervous system: where the good guys go bad. Semin Cell Dev Biol. 19, 42-51.

Aijaz, S., Balda, M.S., Matter, K., 2006. Tight junctions: molecular architecture and function. Int Rev Cytol. 248, 261-298.

Aloisi, F., 2001. Immune function of microglia. Glia. 36, 165-179.

Arora, H., Owens, S.M., Gentry, W.B., 2001. Intravenous (+)-methamphetamine causes complex dose-dependent physiologic changes in awake rats. Eur J Pharmacol. 426, 81-87.

Arundine, M., Tymianski, M., 2003. Molecular mechanisms of calcium-dependent neurodegeneration in excitotoxicity. Cell Calcium. 34, 325-337.

Asahi, M., Asahi, K., Jung, J.C., del Zoppo, G.J., Fini, M.E., Lo, E.H., 2000. Role for matrix metalloproteinase 9 after focal cerebral ischemia: effects of gene knockout and enzyme inhibition with BB-94. J Cereb Blood Flow Metab. 20, 1681-1689.

Asanuma, M., Tsuji, T., Miyazaki, I., Miyoshi, K., Ogawa, N., 2003. Methamphetamine-induced neurotoxicity in mouse brain is attenuated by ketoprofen, a non-steroidal anti-inflammatory drug. Neurosci Lett. 352, 13-16.

Aurrand-Lions, M., Johnson-Leger, C., Wong, C., Du Pasquier, L., Imhof, B.A., 2001. Heterogeneity of endothelial junctions is reflected by differential expression and specific subcellular localization of the three JAM family members. Blood. 98, 3699-3707.

Balda, M.S., Matter, K., 2000. The tight junction protein ZO-1 and an interacting transcription factor regulate ErbB-2 expression. EMBO J. 19, 2024-2033.

Balda, M.S., Whitney, J.A., Flores, C., Gonzalez, S., Cereijido, M., Matter, K., 1996. Functional dissociation of paracellular permeability and transepithelial electrical resistance and disruption of the apical-basolateral intramembrane diffusion barrier by expression of a mutant tight junction membrane protein. J Cell Biol. 134, 1031-1049.

Ballabh, P., Braun, A., Nedergaard, M., 2004. The blood-brain barrier: an overview: structure, regulation, and clinical implications. Neurobiol Dis. 16, 1-13.

Banerjee, A., Zhang, X., Manda, K.R., Banks, W.A., Ercal, N., 2010. HIV proteins (gp120 and Tat) and methamphetamine in oxidative stress-induced damage in the brain: potential role of the thiol antioxidant N-acetylcysteine amide. Free Radic Biol Med. 48, 1388-1398.

Barr, A.M., Panenka, W.J., MacEwan, G.W., Thornton, A.E., Lang, D.J., Honer, W.G., Lecomte, T., 2006. The need for speed: an update on methamphetamine addiction. J Psychiatry Neurosci. 31, 301-313.

Barreiro, O., Yanez-Mo, M., Serrador, J.M., Montoya, M.C., Vicente-Manzanares, M., Tejedor, R., Furthmayr, H., Sanchez-Madrid, F., 2002. Dynamic interaction of VCAM-1 and ICAM-1 with moesin and ezrin in a novel endothelial docking structure for adherent leukocytes. J Cell Biol. 157, 1233-1245.

Battaglia, G., Fornai, F., Busceti, C.L., Aloisi, G., Cerrito, F., De Blasi, A., Melchiorri, D., Nicoletti, F., 2002. Selective blockade of mGlu5 metabotropic glutamate receptors is protective against methamphetamine neurotoxicity. J Neurosci. 22, 2135-2141.

Bauer, P.M., Fulton, D., Boo, Y.C., Sorescu, G.P., Kemp, B.E., Jo, H., Sessa, W.C., 2003. Compensatory phosphorylation and protein-protein interactions revealed by loss of function and gain of function mutants of multiple serine phosphorylation sites in endothelial nitric-oxide synthase. J Biol Chem. 278, 14841-14849.

Bazzoni, G., Dejana, E., 2004. Endothelial cell-to-cell junctions: molecular organization and role in vascular homeostasis. Physiol Rev. 84, 869-901.

Begley, D.J., 2004. ABC transporters and the blood-brain barrier. Curr Pharm Des. 10, 1295-1312.

Begley, D.J., Pontikis, C.C., Scarpa, M., 2008. Lysosomal storage diseases and the blood-brain barrier. Curr Pharm Des. 14, 1566-1580.

Ben-Menachem, E., Johansson, B.B., Svensson, T.H., 1982. Increased vulnerability of the blood-brain barrier to acute hypertension following depletion of brain noradrenaline. J Neural Transm. 53, 159-167.

Bernacki, J., Dobrowolska, A., Nierwinska, K., Malecki, A., 2008. Physiology and pharmacological role of the blood-brain barrier. Pharmacol Rep. 60, 600-622.

Berridge, C.W., Waterhouse, B.D., 2003. The locus coeruleus-noradrenergic system: modulation of behavioral state and state-dependent cognitive processes. Brain Res Brain Res Rev. 42, 33-84.

Betanzos, A., Huerta, M., Lopez-Bayghen, E., Azuara, E., Amerena, J., Gonzalez-Mariscal, L., 2004. The tight junction protein ZO-2 associates with Jun, Fos and C/EBP transcription factors in epithelial cells. Exp Cell Res. 292, 51-66.

Bogdan, C., Rollinghoff, M., Diefenbach, A., 2000. Reactive oxygen and reactive nitrogen intermediates in innate and specific immunity. Curr Opin Immunol. 12, 64-76.

Bojarski, C., Weiske, J., Schoneberg, T., Schroder, W., Mankertz, J., Schulzke, J.D., Florian, P., Fromm, M., Tauber, R., Huber, O., 2004. The specific fates of tight junction proteins in apoptotic epithelial cells. J Cell Sci. 117, 2097-2107.

Boje, K.M., Lakhman, S.S., 2000. Nitric oxide redox species exert differential permeability effects on the blood-brain barrier. J Pharmacol Exp Ther. 293, 545-550.

Boo, Y.C., Hwang, J., Sykes, M., Michell, B.J., Kemp, B.E., Lum, H., Jo, H., 2002. Shear stress stimulates phosphorylation of eNOS at Ser(635) by a protein kinase A-dependent mechanism. Am J Physiol Heart Circ Physiol. 283, H1819-H1828.

Bowyer, J.F., Ali, S., 2006. High doses of methamphetamine that cause disruption of the blood-brain barrier in limbic regions produce extensive neuronal degeneration in mouse hippocampus. Synapse. 60, 521-532.

Bowyer, J.F., Davies, D.L., Schmued, L., Broening, H.W., Newport, G.D., Slikker, W.Jr., Holson, R.R., 1994. Further studies of the role of hyperthermia in methamphetamine neurotoxicity. J Pharmacol Exp Ther. 268, 1571-1580.

Bowyer, J.F., Holson, R.R., Miller, D.B., O'Callaghan, J.P., 2001. Phenobarbital and dizocilpine can block methamphetamine-induced neurotoxicity in mice by mechanisms that are independent of thermoregulation. Brain Res. 919, 179-183.

Bowyer, J.F., Robinson, B., Ali, S., Schmued, L.C., 2008. Neurotoxic-related changes in tyrosine hydroxylase, microglia, myelin, and the blood-brain barrier in the caudate-putamen from acute methamphetamine exposure. Synapse. 62, 193-204.

Bowyer, J.F., Tank, A.W., Newport, G.D., Slikker, W.Jr., Ali, S.F., Holson, R.R., 1992. The influence of environmental temperature on the transient effects of methamphetamine on dopamine levels and dopamine release in rat striatum. J Pharmacol Exp Ther. 260, 817-824.

Breckenridge, D.G., Xue, D., 2004. Regulation of mitochondrial membrane permeabilization by BCL-2 family proteins and caspases. Curr Opin Cell Biol. 16, 647-652.

Brown, J.M., Quinton, M.S., Yamamoto, B.K., 2005. Methamphetamine-induced inhibition of mitochondrial complex II: roles of glutamate and peroxynitrite. J Neurochem. 95, 429-436.

Brown, P.L., Wise, R.A., Kiyatkin, E.A., 2003. Brain hyperthermia is induced by methamphetamine and exacerbated by social interaction. J Neurosci. 23, 3924-3929.

Bucci, M., Roviezzo, F., Posadas, I., Yu, J., Parente, L., Sessa, W.C., Ignarro, L.J., Cirino, G., 2005. Endothelial nitric oxide synthase activation is critical for vascular leakage during acute inflammation in vivo. Proc Natl Acad Sci USA. 102, 904-908.

Burrows, K.B., Gudelsky, G., Yamamoto, B.K., 2000. Rapid and transient inhibition of mitochondrial function following methamphetamine or 3,4-methylenedioxymethamphetamine administration. Eur J Pharmacol. 398, 11-18.

Butt, A.M., Jones, H.C., Abbott, N.J., 1990. Electrical resistance across the blood-brain barrier in anaesthetized rats: a developmental study. J Physiol. 429, 47-62.

Caldwell, J., Dring, L.G., Williams, R.T., 1972. Metabolism of [^{14}C]methamphetamine in man, the guinea pig and the rat. Biochem J. 129, 11-22.

Callahan, B.T., Cord, B.J., Yuan, J., McCann, U.D., Ricaurte, G.A., 2001. Inhibitors of Na^+/H^+ and Na^+/Ca^{2+} exchange potentiate methamphetamine-induced dopamine neurotoxicity: possible role of ionic dysregulation in methamphetamine neurotoxicity. J Neurochem. 77, 1348-1362.

Cao, S., Yao, J., McCabe, T.J., Yao, Q., Katusic, Z.S., Sessa, W.C., Shah, V., 2001. Direct interaction between endothelial nitric-oxide synthase and dynamin-2. Implications for nitric-oxide synthase function. J Biol Chem. 276, 14249-14256.

Cardoso, F.L., Brites, D., Brito, M.A., 2010. Looking at the blood-brain barrier: molecular anatomy and possible investigation approaches. Brain Res Rev. 64, 328-363.

Carman, C.V., Sage, P.T., Sciuto, T.E., de la Fuente, M.A., Geha, R.S., Ochs, H.D., Dvorak, H.F., Dvorak, A.M., Springer, T.A., 2007. Transcellular diapedesis is initiated by invasive podosomes. Immunity. 26, 784-797.

Carman, C.V., Springer, T.A., 2004. A transmigratory cup in leukocyte diapedesis both through individual vascular endothelial cells and between them. J Cell Biol. 167, 377-388.

Carvey, P.M., Hendey, B., Monahan, A.J., 2009. The blood-brain barrier in neurodegenerative disease: a rhetorical perspective. J Neurochem. 111, 291-314.

Carvey, P.M., Zhao, C.H., Hendey, B., Lum, H., Trachtenberg, J., Desai, B.S., Snyder, J., Zhu, Y.G., Ling, Z.D., 2005. 6-Hydroxydopamine-induced alterations in blood-brain barrier permeability. Eur J Neurosci. 22, 1158-1168.

Chan, P., Di Monte, D.A., Luo, J.J., DeLanney, L.E., Irwin, I., Langston, J.W., 1994. Rapid ATP loss caused by methamphetamine in the mouse striatum: relationship between energy impairment and dopaminergic neurotoxicity. J Neurochem. 62, 2484-2487.

Chen, Z.P., Mitchelhill, K.I., Michell, B.J., Stapleton, D., Rodriguez-Crespo, I., Witters, L.A., Power, D.A., Ortiz de Montellano, P.R., Kemp, B.E., 1999. AMP-activated protein kinase phosphorylation of endothelial NO synthase. FEBS Lett. 443, 285-289.

Cho, A.K., 1990. Ice: a new dosage form of an old drug. Science. 249, 631-634.

Choi, Y.K., Kim, K.W., 2008. Blood-neural barrier: its diversity and coordinated cell-to-cell communication. BMB Rep. 41, 345-352.

Cipolla, M.J., Crete, R., Vitullo, L., Rix, R.D., 2004. Transcellular transport as a mechanism of blood-brain barrier disruption during stroke. Front Biosci. 9, 777-785.

Cook, C.E., Jeffcoat, A.R., Hill, J.M., Pugh, D.E., Patetta, P.K., Sadler, B.M., White, W.R., Perez-Reyes, M., 1993. Pharmacokinetics of methamphetamine self-administered to human subjects by smoking S-(+)-methamphetamine hydrochloride. Drug Metab Dispos. 21, 717-723.

Cook, C.E., Jeffcoat, A.R., Sadler, B.M., Hill, J.M., Voyksner, R.D., Pugh, D.E., White, W.R., Perez-Reyes, M., 1992. Pharmacokinetics of oral methamphetamine and effects of repeated daily dosing in humans. Drug Metab Dispos. 20, 856-862.

Cordenonsi, M., D'Atri, F., Hammar, E., Parry, D.A., Kendrick-Jones, J., Shore, D., Citi, S., 1999. Cingulin contains globular and coiled-coil domains and

interacts with ZO-1, ZO-2, ZO-3, and myosin. J Cell Biol. 147, 1569-1582.

Correale, J., Villa, A., 2007. The blood-brain-barrier in multiple sclerosis: functional roles and therapeutic targeting. Autoimmunity. 40, 148-160.

Conant, K., St Hillaire, C., Anderson, C., Galey, D., Wang, J., Nath, A., 2004. Human immunodeficiency virus type 1 Tat and methamphetamine affect the release and activation of matrix-degrading proteinases. J Neurovirol. 10**,** 21-28.

Cruickshank, C.C., Dyer, K.R., 2009. A review of the clinical pharmacology of methamphetamine. Addiction. 104, 1085-1099.

Dallas, S., Miller, D.S., Bendayan, R., 2006. Multidrug resistance-associated proteins: expression and function in the central nervous system. Pharmacol Rev. 58, 140-161.

Davidson, C., Gow, A.J., Lee, T.H., Ellinwood, E.H., 2001. Methamphetamine neurotoxicity: necrotic and apoptotic mechanisms and relevance to human abuse and treatment. Brain Res Brain Res Rev. 36, 1-22.

de Boer, A.G., van der Sandt, I.C., Gaillard, P.J., 2003. The role of drug transporters at the blood-brain barrier. Annu Rev Pharmacol Toxicol. 43, 629-656.

De Keyser, J., Mostert, J.P., Koch, M.W., 2008. Dysfunctional astrocytes as key players in the pathogenesis of central nervous system disorders. J Neurol Sci. 267, 3-16.

de la Torre, R., Farre, M., Navarro, M., Pacifici, R., Zuccaro, P., Pichini, S., 2004. Clinical pharmacokinetics of amphetamine and related substances: monitoring in conventional and non-conventional matrices. Clin Pharmacokinet. 43, 157-185.

de Vries, H.E., Blom-Roosemalen, M.C., van Oosten, M., de Boer, A.G., van Berkel, T.J., Breimer, D.D., Kuiper, J., 1996. The influence of cytokines on the integrity of the blood-brain barrier in vitro. J Neuroimmunol. 64, 37-43.

Dedio, J., Konig, P., Wohlfart, P., Schroeder, C., Kummer, W., Muller-Esterl, W., 2001. NOSIP, a novel modulator of endothelial nitric oxide synthase activity. FASEB J. 15, 79-89.

Defazio, G., Ribatti, D., Nico, B., Ricchiuti, F., De Salvia, R., Roncali, L., Livrea, P., 1997. Endocytosis of horseradish peroxidase by brain microvascular

and umbilical vein endothelial cells in culture: an ultrastructural and morphometric study. Brain Res Bull. 43, 467-472.

Dejana, E., Orsenigo, F., Molendini, C., Baluk, P., McDonald, D.M., 2009. Organization and signaling of endothelial cell-to-cell junctions in various regions of the blood and lymphatic vascular trees. Cell Tissue Res. 335, 17-25.

Deng, X., Cadet, J.L., 1999. Methamphetamine administration causes overexpression of nNOS in the mouse striatum. Brain Res. 851, 254-257.

Deng, X., Cai, N.S., McCoy, M.T., Chen, W., Trush, M.A., Cadet, J.L., 2002a. Methamphetamine induces apoptosis in an immortalized rat striatal cell line by activating the mitochondrial cell death pathway. Neuropharmacology. 42, 837-845.

Deng, X., Jayanthi, S., Ladenheim, B., Krasnova, I.N., Cadet, J.L., 2002b. Mice with partial deficiency of c-Jun show attenuation of methamphetamine-induced neuronal apoptosis. Mol Pharmacol. 62, 993-1000.

Deng, X., Wang, Y., Chou, J., Cadet, J.L., 2001. Methamphetamine causes widespread apoptosis in the mouse brain: evidence from using an improved TUNEL histochemical method. Brain Res Mol Brain Res. 93, 64-69.

Dietrich, J.B., 2009. Alteration of blood-brain barrier function by methamphetamine and cocaine. Cell Tissue Res. 336, 385-392.

Doherty, G.J., McMahon, H.T., 2009. Mechanisms of endocytosis. Annu Rev Biochem. 78, 857-902.

Dohgu, S., Takata, F., Yamauchi, A., Nakagawa, S., Egawa, T., Naito, M., Tsuruo, T., Sawada, Y., Niwa, M., Kataoka, Y., 2005. Brain pericytes contribute to the induction and up-regulation of blood-brain barrier functions through transforming growth factor-beta production. Brain Res. 1038, 208-215.

Dore-Duffy, P., Owen, C., Balabanov, R., Murphy, S., Beaumont, T., Rafols, J. A., 2000. Pericyte migration from the vascular wall in response to traumatic brain injury. Microvasc Res. 60, 55-69.

Drozdzik, M., Bialecka, M., Mysliwiec, K., Honczarenko, K., Stankiewicz, J., Sych, Z., 2003. Polymorphism in the P-glycoprotein drug transporter MDR1 gene: a possible link between environmental and genetic factors in Parkinson's disease. Pharmacogenetics. 13, 259-263.

Dudzinski, D.M., Michel, T., 2007. Life history of eNOS: partners and pathways. Cardiovasc Res. 75, 247-260.

Duran, W.N., Breslin, J.W., Sanchez, F.A., 2010. The NO cascade, eNOS location, and microvascular permeability. Cardiovasc Res. 87, 254-261.

Ebnet, K., Schulz, C.U., Meyer Zu Brickwedde, M.K., Pendl, G.G., Vestweber, D., 2000. Junctional adhesion molecule interacts with the PDZ domain-containing proteins AF-6 and ZO-1. J Biol Chem. 275, 27979-27988.

Eisch, A.J., Marshall, J.F., 1998. Methamphetamine neurotoxicity: dissociation of striatal dopamine terminal damage from parietal cortical cell body injury. Synapse. 30, 433-345.

Eisch, A.J., Schmued, L.C., Marshall, J.F., 1998. Characterizing cortical neuron injury with Fluoro-Jade labeling after a neurotoxic regimen of methamphetamine. Synapse. 30, 329-333.

Escubedo, E., Guitart, L., Sureda, F.X., Jimenez, A., Pubill, D., Pallas, M., Camins, A., Camarasa, J., 1998. Microgliosis and down-regulation of adenosine transporter induced by methamphetamine in rats. Brain Res. 814, 120-126.

Eyerman, D.J., Yamamoto, B.K., 2007. A rapid oxidation and persistent decrease in the vesicular monoamine transporter 2 after methamphetamine. J Neurochem. 103, 1219-1227.

Fanning, A.S., Jameson, B.J., Jesaitis, L.A., Anderson, J.M., 1998. The tight junction protein ZO-1 establishes a link between the transmembrane protein occludin and the actin cytoskeleton. J Biol Chem. 273, 29745-29753.

Feron, O., Belhassen, L., Kobzik, L., Smith, T.W., Kelly, R.A., Michel, T., 1996. Endothelial nitric oxide synthase targeting to caveolae. Specific interactions with caveolin isoforms in cardiac myocytes and endothelial cells. J Biol Chem. 271, 22810-22814.

Finnegan, K.T., Ricaurte, G., Seiden, L.S., Schuster, C.R., 1982. Altered sensitivity to d-methylamphetamine, apomorphine, and haloperidol in rhesus monkeys depleted of caudate dopamine by repeated administration of d-methylamphetamine. Psychopharmacology (Berl). 77, 43-52.

Fischer, J.F., Cho, A.K., 1979. Chemical release of dopamine from striatal homogenates: evidence for an exchange diffusion model. J Pharmacol Exp Ther. 208, 203-209.

Fischmann, T.O., Hruza, A., Niu, X.D., Fossetta, J.D., Lunn, C.A., Dolphin, E., Prongay, A.J., Reichert, P., Lundell, D.J., Narula, S.K., Weber, P.C., 1999. Structural characterization of nitric oxide synthase isoforms reveals striking active-site conservation. Nat Struct Biol. 6, 233-242.

Fisslthaler, B., Loot, A.E., Mohamed, A., Busse, R., Fleming, I., 2008. Inhibition of endothelial nitric oxide synthase activity by proline-rich tyrosine kinase 2 in response to fluid shear stress and insulin. Circ Res. 102, 1520-1528.

Fitzmaurice, P.S., Tong, J., Yazdanpanah, M., Liu, P.P., Kalasinsky, K.S., Kish, S.J., 2006. Levels of 4-hydroxynonenal and malondialdehyde are increased in brain of human chronic users of methamphetamine. J Pharmacol Exp Ther. 319, 703-709.

Fleckenstein, A.E., Volz, T.J., Riddle, E.L., Gibb, J.W., Hanson, G.R., 2007. New insights into the mechanism of action of amphetamines. Annu Rev Pharmacol Toxicol. 47, 681-698.

Fleckenstein, A.E., Wilkins, D.G., Gibb, J.W., Hanson, G.R., 1997. Interaction between hyperthermia and oxygen radical formation in the 5-hydroxytryptaminergic response to a single methamphetamine administration. J Pharmacol Exp Ther. 283, 281-285.

Fleming, I., 2010. Molecular mechanisms underlying the activation of eNOS. Pflugers Arch. 459, 793-806.

Fleming, I., Busse, R., 1999. Signal transduction of eNOS activation. Cardiovasc Res. 43, 532-541.

Fontana, J., Fulton, D., Chen, Y., Fairchild, T.A., McCabe, T.J., Fujita, N., Tsuruo, T., Sessa, W.C., 2002. Domain mapping studies reveal that the M domain of hsp90 serves as a molecular scaffold to regulate Akt-dependent phosphorylation of endothelial nitric oxide synthase and NO release. Circ Res. 90, 866-873.

Forster, C., 2008. Tight junctions and the modulation of barrier function in disease. Histochem Cell Biol. 130, 55-70.

Fujimoto, T., Nakade, S., Miyawaki, A., Mikoshiba, K., Ogawa, K., 1992. Localization of inositol 1,4,5-trisphosphate receptor-like protein in plasmalemmal caveolae. J Cell Biol. 119, 1507-1513.

Fujimura, M., Gasche, Y., Morita-Fujimura, Y., Massengale, J., Kawase, M., Chan, P. H., 1999. Early appearance of activated matrix metalloproteinase-9 and

blood-brain barrier disruption in mice after focal cerebral ischemia and reperfusion. Brain Res. 842, 92-100.

Fukami, G., Hashimoto, K., Koike, K., Okamura, N., Shimizu, E., Iyo, M., 2004. Effect of antioxidant N-acetyl-L-cysteine on behavioral changes and neurotoxicity in rats after administration of methamphetamine. Brain Res. 1016, 90-95.

Fukumura, D., Gohongi, T., Kadambi, A., Izumi, Y., Ang, J., Yun, C.O., Buerk, D.G., Huang, P.L., Jain, R.K., 2001. Predominant role of endothelial nitric oxide synthase in vascular endothelial growth factor-induced angiogenesis and vascular permeability. Proc Natl Acad Sci USA. 98, 2604-2609.

Fukumura, D., Kashiwagi, S., Jain, R.K., 2006. The role of nitric oxide in tumour progression. Nat Rev Cancer. 6, 521-534.

Fulton, D., Church, J.E., Ruan, L., Li, C., Sood, S.G., Kemp, B.E., Jennings, I.G., Venema, R.C., 2005. Src kinase activates endothelial nitric-oxide synthase by phosphorylating Tyr-83. J Biol Chem. 280, 35943-35952.

Fulton, D., Gratton, J.P., Sessa, W.C., 2001. Post-translational control of endothelial nitric oxide synthase: why isn't calcium/calmodulin enough? J Pharmacol Exp Ther. 299, 818-824.

Fulton, D., Ruan, L., Sood, S.G., Li, C., Zhang, Q., Venema, R.C., 2008. Agonist-stimulated endothelial nitric oxide synthase activation and vascular relaxation. Role of eNOS phosphorylation at Tyr83. Circ Res. 102, 497-504.

Funke, L., Dakoji, S., Bredt, D.S., 2005. Membrane-associated guanylate kinases regulate adhesion and plasticity at cell junctions. Annu Rev Biochem. 74, 219-245.

Furuse, M., Fujita, K., Hiiragi, T., Fujimoto, K., Tsukita, S., 1998a. Claudin-1 and -2: novel integral membrane proteins localizing at tight junctions with no sequence similarity to occludin. J Cell Biol. 141, 1539-1550.

Furuse, M., Hirase, T., Itoh, M., Nagafuchi, A., Yonemura, S., Tsukita, S., 1993. Occludin: a novel integral membrane protein localizing at tight junctions. J Cell Biol. 123, 1777-1788.

Furuse, M., Itoh, M., Hirase, T., Nagafuchi, A., Yonemura, S., Tsukita, S., 1994. Direct association of occludin with ZO-1 and its possible involvement in the localization of occludin at tight junctions. J Cell Biol. 127, 1617-1626.

Furuse, M., Sasaki, H., Fujimoto, K., Tsukita, S., 1998b. A single gene product, claudin-1 or -2, reconstitutes tight junction strands and recruits occludin in fibroblasts. J Cell Biol. 143, 391-401.

Furuse, M., Sasaki, H., Tsukita, S., 1999. Manner of interaction of heterogeneous claudin species within and between tight junction strands. J Cell Biol. 147, 891-903.

Gaillard, P.J., de Boer, A.B., Breimer, D.D., 2003. Pharmacological investigations on lipopolysaccharide-induced permeability changes in the blood-brain barrier in vitro. Microvasc Res. 65, 24-31.

Garcia-Cardena, G., Fan, R., Shah, V., Sorrentino, R., Cirino, G., Papapetropoulos, A., Sessa, W.C., 1998. Dynamic activation of endothelial nitric oxide synthase by Hsp90. Nature. 392, 821-824.

Ghosh, S., Gachhui, R., Crooks, C., Wu, C., Lisanti, M.P., Stuehr, D.J., 1998. Interaction between caveolin-1 and the reductase domain of endothelial nitric-oxide synthase. Consequences for catalysis. J Biol Chem. 273, 22267-22271.

Giovanni, A., Liang, L.P., Hastings, T.G., Zigmond, M.J., 1995. Estimating hydroxyl radical content in rat brain using systemic and intraventricular salicylate: impact of methamphetamine. J Neurochem. 64, 1819-1825.

Glass, C.K., Saijo, K., Winner, B., Marchetto, M.C., Gage, F.H., 2010. Mechanisms underlying inflammation in neurodegeneration. Cell. 140, 918-934.

Gloor, S.M., Weber, A., Adachi, N., Frei, K., 1997. Interleukin-1 modulates protein tyrosine phosphatase activity and permeability of brain endothelial cells. Biochem Biophys Res Commun. 239, 804-809.

Gluck, M.R., Moy, L.Y., Jayatilleke, E., Hogan, K.A., Manzino, L., Sonsalla, P.K., 2001. Parallel increases in lipid and protein oxidative markers in several mouse brain regions after methamphetamine treatment. J Neurochem. 79, 152-160.

Gonçalves, J., Baptista, S., Martins, T., Milhazes, N., Borges, F., Ribeiro, C.F., Malva, J.O., Silva, A.P., 2010. Methamphetamine-induced neuroinflammation and neuronal dysfunction in the mice hippocampus: preventive effect of indomethacin. Eur J Neurosci. 31, 315-326.

Gonçalves, J., Martins, T., Ferreira, R., Milhazes, N., Borges, F., Ribeiro, C.F., Malva, J.O., Macedo, T.R., Silva, A.P., 2008. Methamphetamine-induced

early increase of IL-6 and TNF-alpha mRNA expression in the mouse brain. Ann N Y Acad Sci. 1139, 103-111.

Gonul, E., Duz, B., Kahraman, S., Kayali, H., Kubar, A., Timurkaynak, E., 2002. Early pericyte response to brain hypoxia in cats: an ultrastructural study. Microvasc Res. 64, 116-119.

Gonzalez-Mariscal, L., Tapia, R., Chamorro, D., 2008. Crosstalk of tight junction components with signaling pathways. Biochim Biophys Acta. 1778, 729-756.

Gottardi, C.J., Arpin, M., Fanning, A.S., Louvard, D., 1996. The junction-associated protein, zonula occludens-1, localizes to the nucleus before the maturation and during the remodeling of cell-cell contacts. Proc Natl Acad Sci USA. 93, 10779-10784.

Granado, N., Ares-Santos, S., Oliva, I., O'Shea, E., Martin, E.D., Colado, M.I., Moratalla, R., 2011. Dopamine D2-receptor knockout mice are protected against dopaminergic neurotoxicity induced by methamphetamine or MDMA. Neurobiol Dis. 42, 391-403.

Green, A.R., De Souza, R.J., Williams, J.L., Murray, T.K., Cross, A.J., 1992. The neurotoxic effects of methamphetamine on 5-hydroxytryptamine and dopamine in brain: evidence for the protective effect of chlormethiazole. Neuropharmacology. 31, 315-321.

Greenwood, J., Heasman, S.J., Alvarez, J.I., Prat, A., Lyck, R., Engelhardt, B., 2011. Review: leucocyte-endothelial cell crosstalk at the blood-brain barrier: a prerequisite for successful immune cell entry to the brain. Neuropathol Appl Neurobiol. 37, 24-39.

Guillot, F.L., Audus, K.L., Raub, T.J., 1990. Fluid-phase endocytosis by primary cultures of bovine brain microvessel endothelial cell monolayers. Microvasc Res. 39, 1-14.

Gurney, K.J., Estrada, E.Y., Rosenberg, G.A., 2006. Blood-brain barrier disruption by stromelysin-1 facilitates neutrophil infiltration in neuroinflammation. Neurobiol Dis. 23, 87-96.

Han, F., Shirasaki, Y., Fukunaga, K., 2006. Microsphere embolism-induced endothelial nitric oxide synthase expression mediates disruption of the blood-brain barrier in rat brain. J Neurochem. 99, 97-106.

Hanisch, U.K., 2002. Microglia as a source and target of cytokines. Glia. 40, 140-155.

Hanson, G.R., Rau, K.S., Fleckenstein, A.E., 2004. The methamphetamine experience: a NIDA partnership. Neuropharmacology. 47 Suppl 1, 92-100.

Haorah, J., Ramirez, S.H., Schall, K., Smith, D., Pandya, R., Persidsky, Y., 2007. Oxidative stress activates protein tyrosine kinase and matrix metalloproteinases leading to blood-brain barrier dysfunction. J Neurochem. 101, 566-576.

Harris, D.S., Boxenbaum, H., Everhart, E.T., Sequeira, G., Mendelson, J.E., Jones, R.T., 2003. The bioavailability of intranasal and smoked methamphetamine. Clin Pharmacol Ther. 74, 475-486.

Harris, M.B., Ju, H., Venema, V.J., Blackstone, M., Venema, R.C., 2000. Role of heat shock protein 90 in bradykinin-stimulated endothelial nitric oxide release. Gen Pharmacol. 35, 165-170.

Hart, C.L., Ward, A.S., Haney, M., Foltin, R.W., Fischman, M.W., 2001. Methamphetamine self-administration by humans. Psychopharmacology (Berl). 157, 75-81.

Haskins, J., Gu, L., Wittchen, E.S., Hibbard, J., Stevenson, B.R., 1998. ZO-3, a novel member of the MAGUK protein family found at the tight junction, interacts with ZO-1 and occludin. J Cell Biol. 141, 199-208.

Hatakeyama, T., Pappas, P.J., Hobson, R.W.2nd, Boric, M.P., Sessa, W.C., Duran, W.N., 2006. Endothelial nitric oxide synthase regulates microvascular hyperpermeability in vivo. J Physiol. 574, 275-281.

Hawkins, B.T., Davis, T.P., 2005. The blood-brain barrier/neurovascular unit in health and disease. Pharmacol Rev. 57, 173-185.

Hawkins, B.T., Egleton, R.D., 2008. Pathophysiology of the blood-brain barrier: animal models and methods. Curr Top Dev Biol. 80, 277-309.

Hawkins, R.A., O'Kane, R.L., Simpson, I.A., Vina, J.R., 2006. Structure of the blood-brain barrier and its role in the transport of amino acids. J Nutr. 136, 218S-226S.

Hecker, M., Mulsch, A., Bassenge, E., Forstermann, U., Busse, R., 1994. Subcellular localization and characterization of nitric oxide synthase(s) in endothelial cells: physiological implications. Biochem J. 299 (Pt 1), 247-252.

Herve, F., Ghinea, N., Scherrmann, J.M., 2008. CNS delivery via adsorptive transcytosis. AAPS J. 10, 455-472.

Hickey, W.F., 1999. Leukocyte traffic in the central nervous system: the participants and their roles. Semin Immunol. 11, 125-137.

Hirase, T., Staddon, J.M., Saitou, M., Ando-Akatsuka, Y., Itoh, M., Furuse, M., Fujimoto, K., Tsukita, S., Rubin, L.L., 1997. Occludin as a possible determinant of tight junction permeability in endothelial cells. J Cell Sci. 110 (Pt 14), 1603-1613.

Hixenbaugh, E.A., Goeckeler, Z.M., Papaiya, N.N., Wysolmerski, R.B., Silverstein, S.C., Huang, A.J., 1997. Stimulated neutrophils induce myosin light chain phosphorylation and isometric tension in endothelial cells. Am J Physiol. 273, H981-H988.

Hordijk, P.L., 2006. Endothelial signalling events during leukocyte transmigration. FEBS J. 273, 4408-4415.

Hori, S., Ohtsuki, S., Hosoya, K., Nakashima, E., Terasaki, T., 2004. A pericyte-derived angiopoietin-1 multimeric complex induces occludin gene expression in brain capillary endothelial cells through Tie-2 activation in vitro. J Neurochem. 89, 503-513.

Hornung, J.P., 2003. The human raphe nuclei and the serotonergic system. J Chem Neuroanat. 26, 331-343.

Hotchkiss, A.J., Gibb, J.W., 1980. Long-term effects of multiple doses of methamphetamine on tryptophan hydroxylase and tyrosine hydroxylase activity in rat brain. J Pharmacol Exp Ther. 214, 257-262.

Hotchkiss, A.J., Morgan, M.E., Gibb, J.W., 1979. The long-term effects of multiple doses of methamphetamine on neostriatal tryptophan hydroxylase, tyrosine hydroxylase, choline acetyltransferase and glutamate decarboxylase activities. Life Sci. 25, 1373-1378.

Howarth, A.G., Hughes, M.R., Stevenson, B.R., 1992. Detection of the tight junction-associated protein ZO-1 in astrocytes and other nonepithelial cell types. Am J Physiol. 262, C461-C469.

Huber, J.D., Witt, K.A., Hom, S., Egleton, R.D., Mark, K.S., Davis, T.P., 2001. Inflammatory pain alters blood-brain barrier permeability and tight junctional protein expression. Am J Physiol Heart Circ Physiol. 280, H1241-H1248.

Imam, S.Z., el-Yazal, J., Newport, G.D., Itzhak, Y., Cadet, J.L., Slikker, W.Jr., Ali, S.F., 2001. Methamphetamine-induced dopaminergic neurotoxicity: role

of peroxynitrite and neuroprotective role of antioxidants and peroxynitrite decomposition catalysts. Ann N Y Acad Sci. 939, 366-380.

Imam, S.Z., Islam, F., Itzhak, Y., Slikker, W.Jr., Ali, S.F., 2000. Prevention of dopaminergic neurotoxicity by targeting nitric oxide and peroxynitrite: implications for the prevention of methamphetamine-induced neurotoxic damage. Ann N Y Acad Sci. 914, 157-171.

Inoko, A., Itoh, M., Tamura, A., Matsuda, M., Furuse, M., Tsukita, S., 2003. Expression and distribution of ZO-3, a tight junction MAGUK protein, in mouse tissues. Genes Cells. 8, 837-845.

Islas, S., Vega, J., Ponce, L., Gonzalez-Mariscal, L., 2002. Nuclear localization of the tight junction protein ZO-2 in epithelial cells. Exp Cell Res. 274, 138-148.

Itoh, M., Furuse, M., Morita, K., Kubota, K., Saitou, M., Tsukita, S., 1999a. Direct binding of three tight junction-associated MAGUKs, ZO-1, ZO-2, and ZO-3, with the COOH termini of claudins. J Cell Biol. 147, 1351-1363.

Itoh, M., Morita, K., Tsukita, S., 1999b. Characterization of ZO-2 as a MAGUK family member associated with tight as well as adherens junctions with a binding affinity to occludin and alpha catenin. J Biol Chem. 274, 5981-5986.

Itzhak, Y., Ali, S.F., 1996. The neuronal nitric oxide synthase inhibitor, 7-nitroindazole, protects against methamphetamine-induced neurotoxicity in vivo. J Neurochem. 67, 1770-1773.

Itzhak, Y., Martin, J.L., Ail, S.F., 2000. nNOS inhibitors attenuate methamphetamine-induced dopaminergic neurotoxicity but not hyperthermia in mice. Neuroreport. 11, 2943-2946.

Ivanov, D., Philippova, M., Antropova, J., Gubaeva, F., Iljinskaya, O., Tararak, E., Bochkov, V., Erne, P., Resink, T., Tkachuk, V., 2001. Expression of cell adhesion molecule T-cadherin in the human vasculature. Histochem Cell Biol. 115, 231-242.

Jayanthi, S., Deng, X., Bordelon, M., McCoy, M.T., Cadet, J.L., 2001. Methamphetamine causes differential regulation of pro-death and anti-death Bcl-2 genes in the mouse neocortex. FASEB J. 15, 1745-1752.

Jayanthi, S., Deng, X., Noailles, P.A., Ladenheim, B., Cadet, J.L., 2004. Methamphetamine induces neuronal apoptosis via cross-talks between

endoplasmic reticulum and mitochondria-dependent death cascades. FASEB J. 18, 238-251.

Jayanthi, S., Ladenheim, B., Cadet, J.L., 1998. Methamphetamine-induced changes in antioxidant enzymes and lipid peroxidation in copper/zinc-superoxide dismutase transgenic mice. Ann N Y Acad Sci. 844, 92-102.

Jian Liu, K., Rosenberg, G.A., 2005. Matrix metalloproteinases and free radicals in cerebral ischemia. Free Radic Biol Med. 39, 71-80.

Kahlert, S., Zundorf, G., Reiser, G., 2005. Glutamate-mediated influx of extracellular Ca^{2+} is coupled with reactive oxygen species generation in cultured hippocampal neurons but not in astrocytes. J Neurosci Res. 79, 262-271.

Kametani, Y., Takeichi, M., 2007. Basal-to-apical cadherin flow at cell junctions. Nat Cell Biol. 9, 92-98.

Kanmogne, G.D., Schall, K., Leibhart, J., Knipe, B., Gendelman, H.E., Persidsky, Y., 2007. HIV-1 gp120 compromises blood-brain barrier integrity and enhances monocyte migration across blood-brain barrier: implication for viral neuropathogenesis. J Cereb Blood Flow Metab. 27, 123-134.

Kast, R.E., 2009. Use of FDA approved methamphetamine to allow adjunctive use of methylnaltrexone to mediate core anti-growth factor signaling effects in glioblastoma. J Neurooncol. 94, 163-167.

Kast, R.E., Focosi, D., 2010. Three paths to better tyrosine kinase inhibition behind the blood-brain barrier in treating chronic myelogenous leukemia and glioblastoma with imatinib. Transl Oncol. 3, 13-15.

Katsuno, T., Umeda, K., Matsui, T., Hata, M., Tamura, A., Itoh, M., Takeuchi, K., Fujimori, T., Nabeshima, Y., Noda, T., Tsukita, S., 2008. Deficiency of zonula occludens-1 causes embryonic lethal phenotype associated with defected yolk sac angiogenesis and apoptosis of embryonic cells. Mol Biol Cell. 19, 2465-2475.

Kaur, C., Ling, E.A., 2008. Blood brain barrier in hypoxic-ischemic conditions. Curr Neurovasc Res. 5, 71-81.

Keogh, B., Sheahan, B.J., Atkins, G.J., Mills, K.H., 2003. Inhibition of matrix metalloproteinases ameliorates blood-brain barrier disruption and neuropathological lesions caused by avirulent Semliki Forest virus infection. Vet Immunol Immunopathol. 94, 185-190.

Kim, J., Jung, Y., 2011. Different expressions of AQP1, AQP4, eNOS, and VEGF proteins in ischemic versus non-ischemic cerebropathy in rats: potential roles of AQP1 and eNOS in hydrocephalic and vasogenic edema formation. Anat Cell Biol. 44, 295-303.

Kish, S.J., 2008. Pharmacologic mechanisms of crystal meth. Cmaj. 178, 1679-1682.

Kiyatkin, E.A., 2005. Brain hyperthermia as physiological and pathological phenomena. Brain Res Brain Res Rev. 50, 27-56.

Kiyatkin, E.A., Brown, P.L., Sharma, H.S., 2007. Brain edema and breakdown of the blood-brain barrier during methamphetamine intoxication: critical role of brain hyperthermia. Eur J Neurosci. 26, 1242-1253.

Kleinert, H., Pautz, A., Linker, K., Schwarz, P.M., 2004. Regulation of the expression of inducible nitric oxide synthase. Eur J Pharmacol. 500, 255-266.

Koenig, H., Trout, J.J., Goldstone, A.D., Lu, C.Y., 1992. Capillary NMDA receptors regulate blood-brain barrier function and breakdown. Brain Res. 588, 297-303.

Krasnova, I.N., Cadet, J.L., 2009. Methamphetamine toxicity and messengers of death. Brain Res Rev. 60, 379-407.

Krause, G., Winkler, L., Mueller, S.L., Haseloff, R.F., Piontek, J., Blasig, I.E., 2008. Structure and function of claudins. Biochim Biophys Acta. 1778, 631-645.

Kreutzberg, G.W., 1996. Microglia: a sensor for pathological events in the CNS. Trends Neurosci. 19, 312-318.

Kuczenski, R., Everall, I.P., Crews, L., Adame, A., Grant, I., Masliah, E., 2007. Escalating dose-multiple binge methamphetamine exposure results in degeneration of the neocortex and limbic system in the rat. Exp Neurol. 207, 42-51.

Kuhn, D.M., Aretha, C.W., Geddes, T.J., 1999. Peroxynitrite inactivation of tyrosine hydroxylase: mediation by sulfhydryl oxidation, not tyrosine nitration. J Neurosci. 19, 10289-10294.

Kuhn, D.M., Arthur, R.E.Jr., 1997. Inactivation of tryptophan hydroxylase by nitric oxide: enhancement by tetrahydrobiopterin. J Neurochem. 68, 1495-1502.

Kuhn, D.M., Geddes, T.J., 1999. Peroxynitrite inactivates tryptophan hydroxylase via sulfhydryl oxidation. Coincident nitration of enzyme tyrosyl residues has minimal impact on catalytic activity. J Biol Chem. 274, 29726-29732.

Kuhn, D.M., Sadidi, M., Liu, X., Kreipke, C., Geddes, T., Borges, C., Watson, J.T., 2002. Peroxynitrite-induced nitration of tyrosine hydroxylase: identification of tyrosines 423, 428, and 432 as sites of modification by matrix-assisted laser desorption ionization time-of-flight mass spectrometry and tyrosine-scanning mutagenesis. J Biol Chem. 277, 14336-14342.

Ladenheim, B., Krasnova, I.N., Deng, X., Oyler, J.M., Polettini, A., Moran, T.H., Huestis, M.A., Cadet, J.L., 2000. Methamphetamine-induced neurotoxicity is attenuated in transgenic mice with a null mutation for interleukin-6. Mol Pharmacol. 58, 1247-1256.

Lai, C.H., Kuo, K.H., 2005. The critical component to establish in vitro BBB model: Pericyte. Brain Res Brain Res Rev. 50, 258-265.

LaVoie, M.J., Card, J.P., Hastings, T.G., 2004. Microglial activation precedes dopamine terminal pathology in methamphetamine-induced neurotoxicity. Exp Neurol. 187, 47-57.

LaVoie, M.J., Hastings, T.G., 1999. Dopamine quinone formation and protein modification associated with the striatal neurotoxicity of methamphetamine: evidence against a role for extracellular dopamine. J Neurosci. 19, 1484-1491.

Li, C., Ruan, L., Sood, S.G., Papapetropoulos, A., Fulton, D., Venema, R.C., 2007. Role of eNOS phosphorylation at Ser-116 in regulation of eNOS activity in endothelial cells. Vascul Pharmacol. 47, 257-264.

Liaw, C.W., Cannon, C., Power, M.D., Kiboneka, P.K., Rubin, L.L., 1990. Identification and cloning of two species of cadherins in bovine endothelial cells. EMBO J. 9, 2701-2708.

Liebner, S., Fischmann, A., Rascher, G., Duffner, F., Grote, E.H., Kalbacher, H., Wolburg, H., 2000. Claudin-1 and claudin-5 expression and tight junction morphology are altered in blood vessels of human glioblastoma multiforme. Acta Neuropathol. 100, 323-331.

Lin, L.Y., Di Stefano, E.W., Schmitz, D.A., Hsu, L., Ellis, S.W., Lennard, M.S., Tucker, G.T., Cho, A.K., 1997. Oxidation of methamphetamine and methylenedioxymethamphetamine by CYP2D6. Drug Metab Dispos. 25, 1059-1064.

Lippoldt, A., Kniesel, U., Liebner, S., Kalbacher, H., Kirsch, T., Wolburg, H., Haller, H., 2000. Structural alterations of tight junctions are associated with loss of polarity in stroke-prone spontaneously hypertensive rat blood-brain barrier endothelial cells. Brain Res. 885, 251-261.

Liu, Y., Brown, S., Shaikh, J., Fishback, J.A., Matsumoto, R.R., 2008. Relationship between methamphetamine exposure and matrix metalloproteinase 9 expression. Neuroreport. 19, 1407-1409.

Lo, E.H., Dalkara, T., Moskowitz, M.A., 2003. Mechanisms, challenges and opportunities in stroke. Nat Rev Neurosci. 4, 399-415.

Lohmann, C., Krischke, M., Wegener, J., Galla, H.J., 2004. Tyrosine phosphatase inhibition induces loss of blood-brain barrier integrity by matrix metalloproteinase-dependent and -independent pathways. Brain Res. 995, 184-196.

Loscalzo, J., Welch, G., 1995. Nitric oxide and its role in the cardiovascular system. Prog Cardiovasc Dis. 38, 87-104.

Mahajan, S.D., Aalinkeel, R., Sykes, D.E., Reynolds, J.L., Bindukumar, B., Adal, A., Qi, M., Toh, J., Xu, G., Prasad, P.N., Schwartz, S.A., 2008. Methamphetamine alters blood brain barrier permeability via the modulation of tight junction expression: Implication for HIV-1 neuropathogenesis in the context of drug abuse. Brain Res. 1203, 133-148.

Manaenko, A., Chen, H., Kammer, J., Zhang, J.H., Tang, J., 2011. Comparison Evans Blue injection routes: Intravenous versus intraperitoneal, for measurement of blood-brain barrier in a mice hemorrhage model. J Neurosci Methods. 195, 206-210.

Mamdouh, Z., Chen, X., Pierini, L.M., Maxfield, F.R., Muller, W.A., 2003. Targeted recycling of PECAM from endothelial surface-connected compartments during diapedesis. Nature. 421, 748-753.

Mamdouh, Z., Kreitzer, G.E., Muller, W.A., 2008. Leukocyte transmigration requires kinesin-mediated microtubule-dependent membrane trafficking from the lateral border recycling compartment. J Exp Med. 205, 951-966.

Mamdouh, Z., Mikhailov, A., Muller, W.A., 2009. Transcellular migration of leukocytes is mediated by the endothelial lateral border recycling compartment. J Exp Med. 206, 2795-2808.

Maniatis, N.A., Brovkovych, V., Allen, S.E., John, T.A., Shajahan, A.N., Tiruppathi, C., Vogel, S.M., Skidgel, R.A., Malik, A.B., Minshall, R.D., 2006. Novel mechanism of endothelial nitric oxide synthase activation mediated by caveolae internalization in endothelial cells. Circ Res. 99, 870-877.

Mark, K.A., Soghomonian, J.J., Yamamoto, B.K., 2004. High-dose methamphetamine acutely activates the striatonigral pathway to increase striatal glutamate and mediate long-term dopamine toxicity. J Neurosci. 24, 11449-11456.

Martinelli, R., Gegg, M., Longbottom, R., Adamson, P., Turowski, P., Greenwood, J., 2009. ICAM-1-mediated endothelial nitric oxide synthase activation via calcium and AMP-activated protein kinase is required for transendothelial lymphocyte migration. Mol Biol Cell. 20, 995-1005.

Martins, T., Baptista, S., Gonçalves, J., Leal, E., Milhazes, N., Borges, F., Ribeiro, C.F., Quintela, O., Lendoiro, E., Lopez-Rivadulla, M., Ambrosio, A.F., Silva, A.P., 2011. Methamphetamine transiently increases the blood-brain barrier permeability in the hippocampus: Role of tight junction proteins and matrix metalloproteinase-9. Brain Res. 1411, 28-40.

Mayhan, W.G., 2000. Nitric oxide donor-induced increase in permeability of the blood-brain barrier. Brain Res. 866, 101-108.

Mayhan, W.G., Didion, S.P., 1996. Glutamate-induced disruption of the blood-brain barrier in rats. Role of nitric oxide. Stroke. 27, 965-970.

McCabe, T.J., Fulton, D., Roman, L.J., Sessa, W.C., 2000. Enhanced electron flux and reduced calmodulin dissociation may explain "calcium-independent" eNOS activation by phosphorylation. J Biol Chem. 275, 6123-6128.

McCarthy, K.M., Skare, I.B., Stankewich, M.C., Furuse, M., Tsukita, S., Rogers, R.A., Lynch, R.D., Schneeberger, E.E., 1996. Occludin is a functional component of the tight junction. J Cell Sci. 109 (Pt 9), 2287-2298.

McQuaid, S., Cunnea, P., McMahon, J., Fitzgerald, U., 2009. The effects of blood-brain barrier disruption on glial cell function in multiple sclerosis. Biochem Soc Trans. 37, 329-331.

Melega, W.P., Cho, A.K., Harvey, D., Lacan, G., 2007. Methamphetamine blood concentrations in human abusers: application to pharmacokinetic modeling. Synapse 61, 216-220.

Melega, W.P., Williams, A.E., Schmitz, D.A., DiStefano, E.W., Cho, A.K., 1995. Pharmacokinetic and pharmacodynamic analysis of the actions of D-amphetamine and D-methamphetamine on the dopamine terminal. J Pharmacol Exp Ther. 274, 90-96.

Michel, P.P., Hefti, F., 1990. Toxicity of 6-hydroxydopamine and dopamine for dopaminergic neurons in culture. J Neurosci Res. 26, 428-435.

Michel, T., Feron, O., 1997. Nitric oxide synthases: which, where, how, and why? J Clin Invest. 100, 2146-2152.

Michell, B.J., Chen, Z., Tiganis, T., Stapleton, D., Katsis, F., Power, D.A., Sim, A.T., Kemp, B.E., 2001. Coordinated control of endothelial nitric-oxide synthase phosphorylation by protein kinase C and the cAMP-dependent protein kinase. J Biol Chem. 276, 17625-17628.

Michell, B.J., Harris, M.B., Chen, Z.P., Ju, H., Venema, V.J., Blackstone, M.A., Huang, W., Venema, R.C., Kemp, B.E., 2002. Identification of regulatory sites of phosphorylation of the bovine endothelial nitric-oxide synthase at serine 617 and serine 635. J Biol Chem. 277, 42344-42351.

Millan, J., Hewlett, L., Glyn, M., Toomre, D., Clark, P., Ridley, A.J., 2006. Lymphocyte transcellular migration occurs through recruitment of endothelial ICAM-1 to caveola- and F-actin-rich domains. Nat Cell Biol. 8, 113-123.

Miller, D.B., O'Callaghan, J.P., 1994. Environment-, drug- and stress-induced alterations in body temperature affect the neurotoxicity of substituted amphetamines in the C57BL/6J mouse. J Pharmacol Exp Ther. 270, 752-760.

Milward, E.A., Fitzsimmons, C., Szklarczyk, A., Conant, K., 2007. The matrix metalloproteinases and CNS plasticity: an overview. J Neuroimmunol. 187, 9-19.

Mirecki, A., Fitzmaurice, P., Ang, L., Kalasinsky, K.S., Peretti, F.J., Aiken, S.S., Wickham, D.J., Sherwin, A., Nobrega, J.N., Forman, H.J., Kish, S.J., 2004. Brain antioxidant systems in human methamphetamine users. J Neurochem. 89, 1396-1408.

Mitic, L.L., Anderson, J.M., 1998. Molecular architecture of tight junctions. Annu Rev Physiol. 60, 121-142.

Mizoguchi, H., Yamada, K., Mouri, A., Niwa, M., Mizuno, T., Noda, Y., Nitta, A., Itohara, S., Banno, Y., Nabeshima, T., 2007a. Role of matrix

metalloproteinase and tissue inhibitor of MMP in methamphetamine-induced behavioral sensitization and reward: implications for dopamine receptor down-regulation and dopamine release. J Neurochem. 102, 1548-1560.

Mizoguchi, H., Yamada, K., Niwa, M., Mouri, A., Mizuno, T., Noda, Y., Nitta, A., Itohara, S., Banno, Y., Nabeshima, T., 2007b. Reduction of methamphetamine-induced sensitization and reward in matrix metalloproteinase-2 and -9-deficient mice. J Neurochem. 100, 1579-1588.

Mosmann, T., 1983. Rapid colorimetric assay for cellular growth and survival: application to proliferation and cytotoxicity assays. J Immunol Methods. 65, 55-63.

Muller, W.A., 2003. Leukocyte-endothelial-cell interactions in leukocyte transmigration and the inflammatory response. Trends Immunol. 24, 327-334.

Muller, W.A., 2011. Mechanisms of leukocyte transendothelial migration. Annu Rev Pathol. 6, 323-344.

Mun-Bryce, S., Rosenberg, G.A., 1998. Gelatinase B modulates selective opening of the blood-brain barrier during inflammation. Am J Physiol. 274, R1203-R1211.

Nagafuchi, A., Ishihara, S., Tsukita, S., 1994. The roles of catenins in the cadherin-mediated cell adhesion: functional analysis of E-cadherin-alpha catenin fusion molecules. J Cell Biol. 127, 235-245.

Nagy, V., Bozdagi, O., Matynia, A., Balcerzyk, M., Okulski, P., Dzwonek, J., Costa, R.M., Silva, A.J., Kaczmarek, L., Huntley, G.W., 2006. Matrix metalloproteinase-9 is required for hippocampal late-phase long-term potentiation and memory. J Neurosci. 26, 1923-1934.

Nara, A., Aki, T., Funakoshi, T., Uemura, K., 2010. Methamphetamine induces macropinocytosis in differentiated SH-SY5Y human neuroblastoma cells. Brain Res. 1352, 1–10.

Narita, M., Suzuki, M., Kuzumaki, N., Miyatake, M., Suzuki, T., 2008. Implication of activated astrocytes in the development of drug dependence: differences between methamphetamine and morphine. Ann N Y Acad Sci. 1141, 96-104.

Nitta, T., Hata, M., Gotoh, S., Seo, Y., Sasaki, H., Hashimoto, N., Furuse, M., Tsukita, S., 2003. Size-selective loosening of the blood-brain barrier in claudin-5-deficient mice. J Cell Biol. 161, 653-660.

Nordahl, T.E., Salo, R., Leamon, M., 2003. Neuropsychological effects of chronic methamphetamine use on neurotransmitters and cognition: a review. J Neuropsychiatry Clin Neurosci. 15, 317-325.

O'Dell, S.J., Marshall, J.F., 2005. Neurotoxic regimens of methamphetamine induce persistent expression of phospho-c-Jun in somatosensory cortex and substantia nigra. Synapse. 55, 137-47.

Oh, J.W., Schwiebert, L.M., Benveniste, E.N., 1999. Cytokine regulation of CC and CXC chemokine expression by human astrocytes. J Neurovirol. 5, 82-94.

Pacher, P., Beckman, J.S., Liaudet, L., 2007. Nitric oxide and peroxynitrite in health and disease. Physiol Rev. 87, 315-424.

Palmeri, D., van Zante, A., Huang, C.C., Hemmerich, S., Rosen, S.D., 2000. Vascular endothelial junction-associated molecule, a novel member of the immunoglobulin superfamily, is localized to intercellular boundaries of endothelial cells. J Biol Chem. 275, 19139-19145.

Papadopoulos, M.C., Saadoun, S., Binder, D.K., Manley, G.T., Krishna, S., Verkman, A.S., 2004. Molecular mechanisms of brain tumor edema. Neuroscience. 129, 1011-1020.

Parathath, S.R., Parathath, S., Tsirka, S.E., 2006. Nitric oxide mediates neurodegeneration and breakdown of the blood-brain barrier in tPA-dependent excitotoxic injury in mice. J Cell Sci. 119, 339-349.

Park, M., Hennig, B., Toborek, M., 2012. Methamphetamine alters occludin expression via NADPH oxidase-induced oxidative insult and intact caveolae. J Cell Mol Med. 16, 362-375.

Parpura, V., Haydon, P.G., 2000. Physiological astrocytic calcium levels stimulate glutamate release to modulate adjacent neurons. Proc Natl Acad Sci USA. 97, 8629-8634.

Perriere, N., Yousif, S., Cazaubon, S., Chaverot, N., Bourasset, F., Cisternino, S., Decleves, X., Hori, S., Terasaki, T., Deli, M., Scherrmann, J.M., Temsamani, J., Roux, F., Couraud, P.O., 2007. A functional in vitro model of rat blood-brain barrier for molecular analysis of efflux transporters. Brain Res. 1150, 1-13.

Persidsky, Y., Ramirez, S.H., Haorah, J., Kanmogne, G.D., 2006. Blood-brain barrier: structural components and function under physiologic and pathologic conditions. J Neuroimmune Pharmacol. 1, 223-236.

Petty, M.A., Lo, E.H., 2002. Junctional complexes of the blood-brain barrier: permeability changes in neuroinflammation. Prog Neurobiol. 68, 311-323.

Poritz, L.S., Garver, K.I., Tilberg, A.F., Koltun, W.A., 2004. Tumor necrosis factor alpha disrupts tight junction assembly. J Surg Res. 116, 14-18.

Pratt, W.B., 1997. The role of the hsp90-based chaperone system in signal transduction by nuclear receptors and receptors signaling via MAP kinase. Annu Rev Pharmacol Toxicol. 37, 297-326.

Predescu, D., Predescu, S., Shimizu, J., Miyawaki-Shimizu, K., Malik, A.B., 2005. Constitutive eNOS-derived nitric oxide is a determinant of endothelial junctional integrity. Am J Physiol Lung Cell Mol Physiol. 289, L371-L381.

Predescu, S.A., Predescu, D.N., Malik, A.B., 2007. Molecular determinants of endothelial transcytosis and their role in endothelial permeability. Am J Physiol Lung Cell Mol Physiol. 293, L823-L842.

Pritchard, K.A.Jr., Ackerman, A.W., Gross, E.R., Stepp, D.W., Shi, Y., Fontana, J.T., Baker, J.E., Sessa, W.C., 2001. Heat shock protein 90 mediates the balance of nitric oxide and superoxide anion from endothelial nitric-oxide synthase. J Biol Chem. 276, 17621-17624.

Pu, C., Fisher, J.E., Cappon, G.D., Vorhees, C.V., 1994. The effects of amfonelic acid, a dopamine uptake inhibitor, on methamphetamine-induced dopaminergic terminal degeneration and astrocytic response in rat striatum. Brain Res. 649, 217-224.

Pubill, D., Canudas, A.M., Pallas, M., Camins, A., Camarasa, J., Escubedo, E., 2003. Different glial response to methamphetamine- and methylenedioxymethamphetamine-induced neurotoxicity. Naunyn Schmiedebergs Arch Pharmacol. 367, 490-499.

Pun, P.B., Lu, J., Moochhala, S., 2009. Involvement of ROS in BBB dysfunction. Free Radic. Res. 43, 348-364.

Quinton, M.S., Yamamoto, B.K., 2006. Causes and consequences of methamphetamine and MDMA toxicity. AAPS J. 8, E337-E347.

Radi, R., Beckman, J.S., Bush, K.M., Freeman, B.A., 1991. Peroxynitrite oxidation of sulfhydryls. The cytotoxic potential of superoxide and nitric oxide. J Biol Chem. 266, 4244-4250.

Ramirez, S.H., Potula, R., Fan, S., Eidem, T., Papugani, A., Reichenbach, N., Dykstra, H., Weksler, B.B., Romero, I.A., Couraud, P.O., Persidsky, Y., 2009. Methamphetamine disrupts blood-brain barrier function by induction of oxidative stress in brain endothelial cells. J Cereb Blood Flow Metab. 29, 1933-1945.

Remy, S., Beck, H., 2006. Molecular and cellular mechanisms of pharmacoresistance in epilepsy. Brain. 129, 18-35.

Ricaurte, G.A., Guillery, R.W., Seiden, L.S., Schuster, C.R., Moore, R.Y., 1982. Dopamine nerve terminal degeneration produced by high doses of methylamphetamine in the rat brain. Brain Res. 235, 93-103.

Ricaurte, G.A., Schuster, C.R., Seiden, L.S., 1980. Long-term effects of repeated methylamphetamine administration on dopamine and serotonin neurons in the rat brain: a regional study. Brain Res. 193, 153-163.

Roberts, L.M., Black, D.S., Raman, C., Woodford, K., Zhou, M., Haggerty, J.E., Yan, A.T., Cwirla, S.E., Grindstaff, K.K., 2008. Subcellular localization of transporters along the rat blood-brain barrier and blood-cerebral-spinal fluid barrier by in vivo biotinylation. Neuroscience. 155, 423-438.

Rocher, C., Gardier, A.M., 2001. Effects of repeated systemic administration of d-Fenfluramine on serotonin and glutamate release in rat ventral hippocampus: comparison with methamphetamine using in vivo microdialysis. Naunyn Schmiedebergs Arch Pharmacol. 363, 422-428.

Romero, I.A., Radewicz, K., Jubin, E., Michel, C.C., Greenwood, J., Couraud, P.O., Adamson, P., 2003. Changes in cytoskeletal and tight junctional proteins correlate with decreased permeability induced by dexamethasone in cultured rat brain endothelial cells. Neurosci Lett. 344, 112-116.

Rosenberg, G.A., 2002. Matrix metalloproteinases in neuroinflammation. Glia. 39, 279-291.

Rosenberg, G.A., Estrada, E.Y., Dencoff, J.E., 1998. Matrix metalloproteinases and TIMPs are associated with blood-brain barrier opening after reperfusion in rat brain. Stroke. 29, 2189-2195.

Roux, F., Couraud, P.O., 2005. Rat brain endothelial cell lines for the study of blood-brain barrier permeability and transport functions. Cell Mol Neurobiol. 25, 41-58.

Ruan, L., Torres, C.M., Qian, J., Chen, F., Mintz, J.D., Stepp, D.W., Fulton, D., Venema, R.C., 2011. Pin1 prolyl isomerase regulates endothelial nitric oxide synthase. Arterioscler Thromb Vasc Biol. 31, 392-398.

Saitou, M., Furuse, M., Sasaki, H., Schulzke, J.D., Fromm, M., Takano, H., Noda, T., Tsukita, S., 2000. Complex phenotype of mice lacking occludin, a component of tight junction strands. Mol Biol Cell. 11, 4131-4142.

Sanchez, V., Zeini, M., Camarero, J., O'Shea, E., Bosca, L., Green, A.R., Colado, M.I., 2003. The nNOS inhibitor, AR-R17477AR, prevents the loss of NF68 immunoreactivity induced by methamphetamine in the mouse striatum. J Neurochem. 85, 515-524.

Sandoval, K.E., Witt, K.A., 2008. Blood-brain barrier tight junction permeability and ischemic stroke. Neurobiol Dis. 32, 200-219.

Sato, S., Fujita, N., Tsuruo, T., 2000. Modulation of Akt kinase activity by binding to Hsp90. Proc Natl Acad Sci USA. 97, 10832-10837.

Satoh, H., Zhong, Y., Isomura, H., Saitoh, M., Enomoto, K., Sawada, N., Mori, M., 1996. Localization of 7H6 tight junction-associated antigen along the cell border of vascular endothelial cells correlates with paracellular barrier function against ions, large molecules, and cancer cells. Exp Cell Res. 222, 269-274.

Sattler, R., Tymianski, M., 2000. Molecular mechanisms of calcium-dependent excitotoxicity. J Mol Med (Berl). 78, 3-13.

Schep, L.J., Slaughter, R.J., Beasley, D.M., 2010. The clinical toxicology of metamfetamine. Clin Toxicol (Phila). 48, 675-694.

Schmidt, H.H., Hofmann, H., Schindler, U., Shutenko, Z.S., Cunningham, D.D., Feelisch, M., 1996. No .NO from NO synthase. Proc Natl Acad Sci USA. 93, 14492-14497.

Schmitz, Y., Lee, C.J., Schmauss, C., Gonon, F., Sulzer, D., 2001. Amphetamine distorts stimulation-dependent dopamine overflow: effects on D2 autoreceptors, transporters, and synaptic vesicle stores. J Neurosci. 21, 5916-5924.

Schnitzer, J.E., Oh, P., McIntosh, D.P., 1996. Role of GTP hydrolysis in fission of caveolae directly from plasma membranes. Science. 274, 239-242.

Schubert, W., Frank, P.G., Woodman, S.E., Hyogo, H., Cohen, D.E., Chow, C.W., Lisanti, M.P., 2002. Microvascular hyperpermeability in caveolin-1 (-/-) knock-out mice. Treatment with a specific nitric-oxide synthase inhibitor, L-NAME, restores normal microvascular permeability in Cav-1 null mice. J Biol Chem. 277, 40091-40098.

Seiden, L.S., Fischman, M.W., Schuster, C.R., 1976. Long-term methamphetamine induced changes in brain catecholamines in tolerant rhesus monkeys. Drug Alcohol Depend. 1, 215-219.

Seiden, L.S., Sabol, K.E., 1996. Methamphetamine and methylenedioxymethamphetamine neurotoxicity: possible mechanisms of cell destruction. NIDA Res Monogr. 163, 251-276.

Sekine, Y., Ouchi, Y., Sugihara, G., Takei, N., Yoshikawa, E., Nakamura, K., Iwata, Y., Tsuchiya, K.J., Suda, S., Suzuki, K., Kawai, M., Takebayashi, K., Yamamoto, S., Matsuzaki, H., Ueki, T., Mori, N., Gold, M.S., Cadet, J.L., 2008. Methamphetamine causes microglial activation in the brains of human abusers. J Neurosci. 28, 5756-5761.

Sessa, W.C., 2004. eNOS at a glance. J Cell Sci. 117, 2427-2429.

Sessa, W.C., Garcia-Cardena, G., Liu, J., Keh, A., Pollock, J.S., Bradley, J., Thiru, S., Braverman, I.M., Desai, K.M., 1995. The Golgi association of endothelial nitric oxide synthase is necessary for the efficient synthesis of nitric oxide. J Biol Chem. 270, 17641-17644.

Sharma, H.S., Ali, S.F., 2006. Alterations in blood-brain barrier function by morphine and methamphetamine. Ann N Y Acad Sci. 1074, 198-224.

Sharma, H.S., Kiyatkin, E.A., 2009. Rapid morphological brain abnormalities during acute methamphetamine intoxication in the rat: an experimental study using light and electron microscopy. J Chem Neuroanat. 37, 18-32.

Sharp, C.D., Hines, I., Houghton, J., Warren, A., Jackson, T.H.4th, Jawahar, A., Nanda, A., Elrod, J.W., Long, A., Chi, A., Minagar, A., Alexander, J.S., 2003. Glutamate causes a loss in human cerebral endothelial barrier integrity through activation of NMDA receptor. Am J Physiol Heart Circ Physiol. 285, H2592-H2598.

Silva, A.P., Martins, T., Baptista. S., Gonçalves, J., Agasse, F., Malva, J.O., 2010. Brain injury associated with widely abused amphetamines: neuroinflammation, neurogenesis and blood-brain barrier. Curr Drug Abuse Rev. 3, 239-254.

Simionescu, M., Popov, D., Sima, A., 2009. Endothelial transcytosis in health and disease. Cell Tissue Res. 335, 27-40.

Simionescu, M., Simionescu, N., Palade, G. E., 1975. Segmental differentiations of cell junctions in the vascular endothelium. The microvasculature. J Cell Biol. 67, 863-85.

Simões, P.F., Silva, A.P., Pereira, F.C., Marques, E., Grade, S., Milhazes, N., Borges, F., Ribeiro, C.F., Macedo, T.R., 2007. Methamphetamine induces alterations on hippocampal NMDA and AMPA receptor subunit levels and impairs spatial working memory. Neuroscience. 150, 433-441.

Simpson, I.A., Carruthers, A., Vannucci, S.J., 2007. Supply and demand in cerebral energy metabolism: the role of nutrient transporters. J Cereb Blood Flow Metab. 27, 1766-1791.

Sonsalla, P.K., Nicklas, W.J., Heikkila, R.E., 1989. Role for excitatory amino acids in methamphetamine-induced nigrostriatal dopaminergic toxicity. Science. 243, 398-400.

Sriram, K., Miller, D.B., O'Callaghan, J.P., 2006. Minocycline attenuates microglial activation but fails to mitigate striatal dopaminergic neurotoxicity: role of tumor necrosis factor-alpha. J Neurochem. 96, 706-718.

Staszewski, R.D., Yamamoto, B.K., 2006. Methamphetamine-induced spectrin proteolysis in the rat striatum. J Neurochem. 96, 1267-1276.

Steed, E., Balda, M.S., Matter, K., 2010. Dynamics and functions of tight junctions. Trends Cell Biol. 20, 142-149

Stephans, S.E., Yamamoto, B.K., 1994. Methamphetamine-induced neurotoxicity: roles for glutamate and dopamine efflux. Synapse. 17, 203-209.

Stevenson, B.R., Siliciano, J.D., Mooseker, M.S., Goodenough, D.A., 1986. Identification of ZO-1: a high molecular weight polypeptide associated with the tight junction (zonula occludens) in a variety of epithelia. J Cell Biol. 103, 755-766.

Stoll, G., Jander, S., 1999. The role of microglia and macrophages in the pathophysiology of the CNS. Prog Neurobiol. 58, 233-247.

Streit, W.J., 2002. Microglia as neuroprotective, immunocompetent cells of the CNS. Glia. 40, 133-139.

Streit, W.J., Walter, S.A., Pennell, N.A., 1999. Reactive microgliosis. Prog Neurobiol. 57, 563-581.

Sulzer, D., Sonders, M.S., Poulsen, N.W., Galli, A., 2005. Mechanisms of neurotransmitter release by amphetamines: a review. Prog Neurobiol. 75, 406-433.

Svedin, P., Hagberg, H., Savman, K., Zhu, C., Mallard, C., 2007. Matrix metalloproteinase-9 gene knock-out protects the immature brain after cerebral hypoxia-ischemia. J Neurosci. 27, 1511-1518.

Szklarczyk, A., Lapinska, J., Rylski, M., McKay, R.D., Kaczmarek, L., 2002. Matrix metalloproteinase-9 undergoes expression and activation during dendritic remodeling in adult hippocampus. J Neurosci. 22, 920-930.

Takahashi, S., Mendelsohn, M.E., 2003. Synergistic activation of endothelial nitric-oxide synthase (eNOS) by HSP90 and Akt: calcium-independent eNOS activation involves formation of an HSP90-Akt-CaM-bound eNOS complex. J Biol Chem. 278, 30821-30827.

Takayasu, T., Ohshima, T., Nishigami, J., Kondo, T., Nagano, T., 1995. Screening and determination of methamphetamine and amphetamine in the blood, urine and stomach contents in emergency medical care and autopsy cases. J Clin Forensic Med. 2, 25-33.

Tata, D.A., Yamamoto, B.K., 2007. Interactions between methamphetamine and environmental stress: role of oxidative stress, glutamate and mitochondrial dysfunction. Addiction. 102 Suppl 1, 49-60.

Thiel, V.E., Audus, K.L., 2001. Nitric oxide and blood-brain barrier integrity. Antioxid Redox Signal. 3, 273-278.

Thomas, D.M., Dowgiert, J., Geddes, T.J., Francescutti-Verbeem, D., Liu, X., Kuhn, D.M., 2004. Microglial activation is a pharmacologically specific marker for the neurotoxic amphetamines. Neurosci Lett. 367, 349-354.

Thomas, D.M., Kuhn, D.M., 2005a. Attenuated microglial activation mediates tolerance to the neurotoxic effects of methamphetamine. J Neurochem. 92, 790-797.

Thomas, D.M., Kuhn, D.M., 2005b. Cyclooxygenase-2 is an obligatory factor in methamphetamine-induced neurotoxicity. J Pharmacol Exp Ther. 313, 870-876.

Thompson, P.M., Hayashi, K.M., Simon, S.L., Geaga, J.A., Hong, M.S., Sui, Y., Lee, J.Y., Toga, A.W., Ling, W., London, E.D., 2004. Structural abnormalities in the brains of human subjects who use methamphetamine. J Neurosci. 24, 6028-6036.

Thrash, B., Karuppagounder, S.S., Uthayathas, S., Suppiramaniam, V., Dhanasekaran, M., 2010. Neurotoxic effects of methamphetamine. Neurochem Res. 35, 171-179.

Tobias, M.C., O'Neill, J., Hudkins, M., Bartzokis, G., Dean, A.C., London, E.D., 2010. White-matter abnormalities in brain during early abstinence from methamphetamine abuse. Psychopharmacology (Berl). 209, 13-24.

Toborek, M., Lee, Y.W., Flora, G., Pu, H., Andras, I.E., Wylegala, E., Hennig, B., Nath, A., 2005. Mechanisms of the blood-brain barrier disruption in HIV-1 infection. Cell Mol Neurobiol. 25, 181-199.

Tong, X.K., Hamel, E., 1999. Regional cholinergic denervation of cortical microvessels and nitric oxide synthase-containing neurons in Alzheimer's disease. Neuroscience. 92, 163-175.

Traweger, A., Fuchs, R., Krizbai, I.A., Weiger, T.M., Bauer, H.C., Bauer, H., 2003. The tight junction protein ZO-2 localizes to the nucleus and interacts with the heterogeneous nuclear ribonucleoprotein scaffold attachment factor-B. J Biol Chem. 278, 2692-2700.

Tsukita, S., Furuse, M., Itoh, M., 2001. Multifunctional strands in tight junctions. Nat Rev Mol Cell Biol. 2, 285-293.

Tunkel, A.R., Scheld, W.M., 1993. Pathogenesis and pathophysiology of bacterial meningitis. Annu Rev Med. 44, 103-120.

Ueno, M., 2007. Molecular anatomy of the brain endothelial barrier: an overview of the distributional features. Curr Med Chem. 14, 1199-1206.

United Nations Office on Drugs and Crime, 2011. World Drug Report 2011. United Nations Publication, Sales No. E.11.XI.10, Vienna, Austria.

Van Itallie, C.M., Anderson, J.M., 2004. The molecular physiology of tight junction pores. Physiology (Bethesda). 19, 331-338.

Venkiteswaran, K., Xiao, K., Summers, S., Calkins, C.C., Vincent, P.A., Pumiglia, K., Kowalczyk, A.P., 2002. Regulation of endothelial barrier function and growth by VE-cadherin, plakoglobin, and beta-catenin. Am J Physiol Cell Physiol. 283, C811-C821.

Vincent, P.A., Xiao, K., Buckley, K.M., Kowalczyk, A.P., 2004. VE-cadherin: adhesion at arm's length. Am J Physiol Cell Physiol. 286, C987-C997.

Vincent, V.A., Tilders, F.J., Van Dam, A.M., 1997. Inhibition of endotoxin-induced nitric oxide synthase production in microglial cells by the

presence of astroglial cells: a role for transforming growth factor beta. Glia. 19, 190-198.

Vorbrodt, A.W., Dobrogowska, D.H., 2003. Molecular anatomy of intercellular junctions in brain endothelial and epithelial barriers: electron microscopist's view. Brain Res Brain Res Rev. 42, 221-242.

Wachtel, M., Frei, K., Ehler, E., Fontana, A., Winterhalter, K., Gloor, S.M., 1999. Occludin proteolysis and increased permeability in endothelial cells through tyrosine phosphatase inhibition. J Cell Sci. 112 (Pt 23), 4347-4356.

Wagner, G.C., Carelli, R.M., Jarvis, M.F., 1986. Ascorbic acid reduces the dopamine depletion induced by methamphetamine and the 1-methyl-4-phenyl pyridinium ion. Neuropharmacology. 25, 559-561.

Wagner, G.C., Ricaurte, G.A., Seiden, L.S., Schuster, C.R., Miller, R.J., Westley, J., 1980. Long-lasting depletions of striatal dopamine and loss of dopamine uptake sites following repeated administration of methamphetamine. Brain Res. 181, 151-160.

Wang, G., Moniri, N.H., Ozawa, K., Stamler, J.S., Daaka, Y., 2006. Nitric oxide regulates endocytosis by S-nitrosylation of dynamin. Proc Natl Acad Sci USA. 103, 1295-1300.

Watabe, M., Nagafuchi, A., Tsukita, S., Takeichi, M., 1994. Induction of polarized cell-cell association and retardation of growth by activation of the E-cadherin-catenin adhesion system in a dispersed carcinoma line. J Cell Biol. 127, 247-256.

Weil, R.J., Palmieri, D.C., Bronder, J.L., Stark, A.M., Steeg, P.S., 2005. Breast cancer metastasis to the central nervous system. Am J Pathol. 167, 913-920.

Weis, W.I., Nelson, W.J., 2006. Re-solving the cadherin-catenin-actin conundrum. J Biol Chem. 281, 35593-35597.

Weiss, N., Miller, F., Cazaubon, S., Couraud, P.O., 2009. The blood-brain barrier in brain homeostasis and neurological diseases. Biochim Biophys Acta. 1788, 842-857.

Westergren, I., Johansson, B.B., 1992. NBQX, an AMPA antagonist, reduces glutamate-mediated brain edema. Brain Res. 573, 324-326.

Williams, T.M., Lisanti, M.P., 2004. The Caveolin genes: from cell biology to medicine. Ann Med. 36, 584-595.

Willis, C.L., Nolan, C.C., Reith, S.N., Lister, T., Prior, M.J., Guerin, C.J., Mavroudis, G., Ray, D.E., 2004. Focal astrocyte loss is followed by microvascular damage, with subsequent repair of the blood-brain barrier in the apparent absence of direct astrocytic contact. Glia. 45, 325-337.

Wise, R.A., 2004. Dopamine, learning and motivation. Nat Rev Neurosci. 5, 483-494.

Wittchen, E.S., Haskins, J., Stevenson, B.R., 1999. Protein interactions at the tight junction. Actin has multiple binding partners, and ZO-1 forms independent complexes with ZO-2 and ZO-3. J Biol Chem. 274, 35179-35185.

Wolburg, H., Noell, S., Mack, A., Wolburg-Buchholz, K., Fallier-Becker, P., 2009. Brain endothelial cells and the glio-vascular complex. Cell Tissue Res. 335, 75-96.

Wrona, M.Z., Yang, Z., Zhang, F., Dryhurst, G., 1997. Potential new insights into the molecular mechanisms of methamphetamine-induced neurodegeneration. NIDA Res Monogr. 173, 146-174.

Wu, P.H., Shen, Y.C., Wang, Y.H., Chi, C.W., Yen, J.C., 2006. Baicalein attenuates methamphetamine-induced loss of dopamine transporter in mouse striatum. Toxicology. 226, 238-245.

Wu, C.W., Ping, Y.H., Yen, J.C., Chang, C.Y., Wang, S.F., Yeh, C.L., Chi, C.W., Lee, H.C., 2007. Enhanced oxidative stress and aberrant mitochondrial biogenesis in human neuroblastoma SH-SY5Y cells during methamphetamine induced apoptosis. Toxicol Appl Pharmacol. 220, 243-251.

Xu, J., Kausalya, P.J., Phua, D.C., Ali, S.M., Hossain, Z., Hunziker, W., 2008. Early embryonic lethality of mice lacking ZO-2, but Not ZO-3, reveals critical and nonredundant roles for individual zonula occludens proteins in mammalian development. Mol Cell Biol. 28, 1669-1678.

Yamamoto, B.K., Moszczynska, A., Gudelsky, G.A., 2010. Amphetamine toxicities. Ann N Y Acad Sci. 1187, 101-121.

Yamamoto, B.K., Raudensky, J., 2008. The role of oxidative stress, metabolic compromise, and inflammation in neuronal injury produced by amphetamine-related drugs of abuse. J Neuroimmune Pharmacol. 3, 203-217.

Yamamoto, B.K., Zhu, W., 1998. The effects of methamphetamine on the production of free radicals and oxidative stress. J Pharmacol Exp Ther. 287, 107-114.

Yamamoto, T., Harada, N., Kano, K., Taya, S., Canaani, E., Matsuura, Y., Mizoguchi, A., Ide, C., Kaibuchi, K., 1997. The Ras target AF-6 interacts with ZO-1 and serves as a peripheral component of tight junctions in epithelial cells. J Cell Biol. 139, 785-795.

Yang, L., Froio, R.M., Sciuto, T.E., Dvorak, A.M., Alon, R., Luscinskas, F.W., 2005. ICAM-1 regulates neutrophil adhesion and transcellular migration of TNF-alpha-activated vascular endothelium under flow. Blood. 106, 584-592.

Yang, Y., Estrada, E.Y., Thompson, J.F., Liu, W., Rosenberg, G.A., 2007. Matrix metalloproteinase-mediated disruption of tight junction proteins in cerebral vessels is reversed by synthetic matrix metalloproteinase inhibitor in focal ischemia in rat. J Cereb Blood Flow Metab. 27, 697-709.

Yong, V.W., 2005. Metalloproteinases: mediators of pathology and regeneration in the CNS. Nat Rev Neurosci. 6, 931-944.

Yoshida, K., Morimoto, A., Makisumi, T., Murakami, N., 1993. Cardiovascular, thermal and behavioral sensitization to methamphetamine in freely moving rats. J Pharmacol Exp Ther. 267, 1538-1543.

Yu, A.S., McCarthy, K.M., Francis, S.A., McCormack, J.M., Lai, J., Rogers, R.A., Lynch, R.D., Schneeberger, E.E., 2005. Knockdown of occludin expression leads to diverse phenotypic alterations in epithelial cells. Am J Physiol Cell Physiol. 288, C1231-C1241.

Zhang, E.Y., Knipp, G.T., Ekins, S., Swaan, P.W., 2002. Structural biology and function of solute transporters: implications for identifying and designing substrates. Drug Metab Rev. 34, 709-750.

Zhao, C., Ling, Z., Newman, M.B., Bhatia, A., Carvey, P.M., 2007. TNF-alpha knockout and minocycline treatment attenuates blood-brain barrier leakage in MPTP-treated mice. Neurobiol Dis. 26, 36-46.

Zhou, L., Zhu, D.Y., 2009. Neuronal nitric oxide synthase: structure, subcellular localization, regulation, and clinical implications. Nitric Oxide. 20, 223-230.

Zhu, J., Xu, W., Wang, J., Ali, S.F., Angulo, J.A., 2009. The neurokinin-1 receptor modulates the methamphetamine-induced striatal apoptosis and nitric oxide formation in mice. J Neurochem. 111, 656-668.

Zlokovic, B.V., 2008. The blood-brain barrier in health and chronic neurodegenerative disorders. Neuron. 57, 178-201.